Springer Theses

Recognizing Outstanding Ph.D. Research

Aims and Scope

The series "Springer Theses" brings together a selection of the very best Ph.D. theses from around the world and across the physical sciences. Nominated and endorsed by two recognized specialists, each published volume has been selected for its scientific excellence and the high impact of its contents for the pertinent field of research. For greater accessibility to non-specialists, the published versions include an extended introduction, as well as a foreword by the student's supervisor explaining the special relevance of the work for the field. As a whole, the series will provide a valuable resource both for newcomers to the research fields described, and for other scientists seeking detailed background information on special questions. Finally, it provides an accredited documentation of the valuable contributions made by today's younger generation of scientists.

Theses are accepted into the series by invited nomination only and must fulfill all of the following criteria

- They must be written in good English.
- The topic should fall within the confines of Chemistry, Physics, Earth Sciences and related interdisciplinary fields such as Materials, Nanoscience, Chemical Engineering, Complex Systems and Biophysics.
- The work reported in the thesis must represent a significant scientific advance.
- If the thesis includes previously published material, permission to reproduce this must be gained from the respective copyright holder.
- They must have been examined and passed during the 12 months prior to nomination.
- Each thesis should include a foreword by the supervisor outlining the significance of its content.
- The theses should have a clearly defined structure including an introduction accessible to scientists not expert in that particular field.

Camille Petit

Factors Affecting the Removal of Ammonia from Air on Carbonaceous Materials

Investigation of Reactive Adsorption Mechanism

Springer

Author
Dr. Camille Petit
Department of Chemistry
CUNY—City University of New York
New York
NY 10031
USA

Present Address
Department of Earth and Environmental
   Engineering and Chemical Engineering
Columbia University
New York
NY 10027
USA

Supervisor
Prof. Dr. Teresa J. Bandosz
Department of Chemistry
City College of New York
Marshak Science Building
New York
NY 10031
USA

Printed on acid-free paper

Supervisor's Foreword

One may say that today's scientists are runners on a fast track trying to keep up with the considerable number of discoveries and progress. We have sophisticated tools, instruments, and superfast computers with vast databases to help us "digest" all the information we create and are exposed to. Unfortunately, in the quest for scientific solutions to the current problems, in many cases we may accidentally miss the joy of training new scientists who are sometimes better, brighter, and more efficient than we are… so… when opportunity knocks let's embrace it and we will never regret the time spent to teach, to lead, and… to learn.

Marie Sklodowska-Curie once said "I am among those who think that science has great beauty. A scientist in his laboratory is not only a technician: he is also a child placed before natural phenomena which impress him like a fairy tale"… That "fairy tale" is … what leads us through paths of science and let us see the beauty of it and feel the excitement of comprehending, understanding and promoting new ideas, new hypotheses, new proofs… regardless of their magnitude… and often those very small steps built by thousands of scientists enable only very few of us to reach the higher levels honored by the Nobel Prize. Nevertheless, all of us agree that passion for scientific work is one of our motivations and at the same time a great and unique award which we have tremendous luck to receive and experience in almost everyday of our professional careers…

I saw that passion, patience, and brilliance in Camille when as an intern she arrived from her native France to work on the research internship required for a Masters Degree at her school. At that time the US Army Research Office gave us an award for a very demanding research topic, which focuses on the removal of specific toxic gases by existing adsorbents. The challenge was in the required conditions of this adsorption process: ambient air. The Toxic Industrial Compounds (TICs) that we were working on are usually small molecule species whose physical adsorption at room temperature is very weak. Moreover, water in ambient air can compete with the adsorption sites. Overall, the most popular adsorbents (mainly activated carbons and zeolites) existing in 2005 did not look very promising for TICs' removal. The requirements were pretty strict and the adsorbents should not only adsorb a large quantity of toxic species but also have strong

retention properties. The safety of war-fighters and other users of gas filters was at stake here.

At the time, metallic organic frameworks (MOF) were relatively new materials, and graphite oxide (GO) started to experience its renaissance owing to its suitability in one of the synthesis routes for graphene. Thus the idea to build the composites was conceived. Although both materials had good capability to retain ammonia, combining them could result in even better adsorbents! Here the chemistry of MOF could be utilized for surface reactions and GO would provide a dense array of carbon atoms to enhance dispersive forces for physical adsorption. Owing to the specific chemistry of both components, the bonds between two phases were expected. The task was not easy since we did not have any experience in organic synthesis. But Camille took on the challenge. Cautiously, with determined effort and passion, the new materials were built and applied as adsorbents not only for ammonia but also for other TICs such as hydrogen sulfide and nitrogen dioxide. Although removal of the two latter species was beyond Camille's Doctoral Thesis, we consider this finding as important. Thus her work was extended into this area because of the versatility and properties of the new materials.

This book consists of Camille's Doctoral Thesis and describes the story of the Problem Approach. Approach, which started from existing traditional adsorbents and ended at the new and promising structures. Approach, which we hope shows the importance of the chosen research path and of the tools used to accomplish that short, 3-year journey. Approach, in which first we look at the challenge of a scientific problem and then we modify/design materials to meet that challenge. For this we use all our chemistry knowledge, intuition, experience, experience of our predecessors and peers and, of course… passion and enjoyment of science. I wish I have more students with Camille's attitude toward the discoveries of everyday life… and passionate funs of "a fairy tales" of science.

New York, January 2012   Dr. Teresa J. Bandosz

Acknowledgments

I would like to express my sincere gratitude to all of you who contributed, directly or indirectly, to this dissertation… and you are many!

In October 2006, I joined Professor Bandosz' team for what was supposed to be a few months research project to complete my Masters Degree. On the first day, I was welcomed by Anna and Mykola. A few days later, the phone rang in the lab. Professor Bandosz was calling and wanted like to speak with me. She enquired about me and my first results with this communicative enthusiasm that immediately made me feel like I was in the right place. That day, I had met my future Ph.D. mentor. Throughout the past 4 years, her unflinching support, confidence in my work, and excitement for research have guided my study. Not only has she helped me improve my knowledge from a scientific standpoint but she has also provided me with the opportunity to strengthen my communication and professional skills via conferences and collaborations. She has changed the way I look at research and words of thanks are not enough to convey my deep admiration and respect towards her.

Extended thanks to Professors Alexandratos and Couzis, for serving on my Dissertation Committee, and for sharing their invaluable comments and expertise during and after our meetings in spite of their busy schedules. They have been the "third eye" of this thesis, generous with their time and always here to address my questions.

These few years at City College would not have been as enjoyable without the presence of my dear colleagues: Amani, Ammal, Anna, Barbara, Benoit, Danh, Jakub, Karifala, Lena, Mykola, Robert, and Svetlana. Thank you for creating this wonderful atmosphere both diligent and relaxed!

I would like to express my gratitude to Professors Drain, Matsui, Lakshman, Kowach, and Kretzschmar as well as Dr. Morales who have always addressed my many requests and questions and helped me to move forward in the completion of this thesis.

I reserve my last thanks to the one who has the wonderful ability to make me escape from work and to always bring me the balance and support I need, and who, more than anyone else, understands the meaning of these 4 years for me. To the one, whose special inclination for Chemistry, will for sure appreciate to its true worth to have his name on a Chemistry dissertation. Thank you Guillaume.

Contents

Chapter 1
Introduction

1.1 Ammonia and Air Pollution

"There is no such thing as a free lunch". This common saying well illustrates the world industrial development. With its myriad of new technologies constantly improving our daily lives, it also resulted in a dramatic increase of pollution since the beginning of the twentieth century. Air pollution in particular, with the release of greenhouse gases and other volatile toxic compounds, has led to serious environmental issues ranging from climate change to ocean acidification and has thus become the object of many concerns and debates. In response to this global issue, governmental entities impose strict regulations regarding the release of pollutant gases. To prevent/reduce toxic gases emissions and meet these continuously reinforced requirements, the scientific community must find effective pathways toward a safer environment.

As many other gases, ammonia represents a threat to air quality. This small molecule, with a diameter of about 3 Å [1] and easily recognizable by its pungent odor, is one of the most widely produced chemicals and one of the most abundant nitrogen-containing species in the atmosphere [2]. It exhibits Lewis and Brønsted basic characters, both related to the presence of its lone pair of electrons on the nitrogen atom. Owing to its polarity and ability to form hydrogen bonds, ammonia easily dissolves in water. A brief summary of the physical and chemical features of ammonia is presented in Table 1.1. The anthropogenic release of ammonia in the atmosphere related to the agriculture industry (i.e. fertilizer production), manufacturing industry (i.e. ammonia, coke, nitrogen-containing chemicals), sewage treatment plants or refrigeration systems adds up significantly to the natural sources [2]. The latter include mainly animal wastes and microorganisms in soil [2]. This human impact raises serious environmental issues since, in large quantity, ammonia release becomes hazardous. For instance, ammonia easily forms ammonium salts upon reaction with acidic aerosols [2]. These salts are known to be extremely corrosive and are involved in particulate matter formation

Table 1.1 Chemical and
physical properties of
ammonia [8]

Properties	Values
Molecular weight	17 g mol^{-1}
Diameter	3 Å
Dipole moment	1.47 D
pK$_b$	4.75
Solubility in water	89.9 g in 100 mL (cold water)
	7.4 g in 100 mL (hot water)

[2]. Moreover, ammonia also has an impact on the vegetation via, for instance, foliar injury, growth and productivity alteration or reduction of frost tolerance [3]. Ammonia also represents a potential threat to human health since, owing to its high solubility, it can easily react with the skin, eyes and respiratory system to form ammonium hydroxide via an exothermic process responsible for thermal injuries [4]. Considering all of these, the National Research Council (NRC) has identified ammonia emissions as a major air quality concern at regional, national and global levels [5]. Moreover, the American Conference of Governmental Industrial Hygienists (ACGIH) has limited exposure to ammonia to a time-weighted average concentration (TWA) of 25 ppm and short term limit concentration (STEL) of 35 ppm [6], while the immediately dangerous to life and health limit (IDLH) has been set up at 300 ppm [6]. Ammonia is considered as a Toxic Industrial Compound (TIC) [7]. Consequently, facing the accidental or intentional release of that gas is considered an important task for homeland security.

1.2 General Overview on Adsorption and its Applications in Air Pollution

The adsorption of gases on porous materials has been proposed to control the release of toxic pollutants in the atmosphere [9]. Before entering into the details of the specific case of ammonia removal, it seems important to review the general features regarding adsorption mechanisms and adsorbent materials. This section, although not exhaustive, aims at highlighting some of the key properties of adsorption that will be discussed later.

The process of adsorption corresponds to a surface mechanism between two phases (gas–liquid, gas–solid or liquid–solid) that must be distinguished from absorption [10]. In the former case, molecules "stick"/adhere to the surface of a solid or liquid [10]. On the contrary, in absorption phenomena, molecules (or atoms, or ions) "penetrate" inside the bulk phase of a material and become a part of it [10]. Adsorption is thus considered as a surface mechanism whereas absorption corresponds to a volumetric/bulk process. As of terminology, the molecules being adsorbed are referred to as adsorbates and the material on which these species are attached is called the adsorbent. In some cases, the process of adsorption can be reversible as the molecules initially adsorbed can be removed
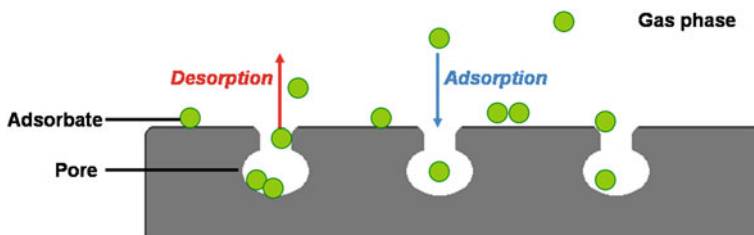
Fig. 1.1 Schematic view of adsorption and desorption processes on porous materials

from the surface [10]. This is called desorption. A schematic view of adsorption and desorption processes is proposed in Fig. 1.1.

In the following, only gas adsorption on solid materials will be considered. This phenomenon can be classified into two categories: physisorption (or physical adsorption) and chemisorption (or chemical adsorption) [9, 10]. During physisorption, the attraction of the gas toward the solid surface is driven by van der Waals forces which include electrostatic, polar and dispersive interactions [10]. Physical adsorption is a non-specific process since the possibility for the adsorbate to be retained on the adsorbent's surface is independent of the chemistry of both entities [10]. It only relies on the porosity of the adsorbent [10]. Physisorption is a rapid mechanism from a kinetic standpoint and represents a necessary path toward chemical adsorption. The latter involves the creation of chemical bonds between the adsorbate and the adsorbent [10]. Unlike physical adsorption, chemisorption is specific since the nature of the two species in contact will enable, favor or prevent binding [10]. Another type of adsorptive interactions is the so-called reactive adsorption where the adsorbent surface chemistry influences the transformations of the adsorbate. Depending on the chemical nature of the adsorbate molecule and the type, number and strength of functional groups on the adsorbent surface, the interactions between the two entities will differ. Usually, chemisorption and reactive adsorption lead to much stronger interactions than physisorption and represents a more selective adsorption process [10]. Enthalpies for physisorption range from about 20 to 50 kJ mol^{-1} whereas enthalpies measured for the other processes are about ten times higher [11].

Adsorbents are usually characterized by a high surface area and porosity and include different types of materials. Among the common adsorbents, one can find: activated carbons, carbon molecular sieves, polymeric resins, zeolites, alumina, silica, metal oxides or metal–organic frameworks [10, 12, 13]. The porosity, although not the only influencing parameter, can greatly modify the ability of an adsorbent to retain molecules. Consequently, when considering adsorption processes, one has to look at the porosity and more specifically at: the shape of the pores (spherical, cylindrical or slit-like pores [9]), the volume of the pores, the pore size and finally the pore size distribution. Considering the latter parameters, it is important to mention that pores are usually classified according to their size,

as micropores (<2 nm), mesopores (2–50 nm) and macropores (>50 nm) [9, 10]. All these features have an impact on the transport/diffusion of the adsorbate as well as on the physical forces exerted by the adsorbent.

To analyze the performance of adsorbents in retaining a targeted molecule, several criteria are considered. One of them is the so-called adsorption capacity. This value represents the amount of adsorbate retained on the surface of the adsorbent per mass or volume of adsorbent. The former unit is useful to analyze the process of gas uptake, and the second has to be considered for practical applications for which the available volume is a limiting factor. The adsorption capacity can be measured by conducting a fixed bed breakthrough test. In a typical run, a well-packed bed of adsorbent is subjected to a constant flow of the specific gas and the concentration of that gas in the outlet stream is measured as a function of time. As seen in Fig. 1.2a, as the adsorption takes place, the adsorbent becomes progressively saturated and the adsorption zone moves toward the end of the bed. At one point, the saturation is such that the adsorbent cannot retain the entire quantity of adsorbate contained in the inlet stream. At this time, the targeted adsorbate is detected in the outlet stream. As the adsorption still progresses, the concentration in the effluent increases until it equals the inlet concentration. A breakthrough curve can be plotted which gives the concentration of the adsorbate in the outlet stream as a function of time (Fig. 1.2b). This curve usually exhibits a sigmoidal shape and two important points can be identified on it. The first point, referred to as the breakthrough, corresponds to the time at which the effluent concentration equals 5–10% of the inlet concentration. The second one is called the quasi-equilibrium and represents the point at which the concentration in the outlet stream equals that of the inlet stream. From this curve, a mass balance between the amount of gas present in the inlet stream and that measured in the outlet stream can be derived and allows for the determination of the adsorption capacity. However, it is important to note that the adsorption capacity can be calculated either at the breakthrough point ("dynamic adsorption") or at quasi-equilibrium ("adsorption at quasi-equilibrium"). In the latter case, higher adsorption capacity values are obtained. In the study described later, adsorbents are always tested in dynamic conditions and the adsorption capacities given refer to those calculated at the breakthrough point. The determination of the breakthrough capacity in this case is presented in Eqs. 1.1 and 1.2. Equation 1.1 gives the amount of adsorbate retained at a specific time per mass of adsorbent. To obtain the capacity at the breakthrough point (or breakthrough capacity), an integration of all the prior values up to the breakthrough time is required as expressed in Eq. 1.2. In other words, the breakthrough capacity corresponds to the area above the breakthrough curve. The main assumption of Eq. 1.1 is that the breakthrough curve between two points used for the calculation is linear. This assumption is easily verified by considering a sufficiently small time interval between two points. It has to be noted that a trivial consideration of the adsorbent bed density can provide the adsorbent capacity per volume of adsorbent.
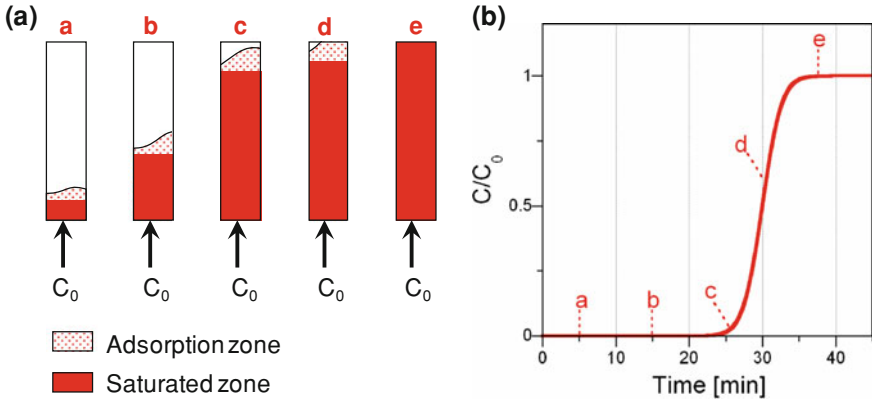
Fig. 1.2 The breakthrough test scheme with the evolution of the saturation and adsorption zones (**a**) and the breakthrough curve with identification of the different steps described in **a** (**b**)

$$A_{t+\mathrm{d}t} = A_t + \mathrm{d}t \times \left(C_0 - \frac{C_t + C_{t+\mathrm{d}t}}{2} \right) \times \frac{Q_{\mathrm{air}}}{m_{\mathrm{ads}}} \times \frac{M_{\mathrm{gas}} \times 273}{10^6 \times 22.4 \times (273 + T)} \quad (1.1)$$

$$A_b = \sum_{t=0}^{t_b} A_t \quad (1.2)$$

In the above two equations, the notation adopted can be summarized as follows:

A_t breakthrough capacity at t (mg g^{-1} of adsorbent)
A_b breakthrough capacity (mg g^{-1} of adsorbent)
t time (min)
t_b breakthrough time (min)
dt time interval between two points of the breakthrough curve (min)
C_0 inlet concentration of targeted gas (ppm)
C_t outlet concentration of targeted gas at t (ppm)
m_{ads} weight of adsorbent's bed (g)
Q total flow rate (mL min^{-1})
M_{gas} gas molecular weight (g mol^{-1})
T temperature (in °C)

1.3 Current Situation on Ammonia Adsorption

Several types of ammonia adsorbents have been tested so far, but most of them remain on a laboratory-scale application. The adsorbents include carbonaceous materials (i.e. activated carbon), zeolites, alumina, silica, polymeric resins, clays or metal–organic frameworks [14–47]. In those studies, ammonia adsorption is

considered either from the air filtration standpoint or as a way to characterize the acid–base nature of an adsorbent. Owing to their diversity of texture and chemistry, the latter materials exhibit quite different performances.

Activated carbons play a large role in retention of various pollutants [9, 13] and in that of ammonia in particular [14–23, 25–27, 29, 45–47]. Their high surface area (about 500–1500 m^2 g^{-1}) and porosity enable physical adsorption whereas their surface chemistry, related to the presence of functional groups, is responsible for specific adsorption via acid–base reactions or hydrogen-bonding [9]. The heat of adsorption of ammonia on carbonaceous materials covers a wide range going from about 20 up to 150 kJ mol^{-1} [19, 45, 48–52]. This large variation is related to the chemical features of the adsorbents. On graphitic surfaces devoid of functional groups, low heats of adsorption are measured [48], whereas in the presence of functionalities able to interact with ammonia, the values are enhanced [45]. Activated carbons exhibit adsorption capacities usually between 0.1 and 20 mg g^{-1} (or higher when tests are performed until thermodynamic equilibrium) [14, 19, 25, 45–47, 53]. Unmodified activated carbons are not ideal adsorbents for ammonia. Indeed, since the average pore size for a common carbon is 10–20 Å, which is much higher than ammonia size, and the physical forces are not sufficiently strong to retain small molecules like ammonia, especially at ambient conditions. Moreover, the surface acidity of carbon materials related to the presence of functionalities is not enough developed to enhance the chemisorption of ammonia. Consequently, the use of untreated activated carbons for ammonia uptake does not look very promising as it only involves weak adsorption forces, which lead to the progressive desorption of the gas over time. Nevertheless, the low cost, high stability and ease of modification of virgin activated carbons represent valuable assets and can be exploited. Various alterations of virgin carbons can be performed to develop stronger forces between ammonia and the adsorbent's surface and have been reported in the literature [15, 23, 27, 53–57]. These modifications address the surface chemistry of activated carbons and can be classified into two categories. The first modification involves direct alteration of the carbon surface with no chemical addition. This category includes the oxidation of the material and results in the formation of new acidic groups on its surface [23, 53–57], a desirable asset in the retention of basic molecules. Nevertheless, an extended oxidation can reduce the physical strength of the adsorbents and thus compromises its potential industrial application. The second type of modification is based on impregnation of the material with a chemical, usually an inorganic compound. Among the inorganic compounds already tested for impregnation on carbon are metal oxides [54], acids and bases [56], or heteropolyacids [15]. Because of the wide diversity of inorganic substances, this method offers an infinite horizon for modifications and enables adapting the material to the specific needs of the adsorption process. In spite of that, only few studies have explored that type of modification for ammonia retention [15, 54, 56]. In addition to activated carbons, other types of carbonaceous materials, such as sludge-derived compounds, carbon nanotubes or carbon fibers, have been tested for ammonia adsorption but their use remains scarce [17, 58, 59].

Ammonia uptake on zeolites, silica or alumina has been extensively studied. While in most cases, ammonia was used as a probe to investigate the acidity of such materials, a few studies have used these materials for gas adsorption purposes [14, 28, 31–36]. It is accepted that ammonia can be physically adsorbed or chemically retained on the Lewis and Brønsted sites of these compounds in its NH_3 or NH_4^+ form. The adsorption of ammonia on these materials is usually characterized by heats of adsorption ranging from 40 to 180 kJ mol^{-1} [60, 61]. The adsorption capacities reported for these materials vary greatly depending on the adsorbent itself and on the conditions of the tests and stretch from 1 to 130 mg g^{-1} [14, 33, 35, 36]. Zeolites, alumina and silica suffer from two main drawbacks in regard to the ammonia removal. One is related to the fact that they are highly hydrophilic [62] and their breakthrough capacity is significantly reduced in ambient/moist air due to a water/ammonia competition for adsorption. Since the presence of humidity on a large-scale application can be difficult and expensive to avoid, this affects the commercialization of such materials for ammonia removal. Another issue is that part of the ammonia adsorbed can progressively desorb from the surface, which is obviously not desired if those materials are employed as gas adsorbents for air quality purposes.

Ammonia adsorption on polymeric resins has already been reported in the literature [14, 37–39]. These materials are mostly encountered in water adsorption processes and, as in the case of zeolites, alumina or silica, ammonia adsorption has been investigated mainly to assess the acidity of the resins and identify the nature of their acidic sites [37–39]. Only a few studies have reported their potential use in gas adsorption and especially ammonia removal [14]. The resins encountered can be ionic or non-ionic resins, porous or non-porous (gel). Depending on their nature, the adsorption can occur via an exchange of cations (i.e. H$^+$/NH$_4^+$), via Lewis/Brønsted interactions between the acidic sites of the resin and ammonia, or via physisorption. The heats of ammonia adsorption on resins vary also greatly depending on the material's features. For instance, on sulfonated gel resins, they can reach 110 kJ mol^{-1} [37, 39]. The limited literature available on ammonia adsorption on resins makes it difficult to evaluate the potential of these materials for ammonia removal applications. However, the well-known swelling of gel resins in the presence of water can raise practical issues and limit their applications in gas adsorption.

In the past decade, the field of adsorption has seen the emergence of a new class of materials, called metal–organic frameworks (MOFs) [12, 63, 64]. These compounds are formed by the self-assembly of metal ions, acting as coordination centers, and polyatomic organic bridging ligands [65]. This results in the formation of highly porous crystalline solids [65]. Owing to the diversity of their metallic centers and organic functionalities, one can tailor materials with specific pore shape, size, volume and chemistry [65]. This feature makes these materials prime candidates for applications in gas purification, gas separation or heterogeneous catalysis [66, 67]. Despite the large enthusiasm surrounding the MOFs, only a few research groups started to investigate their use for ammonia removal [41–44]. Moreover, within these few studies, the potential instability of MOFs in presence

of moisture and their weak dispersive forces in the retention of small molecules of gas at ambient conditions represent two issues scarcely addressed in the literature [41, 42].

Considering the above, one can acknowledge that despite many research efforts, the current pathways envisioned to remove ammonia from air suffer from various deficiencies which are summarized below:

- In many studies, the adsorbent is not specifically designed for ammonia removal. One reason for this is that some of the potential uses of a material are envisioned after its synthesis. Consequently, despite its versatility, the adsorbent may not meet the specific requirements of ammonia adsorption.
- Mostly non-specific forces between the targeted gas and the adsorbent surface have been established and studied, despite the fact that those forces do not guarantee a strong/long-term retention [9, 20].
- No in-depth investigation on the possible desorption of the gas with time has been proposed and yet, a gradual release of the adsorbate over time would significantly question the efficiency of the adsorbent.
- The air stream to be purified and the adsorbent itself are most of the time dried before running adsorption tests in order to avoid competitive adsorption between water and ammonia molecules. Nevertheless, the presence of humidity on a large-scale application can be difficult and expensive to avoid.
- Despite the high solubility of ammonia [8], and the likely presence of water in ambient air, only a few studies have looked into the role of humidity on ammonia retention [42, 54] and they do not lead to a comprehensive description of this factor.

Taking into account these shortcomings, additional research efforts and a deeper insight into the design of ammonia adsorbents are required.

References

1. J. C. Thompson, "Compressibility of Metal-Ammonia Solutions," *Physical Review A,* vol. 4, p. 802, 1971.
2. S. E. Manahan, *Environmental chemistry* vol. 8. Boca Raton, FL: CRC Press, 2005.
3. S. V. Krupa, "Effects of atmospheric ammonia (NH_3) on terrestrial vegetation: a review," *Environmental Pollution,* vol. 124, pp. 179–221, 2003.
4. S. Issley. (2009). *Toxicity, ammonia*. Available: http://emedicine.medscape.com/article/820298-overview.
5. N. R. Council, *Air emissions from animal feeding operations: current knowledge, future needs*: National Academies Press, 2003.
6. OSHA. (2003). *Ammonia*. Available: http://www.osha.gov/dts/chemicalsampling/data/CH_218300.html.
7. I. Cotte-Rodriguez, *et al.*, "Analysis of gaseous toxic industrial compounds and chemical warfare agent simulants by atmospheric pressure ionization mass spectrometry," *Analyst,* vol. 131, pp. 579–589, 2006.
8. R. C. Weast and M. J. Astle, *Handbook of Chemistry and Physics*, 62 ed. Boca Raton, FL: CRC Press, 1981.

9. T. J. Bandosz, *Activated carbon surfaces in environmental remediation*. Oxford, UK: Elsevier, 2006.

10. J. Keller and R. Staudt, *Gas adsorption equilibria*. New York: Springer, 2005.

11. P. Atkins and J. Paula, *Physical chemistry*: W.H. Freeman, 2002.

12. P. Wright, *Microporous framework solids*: RSC Publishing, 2008.

13. R. Bansal and M. Goyal, *Activated carbon adsorption*: Taylor & Francis, 2005.

14. J. Helminen, *et al.*, "Adsorption Equilibria of Ammonia Gas on Inorganic and Organic Sorbents at 298.15 K," *Journal of Chemical & Engineering Data*, vol. 46, pp. 391–399, 2001.

15. A. Lapkin, *et al.*, "Preparation and characterisation of chemisorbents based on heteropolyacids supported on synthetic mesoporous carbons and silica," *Catalysis Today*, vol. 81, pp. 611–621, 2003.

16. M. Molina-Sabio, *et al.*, "Adsorption of NH_3 and H_2S on activated carbon and activated carbon-sepiolite pellets," *Carbon*, vol. 42, pp. 448–450, 2004.

17. C. Canals-Batlle, *et al.*, "Carbonaceous adsorbents for NH_3 removal at room temperature," *Carbon*, vol. 46, pp. 176–178, 2008.

18. W. H. Lee and P. J. Reucroft, "Vapor adsorption on coal- and wood-based chemically activated carbons: (III) NH_3 and H_2S adsorption in the low relative pressure range," *Carbon*, vol. 37, pp. 21–26, 1999.

19. M. Domingo-García, *et al.*, "Dynamic adsorption of ammonia on activated carbons measured by flow microcalorimetry," *Applied Catalysis A: General*, vol. 233, pp. 141–150, 2002.

20. F. Stoeckli, *et al.*, "Specific and non-specific interactions between ammonia and activated carbons," *Carbon*, vol. 42, pp. 1619–1624, 2004.

21. K. Kaneko, *et al.*, "Microporosity and adsorption characteristics against NO, SO_2, and NH_3 of pitch-based activated carbon fibers," *Carbon*, vol. 26, pp. 327–332, 1988.

22. K. Okada, *et al.*, "Adsorption properties of activated carbon from waste newspaper prepared by chemical and physical activation," *Journal of Colloid and Interface Science*, vol. 262, pp. 194–199, 2003.

23. S.-J. Park and B.-J. Kim, "Ammonia removal of activated carbon fibers produced by oxyfluorination," *Journal of Colloid and Interface Science*, vol. 291, pp. 597–599, 2005.

24. L. F. Herrera, *et al.*, "Comparative simulation study of nitrogen and ammonia adsorption on graphitized and nongraphitized carbon blacks," *Journal of Colloid and Interface Science*, vol. 320, pp. 415–422, 2008.

25. C.-C. Huang, *et al.*, "Effect of surface acidic oxides of activated carbon on adsorption of ammonia," *Journal of Hazardous Materials*, vol. 159, pp. 523–527, 2008.

26. B.-J. Kim and S.-J. Park, "Effects of carbonyl group formation on ammonia adsorption of porous carbon surfaces," *Journal of Colloid and Interface Science*, vol. 311, pp. 311–314, 2007.

27. H. Fortier, *et al.*, "Ammonia, cyclohexane, nitrogen and water adsorption capacities of an activated carbon impregnated with increasing amounts of $ZnCl_2$, and designed to chemisorb gaseous NH_3 from an air stream," *Journal of Colloid and Interface Science*, vol. 320, pp. 423–435, 2008.

28. B. Ducourty, *et al.*, "Processes of ammonia adsorption in gallium zeolites as studied by microcalorimetry," *Thermochimica Acta*, vol. 312, pp. 27–32, 1998.

29. W. Shen, *et al.*, "Surface chemistry of pyrolyzed starch carbons on adsorption of ammonia and carbon disulfide," *Colloids and Surfaces A: Physicochemical and Engineering Aspects*, vol. 356, pp. 16–20, 2010.

30. M. P. Bernal and J. M. Lopez-Real, "Natural zeolites and sepiolite as ammonium and ammonia adsorbent materials," *Bioresource Technology*, vol. 43, pp. 27–33, 1993.

31. J. Valyon, *et al.*, "Study of the Dynamics of NH_3 Adsorption in ZSM-5 Zeolites and the Acidity of the Sorption Sites Using the Frequency-Response Technique," *The Journal of Physical Chemistry B*, vol. 102, pp. 8994–9001, 1998.

32. S. Kuo, *et al.*, "Analysis of ammonia adsorption on silica gel using the modified potential theory," *Journal of Chemical & Engineering Data*, vol. 30, pp. 330–332, 1985.

33. G. P. Holland, *et al*., "15 N Solid-State NMR Characterization of Ammonia Adsorption Environments in 3A Zeolite Molecular Sieves," *The Journal of Physical Chemistry B,* vol. 108, pp. 16420–16426, 2004.

34. H. Kosslick, *et al*., "Acidity of substituted MCM-41-type mesoporous silicates probed by ammonia," *Journal of the Chemical Society, Faraday Transactions,* vol. 93, pp. 1849–1854, 1997.

35. S. G. Izmailova, *et al*., "Adsorption of Methanol, Ammonia and Water on the Zeolite-Like Aluminophosphates AlPO4-5, AlPO4-17, and AlPO4-18," *Journal of Colloid and Interface Science,* vol. 179, pp. 374–379, 1996.

36. I. Mishin, *et al*., "Heats of Adsorption of Ammonia and Correlation of Activity and Acidity in Heterogeneous Catalysis," *Adsorption,* vol. 11, pp. 415–424, 2005.

37. M. Hart, *et al*., "Sulfonated poly(styrene-co-divinylbenzene) ion-exchange resins: acidities and catalytic activities in aqueous reactions," *Journal of Molecular Catalysis A: Chemical,* vol. 182–183, pp. 439–445, 2002.

38. C. N. Rhodes, *et al*., "Sulphonated polystyrene resins: acidities and catalytic activities," *Reactive and Functional Polymers,* vol. 40, pp. 187–193, 1999.

39. D. R. Brown and C. N. Rhodes, "A new technique for measuring surface acidity by ammonia adsorption," *Thermochimica Acta,* vol. 294, pp. 33–37, 1997.

40. S. Bodoardo, *et al*., "Ammonia interaction and reaction with Al-pillared montmorillonite: an IR study," *Microporous and Mesoporous Materials,* vol. 20, pp. 187–196, 1998.

41. D. Saha and S. Deng, "Ammonia adsorption and its effects on framework stability of MOF-5 and MOF-177," *Journal of Colloid and Interface Science,* vol. 348, pp. 615–620, 2010.

42. G. W. Peterson, *et al*., "Ammonia Vapor Removal by $Cu_3(BTC)_2$ and Its Characterization by MAS NMR," *The Journal of Physical Chemistry C,* vol. 113, pp. 13906–13917, 2009.

43. C. J. Doonan, *et al*., "Exceptional ammonia uptake by a covalent organic framework," *Nat Chem,* vol. 2, pp. 235–238, 2010.

44. D. Britt, *et al*., "Metal-organic frameworks with high capacity and selectivity for harmful gases," *Proceedings of the National Academy of Sciences,* vol. 105, pp. 11623–11627, August 19, 2008.

45. F. Xie, *et al*., "Microcalorimetric study of acid sites on ammonia- and acid-pretreated activated carbon," *Carbon,* vol. 38, pp. 691–700, 2000.

46. J. Guo, *et al*., "Adsorption of NH_3 onto activated carbon prepared from palm shells impregnated with H_2SO_4," *Journal of Colloid and Interface Science,* vol. 281, pp. 285–290, 2005.

47. C. C. Rodrigues, *et al*., "Ammonia adsorption in a fixed bed of activated carbon," *Bioresource Technology,* vol. 98, pp. 886–891, 2007.

48. W. B. Spencer, *et al*., "Further Studies of Adsorption on Graphitized Carbon Blacks," *The Journal of Physical Chemistry,* vol. 62, pp. 719–723, 1958.

49. R. A. Beebe and R. M. Dell, "Heats of Adsorption of Polar Molecules on Carbon Surfaces. I. Sulfur Dioxide," *The Journal of Physical Chemistry,* vol. 59, pp. 746–754, 1955.

50. R. L. Gale and R. A. Beebe, "Determination of Heats of Adsorption on Carbon Blacks and Bone Mineral by Chromatography Using the Eluted Pulse Technique," *The Journal of Physical Chemistry,* vol. 68, pp. 555–567, 1964.

51. R. B. Anderson and P. H. Emmett, "Surface Complexes on Carbon Blacks. II. The Adsorption of NH_3, C_2H_2, C_4H_{10}, CH_3NH_2 and Water Vapor," *The Journal of Physical Chemistry,* vol. 56, pp. 756–761, 1952.

52. H. Ulbricht, *et al*., "Thermal desorption of gases and solvents from graphite and carbon nanotube surfaces," *Carbon,* vol. 44, pp. 2931–2942, 2006.

53. C. L. Mangun, *et al*., "Oxidation of Activated Carbon Fibers: Effect on Pore Size, Surface Chemistry, and Adsorption Properties," *Chemistry of Materials,* vol. 11, pp. 3476–3483, 1999.

54. L. M. Le Leuch and T. J. Bandosz, "The role of water and surface acidity on the reactive adsorption of ammonia on modified activated carbons," *Carbon,* vol. 45, pp. 568–578, 2007.

55. C. L. Mangun, *et al.*, "Fixed Bed Adsorption of Acetone and Ammonia onto Oxidized Activated Carbon Fibers," *Industrial & Engineering Chemistry Research,* vol. 38, pp. 3499–3504, 1999.
56. S.-J. Park and K.-D. Kim, "Adsorption Behaviors of CO_2 and NH_3 on Chemically Surface-Treated Activated Carbons," *Journal of Colloid and Interface Science,* vol. 212, pp. 186–189, 1999.
57. H. Tamon and M. Okazaki, "Influence of acidic surface oxides of activated carbon on gas adsorption characteristics," *Carbon,* vol. 34, pp. 741–746, 1996.
58. A. Goldoni, *et al.*, "Single-Wall Carbon Nanotube Interaction with Gases: Sample Contaminants and Environmental Monitoring," *Journal of the American Chemical Society,* vol. 125, pp. 11329–11333, 2003.
59. F. Picaud, *et al.*, "A comparative study of single- and multiwalled carbon nanotube sensitivity to ammonia," *Journal of Applied Physics,* vol. 105, pp. 014315–014315-5, 2009.
60. A. Auroux, "Microcalorimetry Methods to Study the Acidity and Reactivity of Zeolites, Pillared Clays and Mesoporous Materials," *Topics in Catalysis,* vol. 19, pp. 205–213, 2002.
61. M. J. Meziani, *et al.*, "Number and Strength of Surface Acidic Sites on Porous Aluminosilicates of the MCM-41 Type Inferred from a Combined Microcalorimetric and Adsorption Study," *Langmuir,* vol. 16, pp. 2262–2268, 2000.
62. J. Pires, *et al.*, "Assessment of Hydrophobic-Hydrophilic Properties of Microporous Materials from Water Adsorption Isotherms," *Adsorption,* vol. 9, pp. 303–309, 2003.
63. J.-R. Li, *et al.*, "Selective gas adsorption and separation in metal-organic frameworks," *Chemical Society Reviews,* vol. 38, pp. 1477–1504, 2009.
64. G. Ferey, "Hybrid porous solids: past, present, future," *Chemical Society Reviews,* vol. 37, pp. 191–214, 2008.
65. S. L. James, "Metal-organic frameworks," *Chemical Society Reviews,* vol. 32, pp. 276–288, 2003.
66. A. U. Czaja, *et al.*, "Industrial applications of metal-organic frameworks," *Chemical Society Reviews,* vol. 38, pp. 1284–1293, 2009.
67. U. Müller, *et al.*, *Chemistry and Applications of Porous Metal–Organic Frameworks*: Wiley-VCH Verlag GmbH & Co. KGaA, 2008.

Chapter 2
Objectives and Research Approach

Considering the above-mentioned issues, our goal is to identify the key parameters enhancing the adsorption of ammonia and thus enable the design of efficient ammonia adsorbents adapted to real-life conditions. In other words, the adsorbent performance must be increased compared to those reported in the literature. The retention of ammonia must be strong so that no desorption of the gas occurs overtime. And finally, the adsorbent must be able to adsorb and retain ammonia at room temperature over a wide range of humidity levels to ensure its industrial sustainability.

To "built the ideal ammonia adsorbent", one has to consider the two main conditions for the good adsorption and sustainable retention of ammonia on solid surfaces and try meet these requirements. One of them is related to physisorption and implies the use of an adsorbent with very small pores, similar in size to that of ammonia molecule. This enhances the physical forces between the pores walls and the molecules to be adsorbed. A second condition is the involvement of chemical transformations (reactive adsorption) of ammonia. Considering the chemistry of this molecule, reactions such as hydrogen bonding, acid–base reactions, and complexation can be envisioned.

The research approach proposed in this study to achieve the above objectives is summarized as follows:

- Synthesis of various materials with porosity and surface chemistry features expected to enhance the strong adsorption of ammonia under ambient conditions.
- Test of the materials prepared for ammonia removal in dynamic conditions, at room temperature, in dry and moist conditions (to assess the potential of the materials for practical applications).
- Study of the strength of ammonia retention.
- Characterization of the adsorbents (textural parameters, porosity and surface chemistry) by various techniques before and after ammonia adsorption.
- Identification of the factors influencing ammonia uptake.
- Proposal of the mechanisms of ammonia retention.

The findings obtained considering this research approach are presented in the following chapters. In Chap. 3, the preparation of the materials tested is described as well as the techniques used to characterize them and to test them for ammonia adsorption. Chapter 4 provides an overview of the materials performance for ammonia removal in terms of adsorption capacity and strength of retention. The role of textural parameters, surface chemistry and moisture is presented in detail in Chap. 5, Chap. 6 and Chap. 7, respectively. A summary on the different mechanisms of ammonia adsorption/retention can be found in Chap. 8. Finally, Chap. 9 offers a conclusion on this research project while Chap. 10 suggests some new paths for future research on ammonia removal from air.

Chapter 3
Materials and Methods

3.1 Materials

3.1.1 Activated Carbons

A first series of samples was prepared by carbonization of different polymers with or without a subsequent oxidation treatment.

In a second series of synthesis, commercial activated carbons were modified with different inorganic chemical compounds. The main step of the modification method involved incipient wetness impregnation followed by an overnight air-drying at 120 °C, overnight. The incipient wetness impregnation consists in adding to the carbon a volume of impregnate solution equal to the adsorbent pore volume.

3.1.1.1 Polymer-Based Activated Carbons

Two series of polymer-based carbons were prepared. The polymer precursors for these two series were poly(4-styrene sulfonic acid co-maleic acid), sodium salt and poly(sodium 4-styrene sulfonate) (Fig. 3.1).

Carbon samples were obtained according to the method described in [1, 2]. Briefly, both polymers were carbonized for 40 min at 800 °C (heating rate of 50 °C min^{-1}) under nitrogen (flow of 300 mL min^{-1}), in a horizontal furnace. The samples were subsequently washed in a Soxhlet extractor with deionized water to remove the excess of water-soluble species. Finally, the samples were dried in air at 120 °C for 24 h. The two resulting carbons are referred to as CP-1 (obtained from poly(4-styrene sulfonic acid co-maleic acid)), and CP-2 (obtained from poly(sodium 4-styrene sulfonate)). "C" stands for "carbon" and "P" for "polymer-based".

poly(4-styrene sulfonic acid co-maleic acid)   poly(sodium 4-styrene sulfonate)
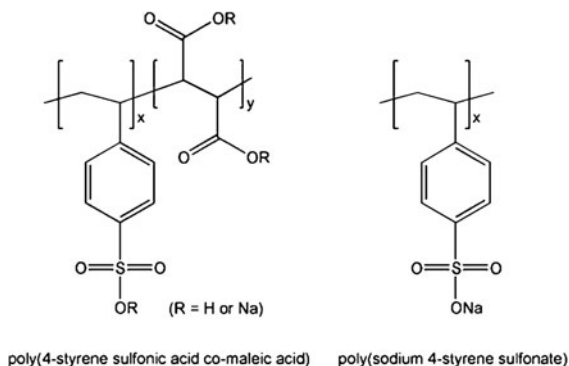
Fig. 3.1 Polymer precursors used for the preparation of activated carbons

CP-1 and CP-2 were then subjected to two different oxidation treatments. In the first oxidation method, CP-1 and CP-2 (10 g) were stirred for 18 h with a saturated solution of ammonium persulfate in sulfuric acid (1 M, 100 mL) [2, 3]. Then, the carbons were washed in a Soxhlet apparatus with deionized water to remove the excess of oxidizing agents and other salts. Finally, the samples were dried in air at 120 °C for 24 h. The resulting materials are referred to as CP-1A and CP-2A, depending on the carbon precursor. In the second type of oxidation, CP-1 and CP-2 were heated at 350 °C (heating rate of 50 °C min^{-1}) for 6 h, in air, in a horizontal furnace. The resulting materials are referred to as CP-1B and CP-2B, depending on the carbon precursor.

3.1.1.2 Activated Carbons Modified with Metal Chlorides

A coal-based activated carbon, BPL (Calgon Carbon Corporation), was modified by impregnation with a solution of either zinc chloride or copper chloride [4]. In the case of copper chloride, two different amounts of metal (5 and 10 wt%) were used. The virgin and modified samples are referred to as: CC, CC-Zn (10 wt%), CC-Cu1 (5 wt%) and CC-Cu2 (10 wt%), respectively. The first "C" stands for "carbon" and the second one for "coal-based".

3.1.1.3 Activated Carbons Modified with Metal Oxides

A wood-based activated carbon, BAX-1500 (Westvaco) was modified with vanadium and molybdenum oxides [5, 6]. Solutions of ammonium vanadate (NH_4VO_3) and ammonium molybdate (($NH_4)_6Mo_7O_{24}\cdot4H_2O$) were used for this impregnation. After drying, the samples were heated at 500 °C under a flow of nitrogen for 3 h, to initiate the release of ammonia and water, and the formation of

V_2O_5, or MoO_3, depending on the impregnate solution. In the case of ammonium molybdate, two different amounts of molybdenum (5 and 10 wt%) were used. The virgin and modified samples are referred to as: CW, CW-V (5 wt%), CC-Mo1 (5 wt%) and CC-Mo2 (10 wt%), respectively. "C" stands for "carbon" and "W" for "wood-based".

In another series of experiments, a coconut shell-based carbon, S208c (Calgon Carbon Corporation), was modified with molybdenum oxide following the same procedure as for BAX-1500 [7]. Like the wood-based carbon, two different amounts of molybdenum were used (5 and 10 wt%). The virgin carbon is referred to as CS and the modified samples as CS-Mo1 and CS-Mo2. "C" stands for "carbon" and "S" for "shell-based".

3.1.1.4 Activated Carbons Modified with Polycations

The wood-based carbon, BAX-1500, was impregnated with hydroxyaluminium and hydroxyaluminium-zirconium polycations [8, 9]. Those polycations were formed upon aging solutions of Chlorhydrol® ($Al_2(OH)_5Cl \cdot 2.5H_2O$) and Rezal® ($Al_{1.2}Zr_{0.3}Cl \cdot 5H_2O$), respectively (Reheis Chemical Company). The formula of the first polycation is $[Al_{13}O_4(OH)_{24}(H_2O)_{12}]^{7+}$ and it has a Keggin Al_{13} unit structure [10]. The derived samples are referred to as CW-Al (from Chlorhydrol) and CW-Zr (from Rezal). Part of CW-Zr sample was then calcined in air for 3 h, leading to CW-Zr-c sample.

3.1.2 Graphite Oxide

Two Graphite Oxide (GO) samples were prepared following two different oxidation methods of graphite called the Hummers [11] and Brodie methods [12]. They both involve the oxidation of graphite but differ in the oxidizing agents used for the treatment. This results in materials of different surface chemistry. When the method of GO preparation is not specified in the name of the sample, it is implied that the sample was prepared via the Hummers method.

3.1.2.1 GO Prepared by the Hummers Method

A commercial graphite powder (Sigma-Aldrich, 10 g) was stirred in concentrated sulfuric acid (230 mL, 0 °C). Potassium permanganate (30 g) was slowly added to the suspension. The rate of addition was controlled to prevent the rapid rise in the temperature of the suspension (should be less than 20 °C). The reaction mixture was then cooled to 2 °C. After removal of the ice bath, the mixture was stirred at room temperature for 30 min. Distilled water (230 mL) was slowly added to the

reaction vessel, keeping the temperature less than 98 °C. The diluted suspension was stirred for an additional 15 min and further diluted with distilled water (1.4 L) and then hydrogen peroxide (100 mL, 30 wt% solution) was added. The mixture was left overnight. GO particles settled at the bottom were separated from the excess liquid by decantation. The remaining suspension was transferred to dialysis tubes (MW cutoff 6,000–9,000). Dialysis was carried out until no more precipitate of $BaSO_4$ was detected by addition of an aqueous solution of $BaCl_2$. Then, the wet form of graphite oxide was separated by centrifugation. The gel-like material was freeze-dried and a fine dark brown powder of the initial graphite oxide was obtained. The resulting material is referred to as GO-H.

3.1.2.2 GO Prepared by the Brodie Method

In this method, a commercial graphite powder (Sigma-Aldrich, 10 g) was thoroughly mixed with potassium chlorate (50 g) in a flask placed into an ice bath. Then, fuming nitric acid (100 mL) was slowly added to liquefy the mixture. After removal of the ice bath, the mixture was left at room temperature for 24 h. Another portion of nitric acid (60 mL) was then added to the reaction vessel. Following this, the slurry was placed in a water bath at 60 °C for 4 days (until no more emission of yellow vapors) and further diluted to 6 L. Then, the GO particles settled at the bottom were separated from the excess liquid by decantation and washed with distilled water until all acids and salts were removed. The wet form of GO was centrifuged and the resulting material was freeze-dried. The fine brown powder obtained is referred to as GO-B.

3.1.3 Metal-Organic Frameworks

Two metal organic frameworks (MOFs) with different metal and organic components were synthesized.

3.1.3.1 Zinc-Based MOF

A zinc-based MOFs was prepared by mixing zinc nitrate hexahydrate (10.4 g) and 1,4 benzenedicarboxylate (2 g) in N,N dimethylformamide (DMF, 140 mL) until complete dissolution of the solids. Then, the mixture was transferred to a round flask connected to a condenser and heated at 115–120 °C for 24 h. After cooling, the supernate was removed and crystals deposited on the bottom of the flask were collected, washed with DMF and immersed in fresh chloroform overnight. Chloroform was changed twice during two days. Crystals were collected after filtration and washing with chloroform. Drying was then performed by heating the crystals

Fig. 3.2 Representation of
MOF-5 unit
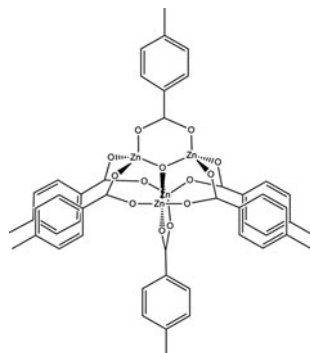
at 130–135 °C for 6 h inside a closed filtering flask connected to an aspirator. The aspirator was used to create a vacuum inside the flask. The resulting product was kept in a desiccator and is referred to as MOF-5. A representations of MOF-5 is shown in Fig. 3.2 and other schematics of its structure can be found in [13–15].

3.1.3.2 Copper-Based MOF

A copper-based MOF was prepared by mixing copper nitrate hemipentahydrate (10 g) and 1,3,5 benzenetricarboxylic acid (5 g) in N,N dimethylformamide (DMF, 85 mL) followed by stirring and sonication for 5 min. Ethanol (85 mL) was then added to the mixture, which was then stirred and sonicated for 5 min. Finally, deionized water (85 mL) was added to the mixture and then stirring and sonication for 30 min were carried out. All crystals were dissolved at this point. Then, the mixture was transferred to a round bottom flask (500 mL) and heated at 85 °C in an oil bath for 21 h under shaking (intensely for the first 4 h, and then the shaking was reduced and finally stopped after 20 h). After cooling, the crystals were filtered using a Büchner funnel, washed and immersed in dichloromethane. Dichloromethane was changed twice during three days. The crystals were collected after filtration and washing with dichloromethane. Drying was then performed by heating the crystals at 170 °C for 28 h inside a closed filtering flask connected to an aspirator. The aspirator was used to create a vacuum inside the flask. The resulting product was kept in a desiccator and is referred to as HKUST-1. A representations of HKUST-1 is shown in Fig. 3.3 and other schematics of its structure can be found in [13] and [16].

3.1.4 Graphite Oxide-Based Composites

Three types of composite were prepared. They differ in the component/substrate used to form the materials in addition to GO.
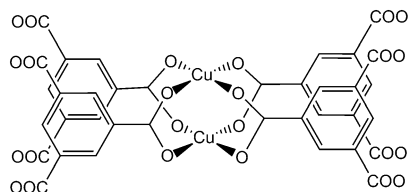
3.1.4.1 Composites of GO and Polyoxometalates

The composites were formed by mixing GO-H (Sect. 3.1.2) with a polymeric
solution and then polyoxometalates (POMs) species [17–19]. More precisely,
GO-H was first dispersed in a diluted solution of $NaNO_3$ (0.01 M) and soni-
cated for 10 min. A few drops of concentrated NaOH (3 M) were then added to
the suspension to reach a pH value related to a proper cation exchange capacity
(CEC) (pH = 6). This is because the pH, the electrolyte type and concentration
of the solution used to disperse GO-H have a significant influence on its surface
charge [20]. The CEC is calculated from the proton binding curve. The
suspension was further sonicated for 50 min. Then a solution of poly(diallyl-
dimethylammonium chloride) (PDDA) (20 wt% in water—Sigma-Aldrich) was
added to the GO-H aqueous suspension under vigorous stirring. The volume of
the polymer solution was chosen to get a charge ratio 1:1 compared to the CEC
value. The mixture was sonicated for 2 h, centrifuged and washed with distilled
water. The obtained wet material was then dispersed in an aqueous solution of
POMs being either hydrated phosphotungstic acid ($H_3PW_{12}O_{40}$) or phospho-
molybdic acid ($H_3PMo_{12}O_{40}$). The amount of acid added was chosen to get a
charge ratio 1:3 (POM/H in GO) compared to the CEC value of GO-H. The
mixture was then centrifuged, and the obtained material was dried in air at
60 °C for 3 days to favor a restacking of the layers [19]. The final materials are
referred to as either GP-W or GP-Mo, depending on the type of POM used.
"G" stands for "graphite oxide" and "P" for "polyoxometalate". Figure 3.4
shows the polymer used to prepare the materials. The structure of the POMs is
similar to that of the polycations used to prepare CW-Al and CW-Zr samples
(Keggin Al_{13} structure) [21, 22].

3.1.4.2 Composites of GO and Zinc-Based Metal–Organic Frameworks

The composites were prepared by dispersing GO-H powder (Sect. 3.1.2) in the
precursors and solvent mixture used to prepare MOF-5 (Sect. 3.1.3). The resulting
suspension was subsequently stirred and subjected to the same synthesis procedure
as for MOF-5 (Sect. 3.1.3). The added GO-H consisted of 5, 10, 20 and 55 wt% of
the final material weight [23]. The composites are referred to as GM-Zn*n* with
n = 1, 2, 3 and 4 for the different GO contents. "G" stands for "graphite oxide"
and "M" for "metal–organic framework".

Fig. 3.4 Polymer used to prepare the composites
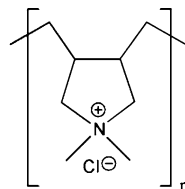
3.1.4.3 Composites of GO and Copper-Based Metal–Organic Frameworks

The composites were prepared by dispersing GO-H powder (Sect. 3.1.2) in the precursors and solvent mixture used to prepare HKUST-1 (Sect. 3.1.3). The resulting suspension was stirred for 5 min, sonicated for another 30 min and then subjected to the same synthesis procedure as for HKUST-1 (Sect. 3.1.3). The added GO consisted of 5, 9, 18, 38 and 46 wt% of the final material weight [24]. The composites are referred to as GM-Cun with $n = 1, 2, 3, 4$ and 5, for the different GO-H contents. "G" stands for "graphite oxide" and "M" for "metal–organic framework".

3.1.5 Resins

Two sulfonated resins were tested for ammonia adsorption. One, referred to as R1, was supplied by Purolite (MN200) and the other one, referred to as R2, was provided by Professor Alexandratos (Hunter College, The City University of New York).

3.2 Methods

3.2.1 Ammonia Breakthrough and Desorption Test

The breakthrough capacity of the different materials prepared for removal of ammonia was assessed by carrying out dynamic tests at room temperature. In this process, a flow of ammonia diluted in air went through a fixed bed of an adsorbent sample. The adsorbent bed contained the adsorbent packed into a glass column. Ammonia concentration in the inlet stream was 1000 ppm. Ammonia concentration in the outlet stream was measured using an electrochemical sensor (Multi-Gas Monitor ITX system). Breakthrough tests were arbitrarily stopped when ammonia concentration reached 100 ppm (10% of the feed) and were immediately followed by the desorption tests. The latter tests were performed by purging the bed with air only. The breakthrough capacity of each sample was then calculated using Eqs. 1.1 and 1.2 provided in Chap. 1 (Sect. 1.2). To evaluate the influence of water, the experiments were performed with a flow of ammonia gas diluted either

Table 3.1 The parameters of the breakthrough experiments

Sample	Bed		Flow rate	
	Volume (cm³)	Adsorbent's particle size	Total (mL min⁻¹)	Ammonia (mL min⁻¹)
Polymer-based carbons	2	Powder	450	90
Modified activated carbons	6	1–2 mm	900 or 450[a]	180 or 90[b]
Graphite oxides	2	Powder	450 or 225	90 or 45
Copper-based metal–organic framework	2	Powder (mixed with glass beads)	225	45
Zinc-based metal–organic framework	2	Powder	450	180
Graphite oxide/Polyoxometalates composites	2	Powder	450	90
Copper-based graphite oxide/metal–organic frameworks composites	2	Powder (mixed with glass beads)	225	45
Zinc-based graphite oxide/metal–organic frameworks composites	2	Powder	450	90
Resins	2	Beads	450	90

[a] 900 mL min⁻¹ for the carbon modified with metal chlorides and 450 mL min⁻¹ for the others
[b] 180 mL min⁻¹ for the carbon modified with metal chlorides and 90 mL min⁻¹ for the others

in dry air (-ED) or in moist air (70% humidity) (-EM). The latter experiments were also performed after prehumification of the samples (2 h, 70% humidity). The suffix -EPD or -EPM is then added to the resulting exhausted samples.

It has to be noted that the bed preparation and flow rates may differ from one sample to another. Details on these parameters are provided in Table 3.1. A schematic of the experimental set up used to perform the breakthrough tests is proposed in Fig. 3.5.

3.2.2 Nitrogen Sorption

Nitrogen sorption analyses were performed to evaluate the porosity and surface area of the materials. The isotherms were obtained at $-196\ °C$ using an ASAP 20 (Micromeritics). Prior to each measurement, samples were outgassed at 120 °C. The apparent surface area, S_{BET} (BET method), the total volume of pores, V_{tot} (calculated from the volume of nitrogen adsorbed at $P/P_0 = 0.985$), the microporous volume, V_{mic} (calculated by the Dubinin–Radushkevitch method [25]) and the volume of mesopores, V_{meso} (calculated as the difference between V_t and V_{mic}) were determined from the isotherms. Pore size distributions (PSDs) were obtained using the density functional theory method (DFT) described elsewhere [26].
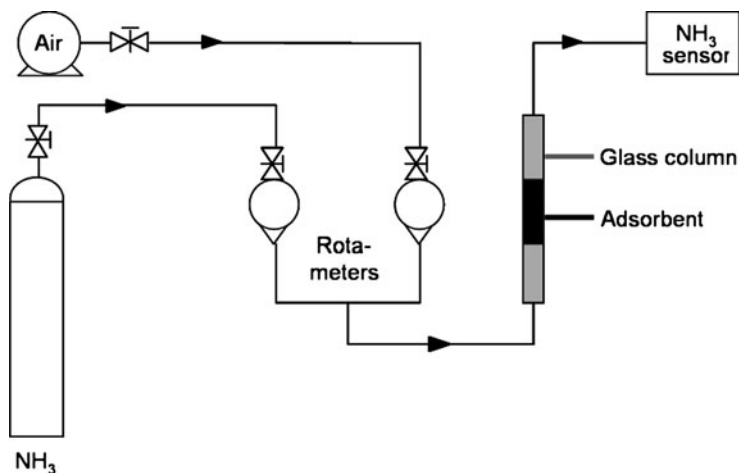
Fig. 3.5 Schematic of the experimental set up for ammonia breakthrough tests

3.2.3 Thermogravimetric Analysis

Thermogravimetric (TG) curves and their derivatives (DTG) were obtained using a TA Instrument thermal analyzer. The samples were heated up to 1000 °C with the heating rate 10 deg min^{-1} under a flow of nitrogen of 100 mL min^{-1}.

3.2.4 Surface pH Measurement

The surface pH of the samples was determined after an overnight stirring of a solution containing the sample powder and deionized water (ratio 1:50. e.g. 0.1 g of material in 5 mL of water).

3.2.5 Potentiometric Titration

Potentiometric titration provides an indication of the strength and number of functional groups present on the materials. The measurements were performed with a DMS Titrino 716 automatic titrator (Metrohm). The instrument was set at the mode when the equilibrium pH was collected. Samples (about 50–100 mg) were placed in a container, dispersed in $NaNO_3$ (0.01 M, 50 mL) and equilibrated overnight with the electrolyte solution. Prior to the titration with NaOH (0.1 M), the suspension was acidified to a pH of 3.20 or below by addition of HCl (0.1 M).

The titration was performed in the pH range 3–10, with constant stirring and continuous saturation with nitrogen to eliminate the influence of atmospheric CO_2.

The surface properties were evaluated using potentiometric titration experiments [27, 28]. Here, it is assumed that the population of sites can be described by a continuous pK_a distribution, $f(pK_a)$. The experimental data can be transformed into a proton binding isotherm, Q, representing the total amount of protonated sites, which is related to the pK_a distribution by the following integral Eq. 3.3.

$$Q(pH) = \int\limits_{-\infty}^{+\infty} q(pH, pK_a)f(pK_a)dpK_a \qquad (3.3)$$

The solution of this equation is obtained using the numerical procedure [27, 28], which applies regularization combined with non-negativity constraints. Based on the spectrum of acidity constants and the history of the samples, the detailed surface chemistry can be evaluated.

3.2.6 Fourier Transform Infrared Spectroscopy

Fourier Transform infrared spectroscopy (FT-IR) spectra were obtained using a Nicolet Magna-IR 830 spectrometer in the attenuated total reflectance mode (ATR). Spectra were collected 16 times and corrected for the background noise. The experiments were done on the powdered samples, without KBr addition.

3.2.7 Elemental Analysis

Carbon, nitrogen, sulfur and hydrogen contents of the two initial GOs were analyzed by Galbraith laboratories. The oxygen content was derived as a difference to 100%.

3.2.8 X-ray Diffraction Spectroscopy

X-ray diffraction spectroscopy (XRD) measurements were conducted using a standard powder diffraction procedure. Samples were ground in a small agate mortar and a few drops of solvent were added (ethanol, methanol or dimethylformamide). The mixture was smear-mounted onto a glass slide and allowed to air-dry. Samples were analyzed by Cu $_{K\alpha}$ radiation generated in a Philips XRG 300 (activated carbon modified with metal chlorides) or a Philips X'Pert (all other samples) X-ray diffractometer. A diffraction experiment was run on standard glass slide for the background correction.

3.2.9 X-ray Photoelectron Spectroscopy

Identification of the elements present in the sample studies as well as their chemical state was obtained by X-ray photoelectron spectroscopy (XPS). These analyses were performed by Evans Analytical Group laboratories with a PHI 5701 LSci instrument, a monochrome Al K_α source (1486.6 eV) and an analysis area of about 2.0×0.8 mm.

3.2.10 Energy Dispersive X-ray Spectroscopy

Energy dispersive X-ray spectroscopy (EDX) was conducted on a Zeiss Supra 55 instrument. The instrument has a resolution of 5 nm at 30 kV. Analyses were performed on a sample powder previously dried and sputter coated with a thin layer of gold to avoid charging. From EDX analyses, the content of elements on the surface was calculated and the maps of the elements derived.

3.2.11 Scanning Electron Microscopy

Scanning electron microscopy (SEM) was performed on a Zeiss Supra 55 instrument. The instrument has a resolution of 5 nm at 30 kV. Scanning was performed on a sample powder previously dried. For some samples, a sputter coating with a thin layer of gold or carbon was performed to avoid charging.

3.2.12 Transmission Electron Microscopy

High resolution transmission electron microscopy (HRTEM) was performed on a JEOL 2100F instrument with an accelerating voltage of 200 kV. Analyses were conducted on the powdered samples previously dispersed in N, N dimethylform-amide and then deposited on copper grids.

References

1. D. Hines, *et al*., "Surface Properties of Porous CarbonCarbon Obtained from Polystyrene Sulfonic Acid-Based Organic Salts," *Langmuir,* vol. 20, pp. 3388–3397, 2004.
2. C. Petit, *et al*., "The role of sulfur-containing groups in ammonia retention on activated carbons," *Carbon,* vol. 48, pp. 654–667, 2010.

3. I. I. Salame and T. J. Bandosz, "Study of Water Adsorption on Activated Carbons with Different Degrees of Surface Oxidation," *Journal of Colloid and Interface Science,* vol. 210, pp. 367–374, 1999.

4. C. Petit, *et al.*, "Interactions of Ammonia with the Surface of Microporous Carbon Impregnated with Transition Metal Chlorides," *The Journal of Physical Chemistry C,* vol. 111, pp. 12705–12714, 2007.

5. C. Petit and T. J. Bandosz, "Complexity of ammonia interactions on activated carbons modified with V_2O_5," *Journal of Colloid and Interface Science,* vol. 325, pp. 301–308, 2008.

6. C. Petit and T. J. Bandosz, "Role of surface heterogeneity in the removal of ammonia from air on micro/mesoporous activated carbons modified with molybdenum and tungtsen oxides," *Microporous and Mesoporous Materials,* vol. 118, pp. 61–67, 2009.

7. C. Petit and T. J. Bandosz, "Removal of Ammonia from Air on Molybdenum and Tungsten Oxide Modified Activated Carbons," *Environmental Science & Technology,* vol. 42, pp. 3033–3039, 2008.

8. C. Petit and T. J. Bandosz, "Role of Aluminum Oxycations in Retention of Ammonia on Modified Activated Carbons," *The Journal of Physical Chemistry C,* vol. 111, pp. 16445–16452, 2007.

9. C. Petit and T. J. Bandosz, "Activated carbons modified with aluminium-zirconium polycations as adsorbents for ammonia," *Microporous and Mesoporous Materials,* vol. 114, pp. 137–147, 2008.

10. T. J. Bandosz, *et al.*, "Surface acidity of pillared taeniolites in terms of their proton affinity distributions," *The Journal of Physical Chemistry,* vol. 99, pp. 13522–13527, 1995.

11. W. S. Hummers and R. E. Offeman, "Preparation of Graphitic Oxide," *Journal of the American Chemical Society,* vol. 80, pp. 1339–1339, 1958.

12. M. B. C. Brodie, "Sur le poids atomique du graphite," *Ann. Chim. Phys.,* vol. 59, pp. 466–472, 1860.

13. U. Mueller, *et al.*, "Metal-organic frameworks-prospective industrial applications," *Journal of Materials Chemistry,* vol. 16, pp. 626–636, 2006.

14. O. M. Yaghi, *et al.*, "Reticular synthesis and the design of new materials," *Nature,* vol. 423, pp. 705–714, 2003.

15. O. M. Yaghi. *MOF-5 network.* Available: http://yaghi.chem.ucla.edu/gallery/photo?photo_id=10454.

16. S. S.-Y. Chui, *et al.*, "A Chemically Functionalizable Nanoporous Material [$Cu_3(TMA)_2(H_2O)_3]_n$]," *Science,* vol. 283, pp. 1148–1150, 1999.

17. T. Cassagneau, *et al.*, "Preparation and Characterization of Ultrathin Films Layer-by-Layer Self-Assembled from Graphite Oxide Nanoplatelets and Polymers," *Langmuir,* vol. 16, pp. 7318–7324, 2000.

18. Y. Song, *et al.*, "Synthesis of polyoxometalates-functionalized carbon nanotubes composites and relevant electrochemical properties study," *Materials Research Bulletin,* vol. 42, pp. 1485–1491, 2007.

19. Z.-H. Liu, *et al.*, "Intercalation of Organic Ammonium Ions into Layered Graphite Oxide," *Langmuir,* vol. 18, pp. 4926–4932, 2002.

20. T. Szabó, *et al.*, "Enhanced acidity and pH-dependent surface charge characterization of successively oxidized graphite oxides," *Carbon,* vol. 44, pp. 537–545, 2006.

21. M. J. Janik, *et al.*, "A computational and experimental study of anhydrous phosphotungstic acid and its interaction with water molecules," *Applied Catalysis A: General,* vol. 256, pp. 51–68, 2003.

22. Wkipedia. *Phosphotungstic acid.* Available: http://en.wikipedia.org/wiki/Phosphotungstic_acid.

23. C. Petit and T. J. Bandosz, "MOF–Graphite Oxide Composites: Combining the Uniqueness of Graphene Layers and Metal–Organic Frameworks," *Advanced Materials,* vol. 21, pp. 4753–4757, 2009.

24. C. Petit and T. J. Bandosz, "The synthesis and characterization of copper-based metal organic framework/graphite oxide composites," *Carbon,* vol. 49, pp. 563–572, 2011.

25. M. M. Dubinin, Ed., *Chemistry and physics of carbon*. New York: Dekker, 1966, p.^pp. Pages.
26. C. Lastoskie, *et al*., "Pore size distribution analysis of microporous carbons: a density functional theory approach," *The Journal of Physical Chemistry,* vol. 97, pp. 4786–4796, 1993.
27. J. Jagiello, "Stable Numerical Solution of the Adsorption Integral Equation Using Splines," *Langmuir,* vol. 10, pp. 2778–2785, 1994.
28. J. Jagiello, *et al*., "Carbon surface characterization in terms of its acidity constant distribution," *Carbon,* vol. 32, pp. 1026–1028, 1994.

Chapter 4
Performance of the Materials Tested for Ammonia Removal

As explained in Chap. 1, the performance of adsorbents is characterized by their adsorption (or breakthrough) capacity. The values obtained for the carbon-based and graphite oxide-based samples tested in various experimental conditions are presented in Figs. 4.1 and 4.2 respectively. The capacities are reported per mass of adsorbent (as compared to per volume of adsorbent) since the prime objective of this study is to investigate the mechanisms of ammonia adsorption.

The average breakthrough capacity for the virgin commercial carbon samples is about 1 mg g^{-1} for CC and CS carbons whereas an average of 9 mg g^{-1} is reached for CW carbon. For the polymer-based carbons, CP-1 and CP-2, the average adsorption capacities measured are 16 and 18 mg g^{-1}, respectively. Graphite oxide, on the other hand, exhibits a much higher breakthrough capacity that ranges from 20 to 60 mg g^{-1}, depending on the preparation method and the experimental conditions. Finally, the highest breakthrough capacity for the "unmodified" materials is obtained with HKUST-1. Up to 170 mg g^{-1} of ammonia can be adsorbed on its surface.

A significant improvement is obtained after the modifications of commercial activated carbons. Overall, the greatest improvement is obtained for the coal-based carbon, CC, modified with metal chlorides. Adsorption capacities for impregnated CC adsorbents run in moist air without prehumidification (EM) are 43–70 times the ones obtained on the corresponding virgin carbon. A significant improvement is also reached for the coconut shell-based carbon impregnated with metal oxides (CS-Mo1 and CS-Mo2). Oxidation of the polymer-based carbons (CP-1 and CP-2) causes an increase in the adsorption capacities of the materials as well, especially when oxidation is performed in the liquid phase (CP-1A and CP-2A). The composite materials exhibit enhanced capacities compared to GO. This improvement is better defined for the MOFs-based composites than for the POMs-based ones. It has to be noted that the GM-Znn and GM-Cun composites are better ammonia adsorbents than the corresponding MOF parent materials.
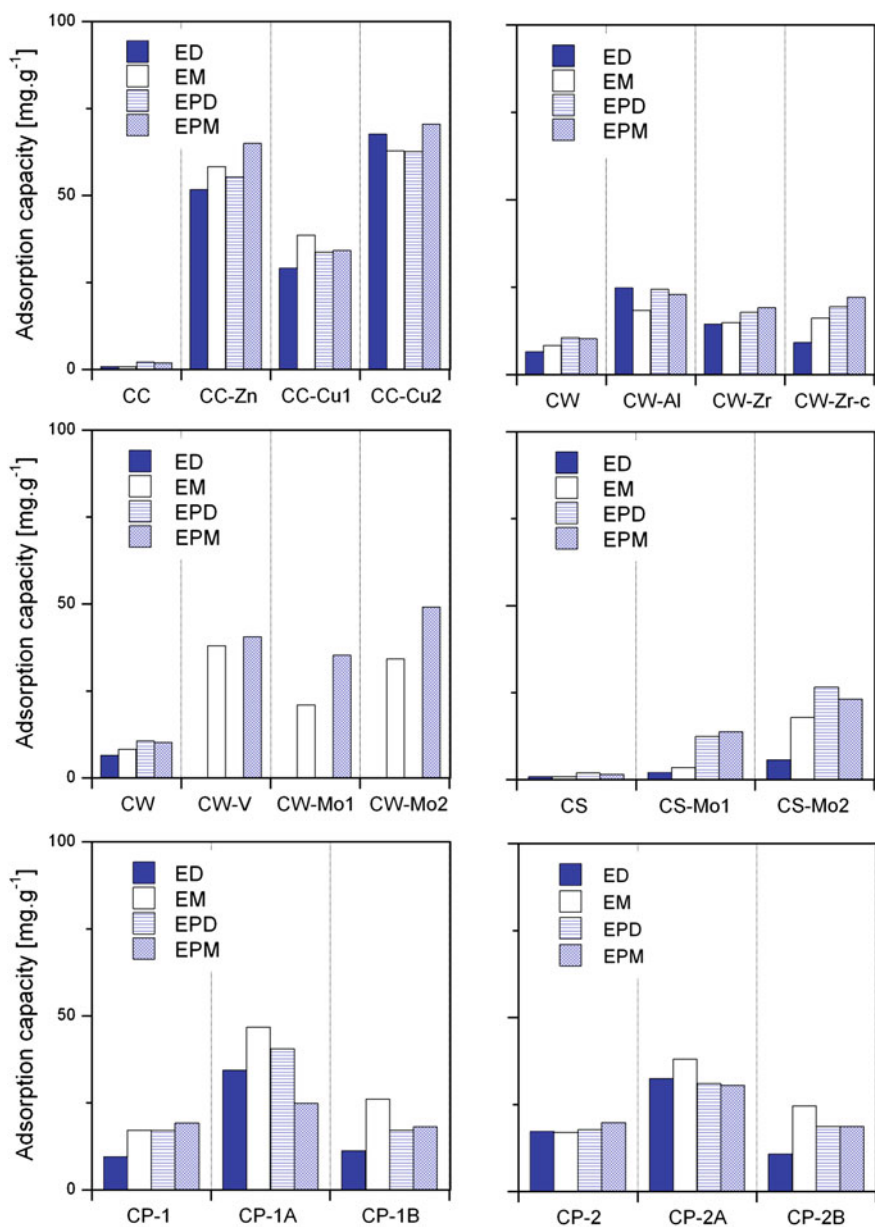
Fig. 4.1 Ammonia adsorption capacities for the untreated and modified activated carbons in various experimental conditions

Overall, the GM-Cu*n* samples are the best performing materials in ammonia adsorption from the point of view of breakthrough capacity with up to 23 wt% of ammonia adsorbed on their surface (see GM-Cu2 sample). Among the activated
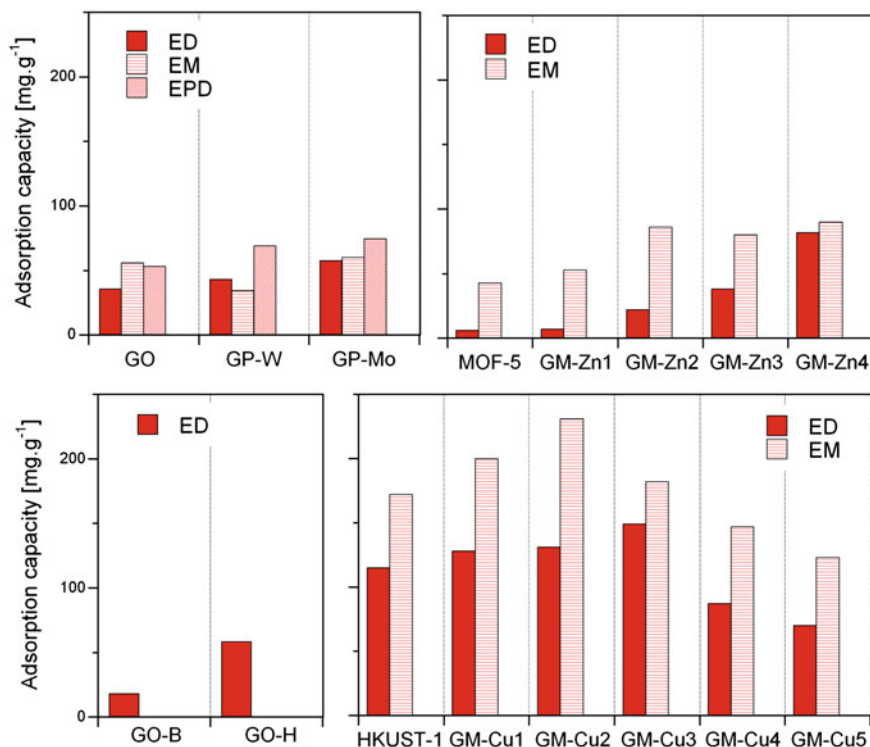
Fig. 4.2 Ammonia adsorption capacities for GO and GO-based composites in various experimental conditions

carbons, CC carbon impregnated with metal chlorides exhibits the best performance with about 7 wt% of ammonia adsorbed. The wood-based carbon impregnated with metal oxides (CW) acts as a good adsorbent as well and shows adsorption capacities reaching about 3–4 wt%. Overall, the performance of the adsorbents studied is at least similar to or much higher than the values reported in the literature for other adsorbents [1–6].

It has to be mentioned here that some precautions must be taken when comparing the performance of materials since the inlet flow rate can be different from one sample to another (Table 3.1) and that flow rate can influence the breakthrough capacity [7]. Although a direct comparison cannot be presented, the values reported in Figs. 4.1 and 4.2 still indicate a trend in the performance of the various materials.

Figure 4.3 shows the examples of breakthrough and desorption curves for the selected materials. The breakthrough curves for all the materials can be found in the Appendix (Figs. A.1, A.2, A.3, A.4, A.5, A.6). These curves contain two parts. The first curve represents the breakthrough curve and is related to the adsorption step when the adsorbent bed is exposed to ammonia (Chap. 1, Sect. 1.2).
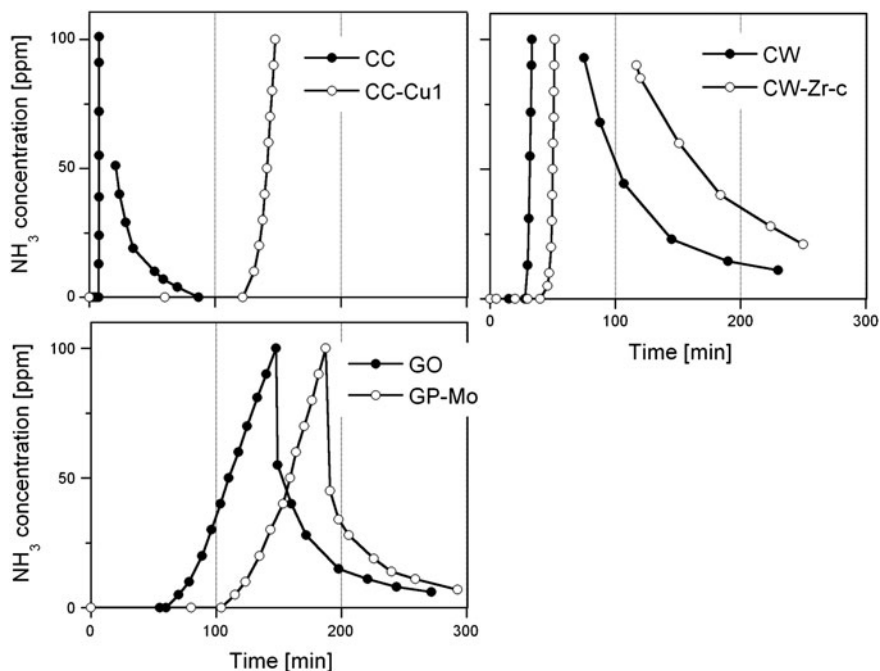
Fig. 4.3 Ammonia breakthrough and desorption curves for selected materials run in dry conditions

The second part of the curve represents the desorption curve and corresponds to the step when the bed is purged with air only (Chap. 1, Sect. 1.2). The desorption curve can be used to assess the strength of interactions between the targeted molecule and the adsorbent surface [8]. The stronger the interactions, the steeper the desorption curve. In an ideal situation, ammonia is strongly retained on the adsorbent's surface and does not desorb when purging the bed with air leading to a zero concentration after the adsorption test stops. As seen in Fig. 4.3, all the breakthrough curves look similar and show a rather steep slope suggesting fast kinetics of interactions between ammonia and the adsorbents' surfaces. On the contrary, the desorption curves differ between the samples and should be analyzed carefully. For the carbon-based samples, the concentration of ammonia recorded right after the adsorption step is always higher than 100 ppm, which corresponds to the detection limit of the sensor used to run the tests. This limit causes that a "gap" is observed between the breakthrough curve and the desorption curve (no data point could be measured), where the ammonia concentration is higher than 100 ppm in that range. This behavior indicates that ammonia is released in relatively high concentration after the breakthrough test and thus suggests that adsorbents work as ammonia "pseudo-concentrators" and that a part of the adsorbed gas is only weakly retained on the surface. This unfavorable feature is more or less

pronounced depending on the sample. For instance, the gap between the break-through curve and the desorption curve is smaller for the untreated carbons (CC, CW) than for the corresponding modified samples. It has to be noted that no desorption curve is plotted for the CC-Cu1 sample since the concentration of ammonia was above 100 ppm for 3 hours, indicating a very weak retention. On the contrary, for the GO-based samples, no gap is observed between the adsorption and desorption curves, evidencing a much stronger retention of ammonia on these materials. All of these underline the different mechanisms of ammonia retention on the various samples and will be discussed in detail later.

Considering the above, one can notice variations in the behavior of the samples studied as ammonia adsorbents. These differences must be linked to various parameters influencing the removal process in terms of breakthrough capacity and strength of retention. In the case of the carbon-based samples, these factors include the type of activated carbon (Fig. 4.1, compare CS and CW), the type of impregnate (Fig. 4.1, compare CW-Zr and CW-Mo2), the amount of impregnate (Fig. 4.1, compare CC-Cu1 and CC-Cu2), and the presence of water (Fig. 4.1, compare CS-Mo2-ED and CS-Mo2-EPD). Similarly, for the GO-based samples, parameters such as the materials preparation method (Fig. 4.2, compare GO-H and GO-B), the type of substrate used to build the composite (Fig. 4.2, compare GM-Zn1 and GM-Cu1), and the composition of the composites (Fig. 4.2, compare GM-Zn1-ED and GM-Zn4-ED), seem to modify the performance of the materials. An extensive investigation of all these parameters is thus required to better understand the mechanisms of ammonia adsorption.

References

1. M. Domingo-García, *et al.*, "Dynamic adsorption of ammonia on activated carbons measured by flow microcalorimetry," *Applied Catalysis A: General,* vol. 233, pp. 141–150, 2002.
2. C.-C. Huang, *et al.*, "Effect of surface acidic oxides of activated carbon on adsorption of ammonia," *Journal of Hazardous Materials,* vol. 159, pp. 523–527, 2008.
3. F. Xie, *et al.*, "Microcalorimetric study of acid sites on ammonia- and acid-pretreated activated carbon," *Carbon,* vol. 38, pp. 691–700, 2000.
4. J. Guo, *et al.*, "Adsorption of NH_3 onto activated carbon prepared from palm shells impregnated with H_2SO_4," *Journal of Colloid and Interface Science,* vol. 281, pp. 285–290, 2005.
5. C. L. Mangun, *et al.*, "Oxidation of Activated Carbon Fibers: Effect on Pore Size, Surface Chemistry, and Adsorption Properties," *Chemistry of Materials,* vol. 11, pp. 3476–3483, 1999.
6. J. Helminen, *et al.*, "Adsorption Equilibria of Ammonia Gas on Inorganic and Organic Sorbents 784 at 298.15 K," *Journal of Chemical & Engineering Data,* vol. 46, pp. 391–399, 2001.
7. T. J. Bandosz, *Activated carbon surfaces in environmental remediation*. Oxford, UK: Elsevier, 2006.
8. M. Seredych, *et al.*, "Role of graphite precursor in the performance of graphite oxides as ammonia adsorbents," *Carbon,* vol. 47, pp. 445–456, 2009.

Chapter 5
Role of Textural Parameters

Adsorbents are usually selected based on their textural properties. These properties include several parameters such as a high surface area and volume of pores. In some cases, the distribution of pores sizes becomes important because it may impact the selectivity of adsorption [1]. Overall, these features are essential when the vapors to be adsorbed are retained on the surface by physisorption but they are also useful to initiate chemisorption or reactive adsorption [2]. Indeed, a reaction between the adsorbent surface groups and the targeted molecule requires that the vapor is temporarily immobilized on the surface [2]. For these reasons, it is paramount to study in detail the textural parameters of the adsorbents tested for the removal of ammonia from air. This chapter provides a description of the porosity of the samples tested and then discusses the various effects of porosity on the ammonia adsorption. In this study, the porosity is evaluated by measuring nitrogen adsorption and the parameters of porous structure are determined from the isotherms (Chap. 3, Sect. 3.2).

5.1 Characterization of the Materials Studied

The parameters of porous structure for all samples are listed in Table 5.1. It has to be noted that GO is not presented in this table as its porosity is negligible [3]. Similarly, the GP-Mo and GP-W composites were found to be nonporous and are thus not shown here.

While the CC and CW carbons are micro/mesoporous, the CS carbon is more homogeneous and can be considered as only microporous. The surface area of the untreated commercial carbons CC and CS is about 1,000 $m^2 g^{-1}$, and for CW—2,000 $m^2 g^{-1}$. A decrease in the surface area and volume of pores is observed after modifications, as a result of inorganic matter deposition. Both the volume of micropores and mesopores are reduced after modifications, suggesting

Table 5.1 The parameters of porous structure for the samples studied

Sample	S_{BET} (m^2 g^{-1})	V_{tot} (cm^3 g^{-1})	V_{meso} (cm^3 g^{-1})	V_{mic} (cm^3 g^{-1})	V_{mic}/V_{tot}
CC	1,033	0.614	0.139	0.475	0.77
CC-Zn	726	0.437	0.095	0.342	0.78
CC-Cu1	914	0.539	0.124	0.415	0.77
CC-Cu2	565	0.345	0.095	0.250	0.73
CW	2,176	1.519	0.701	0.818	0.54
CW-Al	1,929	1.324	0.598	0.726	0.55
CW-Zr	1,958	1.334	0.597	0.737	0.55
CW-Zr-c	1,832	1.268	0.583	0.685	0.54
CW-V	1,513	1.006	0.434	0.572	0.57
CW-Mo1	1,807	1.272	0.611	0.661	0.52
CW-Mo2	1,606	1.334	0.752	0.582	0.44
CS	1,069	0.554	0.018	0.536	0.97
CS-Mo1	850	0.433	0.003	0.430	0.99
CS-Mo2	684	0.355	0.011	0.344	0.97
CP-1	1,331	0.991	0.370	0.621	0.63
CP-1A	1,049	0.871	0.375	0.496	0.57
CP-1B	1,449	1.076	0.385	0.691	0.64
CP-2	334	0.265	0.095	0.170	0.64
CP-2A	531	0.399	0.140	0.259	0.65
CP-2B	742	0.533	0.164	0.369	0.69
MOF-5	793	0.408	0.023	0.385	0.94
GM-Zn-1	706	0.365	0.024	0.341	0.93
GM-Zn-2	806	0.476	0.028	0.388	0.93
GM-Zn-3	603	0.325	0.037	0.288	0.89
GM-Zn-4	742	0.399	0.002	0.397	0.99
HKUST-1	909	0.471	0.022	0.449	0.95
GM-Cu-1	989	0.515	0.037	0.478	0.93
GM-Cu-2	1,002	0.527	0.049	0.478	0.91
GM-Cu-3	996	0.566	0.044	0.522	0.92
GM-Cu-4	704	0.370	0.052	0.348	0.94
GM-Cu-5	620	0.345	0.051	0.294	0.85

that impregnates are located in both mesopores and micropores. Nevertheless, the volume of micropores can also decrease as a result of a pore blocking effect induced by the deposition of inorganic matter at the pore entrances. Finally, the oxidative effect of the inorganic matter or the oxygen during the calcination represents another possible cause for the reduction of porosity for the samples loaded with metal oxides (CW-V, CW-Mo1, CW-Mo2) or calcined in air (CW-Zr-c) [4].

The polymer-based carbons exhibit a large range of porosity. While the CP-1 series exhibits surface areas and volumes of pores similar to those of the commercial carbons (around 1200 m^2 g^{-1}, 1 cm^3 g^{-1}), the CP-2 series has more resemblance to the impregnated carbon samples (S$_{BET}$ ∼ 550 m^2 g^{-1}, V$_{tot}$ ∼ 0.4 cm^3 g^{-1}). Interestingly, for both series, oxidation treatments caused an activation of the starting

materials leading to an increased porosity (between 8 and 76%) (except for CP-1A). This effect is more pronounced for the CP-2 series. As for CW carbon, these materials contain both micropores and mesopores.

The GO-based composites (GM-Zn*n* and GM-Cu*n*) are predominantly microporous with a degree of microporosity equal to or higher than 90%. Their surface area and volume of pores are smaller than the untreated activated carbons and vary depending on their composition. The GM-Cu*n* materials are more porous than the GM-Zn*n* ones, which is likely related to the different porosity of the MOF parent materials. Except for GM-Zn4, an increase in the mesopores volume is noticed for the composites compared to the parent MOF.

Pore size distributions (PSDs) for the virgin and impregnated/oxidized samples are plotted in Fig. 5.1. They provide a deep insight into the porosity for the samples tested. For CC and CS carbons, most of the pores are smaller than 30 Å, whereas for CW carbon, a wide range of pore sizes is revealed. After impregnation, the porous structure changes, especially for the samples impregnated with metal chlorides. This can be the result of a "mass dilution effect" since the inorganic matter contributes to the mass of the final adsorbent but, owing to the lack of pores it does not add any porosity. It is interesting to notice that the pores smaller than 10 Å are not really affected, except for CC-Cu2 and CS-Mo2. This is likely due to the size of the impregnates. For instance, the polycations used in the preparation of CW-Al and CW-Zr have a size of about 9.8 Å [5] which prevents them from entering very small pores. The pores size in the polymer-based carbons covers a rather wide range but the effect of oxidation is mainly detected in the micropore range with an increase in the volume of micropores smaller than 10 Å. PSDs for the GO-based samples and MOF samples are not presented since the calculation method to derive these curves (DFT method) is not adapted to such materials.

5.2 Porosity: A Necessary but Non-Sufficient Condition

Based on the knowledge of adsorption phenomena, it is reasonable to assume that a high surface area with a predominance of micropores should play an important role in the ammonia retention. The size of pores is especially essential for physical adsorption of small molecules as ammonia (diameter of about 3.0 Å [6]) [2, 7].

To evaluate to what extent this "statement" applied to the features of our adsorbents, the changes in the breakthrough capacity with variations in the porosity were studied. Interestingly, the only trend observed was for the untreated commercial activated carbons as it can be seen in Fig. 5.2. In spite of the limited number of samples, a good linear trend with correlation factors above 0.95 (0.99 for the correlations based on surface area and total volume of pores) is found for the virgin carbons. Although more points would be needed to confirm this, this trend tends to suggest that in the absence of functional groups, the adsorbent's porosity influences ammonia adsorption. However, the most important point here
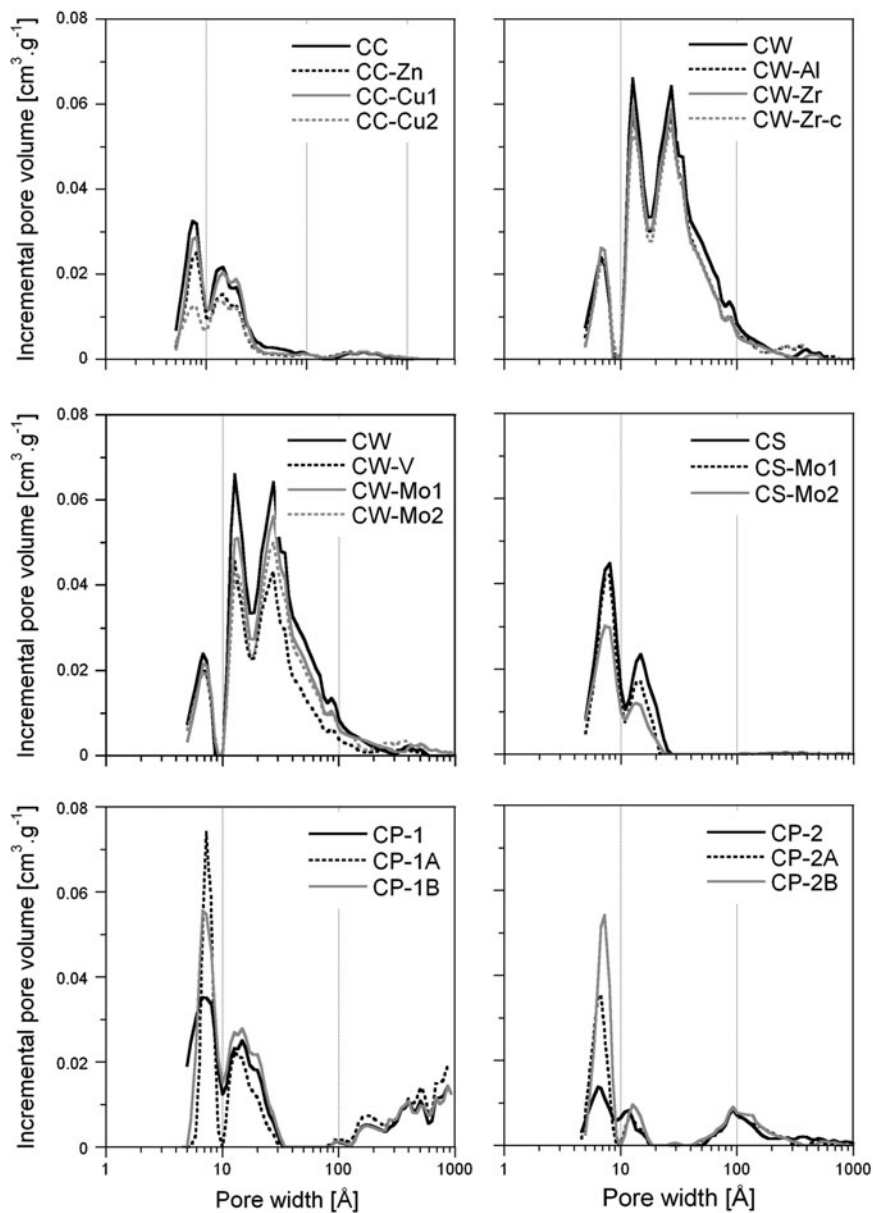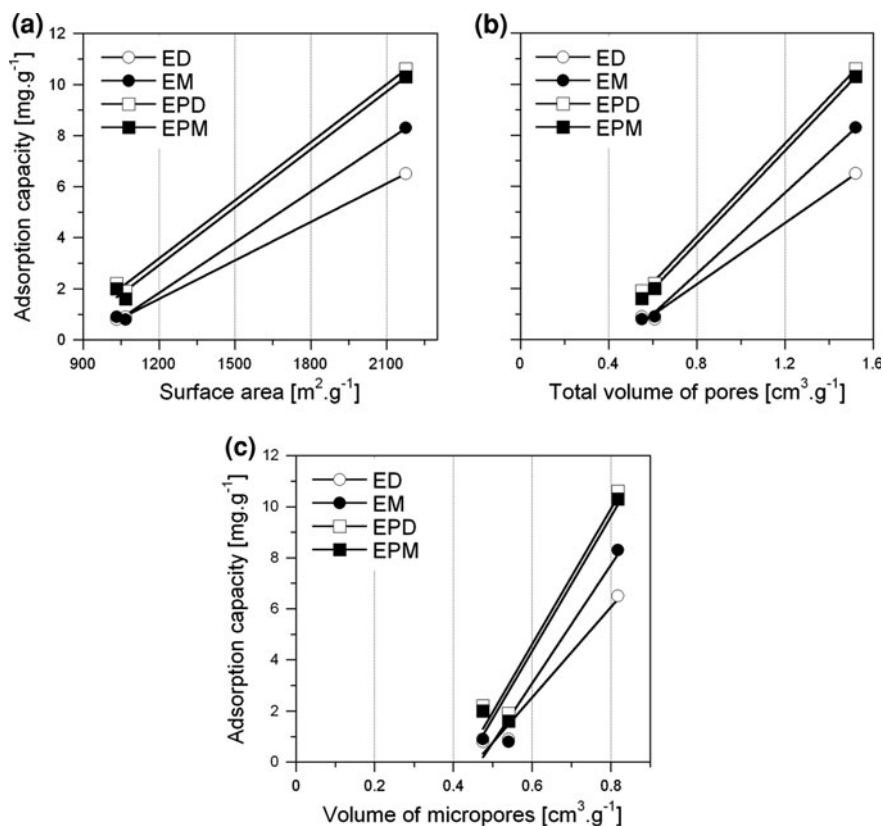
Fig. 5.1 Pore size distributions for various activated carbons

is to notice that no correlation exists for the other materials whether the surface area, volume of pores or volume of micropores is considered. Not only is it observed when all the materials are compared but it is also true within the series of samples.

Fig. 5.2 Dependence of ammonia breakthrough capacity on the surface area (**a**), the total volume of pores (**b**) and the volume of micropores (**c**) for the virgin commercial carbons (CC, CS, CW) in various conditions. Reprinted from Ref. [8], Copyright 2009, with permission from Elsevier

For instance, one can see that even though the untreated carbon CW is more porous and especially contains higher volume of micropores than the derived sample CW-Mo2, it still adsorbs less ammonia. Similar observations can be made for other commercial carbons studied. Regarding the polymer-based carbons, a factor of 2–4 difference in terms of surface area and volume of pores is observed between the CP-1 and CP-2 series of samples. Nevertheless, the ammonia adsorption capacities of the materials are in the same range. All of these suggest that the porosity is not a governing factor in the ammonia retention at ambient conditions. Moreover, since the only trend found was for the samples deprived of surface chemistry, it indicates that the presence of functional groups and inorganic matter on the surface of the adsorbents must be prevalent parameters in the removal of ammonia from air. This will be discussed in more detail later (Chap. 6).

Table 5.2 The parameters of porous structure derived from nitrogen isotherms for the selected samples before and after exposure to ammonia

Sample	S_{BET} $(m^2 \, g^{-1})$	V_{tot} $(cm^3 \, g^{-1})$	V_{meso} $(cm^3 \, g^{-1})$	V_{mic} $(cm^3 \, g^{-1})$	V_{mic}/V_{tot}
CC-Zn	726	0.437	0.095	0.342	0.78
CC-Zn-ED	562	0.353	0.096	0.257	0.73
CC-Zn-EM	593	0.370	0.102	0.268	0.72
CC-Zn-EPD	603	0.373	0.102	0.271	0.73
CC-Zn-EPM	555	0.349	0.104	0.245	0.70
CC-Cu2	565	0.345	0.095	0.250	0.73
CC-Cu2-ED	552	0.339	0.089	0.250	0.74
CC-Cu2-EM	648	0.387	0.090	0.297	0.77
CC-Cu2-EPD	580	0.353	0.092	0.261	0.74
CC-Cu2-EPM	558	0.339	0.085	0.254	0.75
CP-2	334	0.265	0.095	0.170	0.64
CP-2-ED	295	0.263	0.120	0.143	0.54
CP-2-EM	308	0.279	0.131	0.148	0.53
CP-2-EPD	311	0.294	0.147	0.147	0.50
CP-2-EPM	257	0.243	0.118	0.125	0.51
CP-2A	531	0.399	0.140	0.259	0.65
CP-2A-ED	508	0.391	0.147	0.244	0.62
CP-2A-EM	501	0.380	0.136	0.244	0.64
CP-2A-EPD	493	0.374	0.131	0.243	0.65
CP-2A-EPM	494	0.378	0.136	0.242	0.64

Although porosity (and thus physisorption) does not control ammonia adsorption for the samples discussed, it can still play a role in this process. For instance, the presence of pores is necessary to drive ammonia molecules to the adsorbent's active sites. Besides, as addressed in more detail in Chap. 7, one way of ammonia adsorption is its dissolution in water when water is present in the carrier gas or on the surface of the adsorbent. Since small pores favor water adsorption [9], adsorbents with micropores will enhance ammonia retention via dissolution. In addition, in the case of impregnated carbons, it is usually agreed that a large surface area combined with a proper pore size distribution tend to favor the good dispersion of the impregnant [10]. The high and well-defined porosity of the support offers some control on the inorganic matter deposition and reduces the extent of agglomeration. Consequently, by improving impregnation, the porosity indirectly influences the chemical interactions of ammonia with the inorganic matter (discussed in Chap. 6). Finally, pores also serve as a storage space for products of reactive adsorption (discussed in Chap. 6). Table 5.2 lists the parameters of porous structure before and after exposure to ammonia for the selected materials. The data for the other materials studied can be found in the Appendix (Tables A.1 to A.3). As seen in Table 5.2, the surface area and volume of pores decrease after the exposure to ammonia suggesting the deposition of species inside or at the entrance of the pores. It is interesting to note that the

decrease in porosity does not necessarily follow the trend in the breakthrough capacity, which indicates once again that other mechanisms than physisorption are involved in the ammonia removal [8]. On the basis of the apparent absence of porosity of GO, one could argue on the actual role of porosity in ammonia adsorption. For this material, however, it is important to remember that ammonia molecule diameter (3 Å [6]) is slightly smaller than that of nitrogen molecule (3.6 Å [11]). Consequently, even though no porosity is detected by nitrogen adsorption, ammonia can still enter the small pores/interlayer space of GO. This ammonia intercalation between the hydrophilic GO layers is promoted by the polar character of ammonia molecule [12].

5.3 Importance of Dispersive Forces

One way to strengthen the impact of porosity in the ammonia adsorption is by enhancing the dispersive forces of the adsorbents. Although this might be difficult to achieve in the case of activated carbons due to the hardly controllable character of their structure, this can be applied to other types of adsorbents such as MOFs. They exhibit a low density of atoms. While this feature causes high diffusion coefficients and is thus of interest in catalysis [13], it may affect the gas breakthrough capacity by decreasing the dispersive forces, especially at supercritical conditions. To address this issue, the composites GM-Znn and GM-Cun were prepared (Sect. 3.1). The GO component, owing to the dense arrangement of atoms of the graphene layers, was expected to enhance these physical forces. Confirmation of the latter hypothesis is described below.

Figure 5.3 provides a comparison between the adsorption capacities measured and the ones calculated assuming a physical mixture between the two components of the composites. The latter capacities ("hypothetical capacities") were calculated as detailed in Eq. 5.4.

$$A_{composite} = A_{GO} \times wt\%GO + A_{MOF} \times wt\%MOF \qquad (5.4)$$

In the above equation, "A_i" refers to the breakthrough capacity (in mg g^{-1}) of the compound "i" (i = MOF or GO) and "wt%$_i$" to the content of compound "i" in the specific composite. As seen in Fig. 5.3, the measured breakthrough capacities are always higher than the "hypothetical" ones. This suggests that a synergistic effect occurs between the components of the composites. This phenomenon is the result of the presence of increased dispersive forces in the composites owing to the graphene layers [14, 15]. However, it is important to mention that the presence of GO alone cannot enhance the retention forces. The particular arrangement of GO and MOF components in the materials is of prime importance. For instance, we found that replacing GO by graphite did not lead to the enhanced breakthrough capacity. That is why, the description of the composites' structure and formation is of interest and is addressed below.
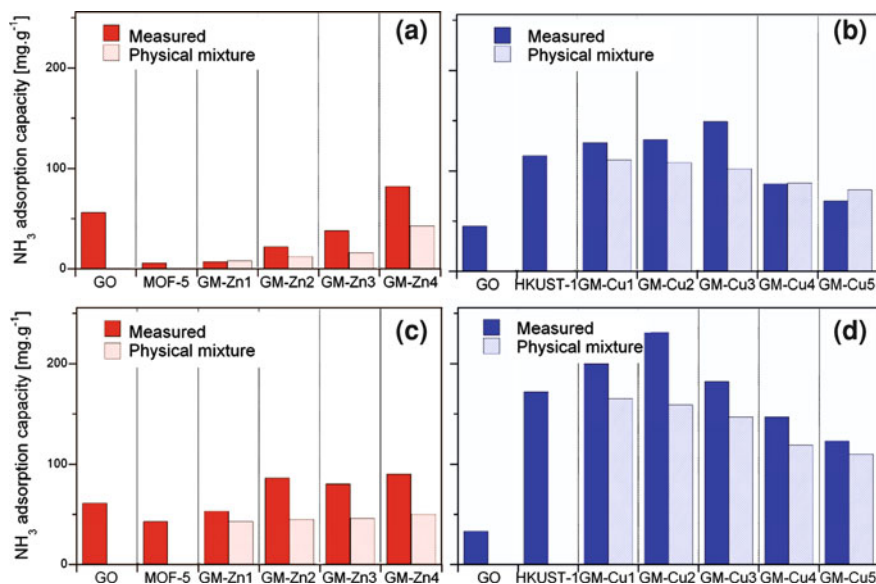
Fig. 5.3 Measured and hypothetical ammonia adsorption capacities for GO, and the zinc-based and copper-based materials in dry (**a**, **b**) and moist conditions (**c**, **d**)

X-ray diffraction patterns of the parent materials and selected composites (Fig. 5.4) provide information on their structure. The diffraction patterns of the other composites can be found in the Appendix (Fig. A.7). The two MOFs samples show the expected pattern for MOF-5 and HKUST-1 [16, 17]. A single peak at about 2 Theta 9.3° (d_{002} peak) is seen on the pattern of GO and is related to an interlayer distance of 9.5 Å. The patterns of the composites are rather similar to those of the parent MOFs for both the GM-Znn and GM-Cun series of samples. This suggests that the presence of graphene layers did not prevent the formation of the crystalline frameworks [18, 19]. The peak corresponding to GO is absent from the composites' diffraction patterns which is due to the fact that DMF (solvent used in the preparation of these materials) caused the dispersion/exfoliation of GO.

In Fig. 5.5, both the measured volumes of pores and the hypothetical ones calculated assuming the physical mixture of MOF and GO are presented for the composites. One can notice that for the GM-Cun samples, the measured porosity is always higher than the hypothetical one. This increase is enhanced as the GO content increases from 5 to 18 wt% and then it decreases. This trend can be due to the presence of increased amounts of GO causing too much distortion in the structure of the materials. Another explanation could be that when a high amount of GO is present, the number of groups on GO exceeds the numbers of accessible sites on MOF with which they can react. Overall, this enhanced porosity is likely due to the creation of new pores at the interface between the MOF component and the graphene layers [19]. It is interesting to see that the degree of enhancement in

Fig. 5.4 X-ray diffraction patterns for GO, and selected zinc-based and copper-based materials. With kind permission from Springer Science + Business Media. Ref. [20], Copyright 2010
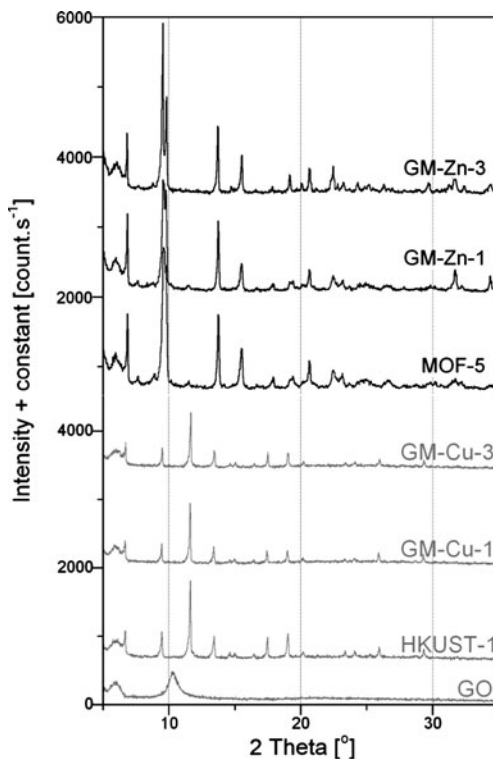

the volume of pores follows the same trend as the ammonia breakthrough capacity. This represents another support for the fact that this new porosity, where the dispersive forces are the strongest, is responsible for the enhanced ammonia breakthrough capacity. For the GM-Znn samples, the porosity is not always higher than that of MOF-5 and than the one calculated for the physical mixture of MOF and GO. Actually, for most samples, the differences between the measured porosity and the one for the physical mixture can be considered within the experimental error range and might thus be negligible. Nevertheless, this does not contradict the existence of enhanced dispersive forces observed based on the amount of ammonia adsorbed [15].

Thermal analyses results, presented in Fig. 5.6 for selected samples, provide insight into the mechanism of composites' formation. The DTG curves for the other samples can be found in the Appendix (Fig. A.8). The DTG curve for GO reveals a major peak at about 200 °C related to the decomposition of epoxy groups [21]. As concluded from X-ray diffraction and nitrogen adsorption analyses, the features of the composites resemble the ones of the parent MOFs. The major peak at 540 °C for MOF-5 and GM-Znn samples, and at 350 °C for HKUST-1 and GM-Cun samples, is due to the decomposition of the organic ligand (BDC or BTC) with release of CO_2 and collapse of the MOF structure [22, 23]. An interesting
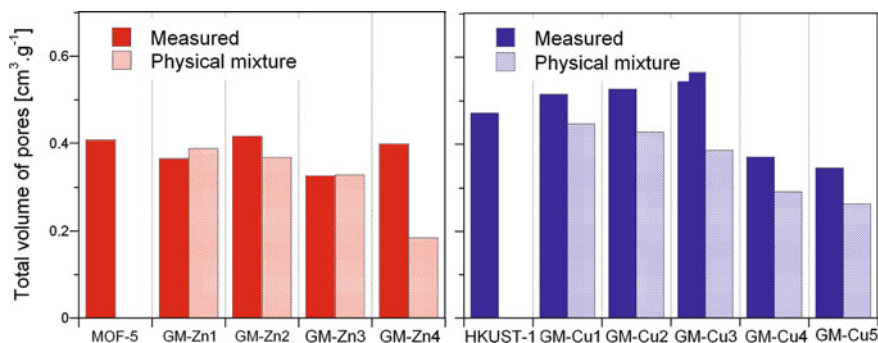
Fig. 5.5 Measured and hypothetical pores volumes for the zinc-based and copper-based samples

Fig. 5.6 DTG curves for the GO, MOF-5, HKUST-1 materials and selected composites. With kind permission from Springer Science + Business Media. Ref. [20], Copyright 2010
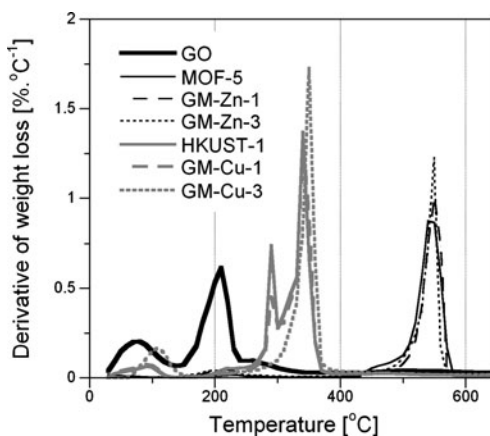
feature of the composites DTG curves is the absence of the intense peak from GO epoxy groups. This suggests that these functionalities are involved in the building process of the new materials. In fact, the formation of MOF occurs via the coordination of carboxylates groups (and thus oxygen groups) and metallic centers. Consequently, it seems possible that the GO functionalities (epoxy, carboxyl, hydroxyl and sulfonic groups) can bind the metallic sites. To verify that the absence of the peak at 200 °C on the composites DTG curves was not due to the reaction of the epoxy groups with compounds other than HKUST-1 during the synthesis of the composites, we subjected GO to the same synthesis process as for the composites but in the absence of copper nitrate and BTC [19]. We then run thermal analyses on the resulting sample. The DTG curves of the latter material exhibited a peak at 200 °C [19]. This supports our hypothesis that the absence of GO epoxy groups on the DTG curves of the composites is related to an interaction of these groups with the MOF. Due to these chemical interactions between the metallic sites of MOF and the functional groups of GO, a new pore space can be
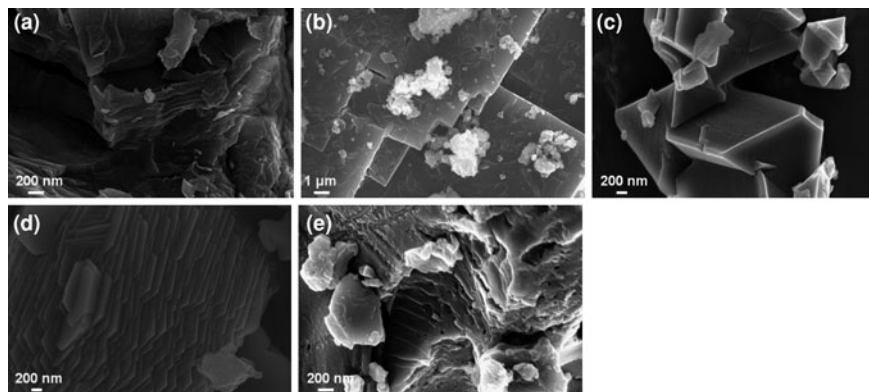
Fig. 5.7 SEM images of GO (**a**), MOF-5 (**b**), HKUST-1 (**c**) and selected composites (**d** GM-Zn1, **e** GM-Cu2). Reprinted from Ref. [18] and [19], Copyright 2009 and 2011, with permission from Wiley and Elsevier

created at the interface between GO carbon layers and the MOF units. This porosity, where the dispersive forces are strong, enables enhanced ammonia adsorption compared to the physical mixture. In fact, it was found that composites of the copper-based MOF and graphite (no oxygen group, thus no chemical interactions) did not exhibit higher porosity and breakthrough capacity than the physical mixture of the MOF and GO.

SEM images of the parent materials and selected composites are presented in Fig. 5.7. The SEM micrographs for the other composites can be found in the Appendix (Fig. A.9). For the two series of samples, the texture of the composites is different from that of the parent materials. In the case of GO, we observe a dense packing of graphene layers whereas both MOF-5 and HKUST-1 exhibit crystalline structures with some defects and remains of an amorphous phase. The GM-Zn1 sample appears as a layered material. These layers likely correspond to an alternation between layers of graphene and MOF blocks [18]. The GM-Cu2 sample exhibits a more heterogeneous structure where only a few distorted layers are observed [19].

HRTEM images of composites GM-Cu1, 3 and 5 support the data obtained from other analyses (Fig. 5.8). In the case of GM-Cu1, well-defined graphene-based layers with embedded HKUST-1 units are observed. On GM-Cu3 sample, more graphene-based layers are present and a rather well-defined lattice image appears within the layers of GO. It is known that electron beam illumination can cause the breakdown of HKUST-1 and can thus prevent any visualization of its lattice structure [24]. Nevertheless, the pattern observed can be considered as representing the lattice image of HKUST-1. It is likely that GO distorted graphene-based layers present in the composite helped MOF to retain its crystalline structure by dissipating the electrostatic charges [25]. Another explanation could be that the lattice image is related to a regular structure formed by stacked GO distorted
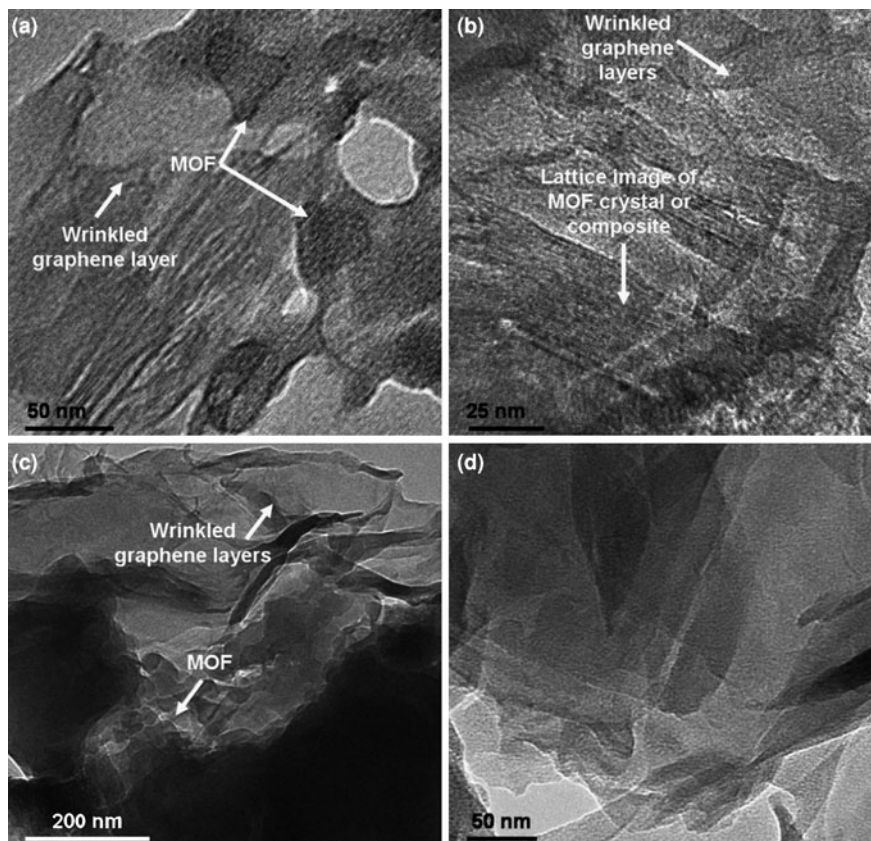
Fig. 5.8 HRTEM images of GM-Cu1 (**a**), GM-Cu3 (**b**) and GM-Cu (**c**, **d**). Reprinted from Ref. [19], Copyright 2011, with permission from Elsevier

Fig. 5.9 Oxygen coordination sites available in MOF-5 (**a**), and HKUST-1 (**b**). With kind permission from Springer Science + Business Media: Ref. [20], Copyright 2010
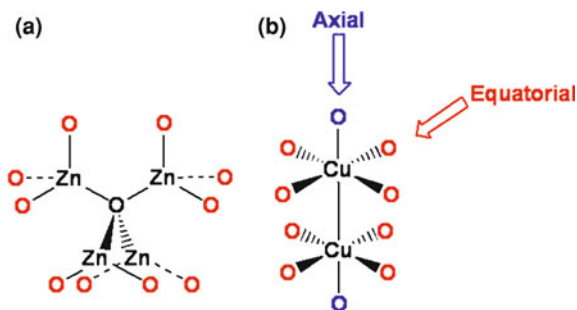
graphene-based layers and HKUST-1 units. For the GM-Cu5 sample, the GO component becomes predominant. Although some HKUST-1 units can be observed within the GO distorted graphene-based layers, separate agglomerates
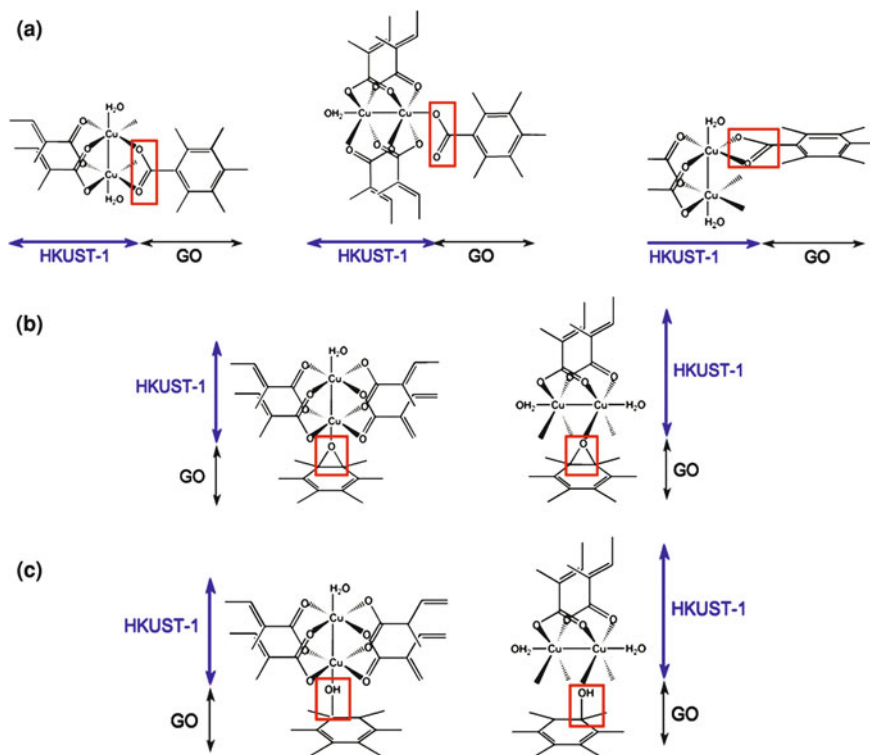
Fig. 5.10 Possible coordinations of the copper sites in HKUST-1 with the carboxyl (**a**), epoxy (**b**) and hydroxyl (**c**) groups of GO. Reprinted from Ref. [19], Copyright 2011, with permission from Elsevier

only with stacked distorted graphene-based layers are seen as well. From a general point of view, these micrographs evidenced that the two composite components are well-dispersed within our materials. This supports the results of thermal analyses and the hypothesis that chemical interactions are involved in the formation on the composites. Moreover, we can see that the GO distorted graphene-based layers are rather well-dispersed in the materials and do not form densely packed agglomerates, which is supported by the XRD results.

Considering these differences in texture between the two series of composites and taking into account the data from thermal analyses, we believe that the formation of the materials is governed by interactions between the GO oxygen groups and the MOFs metallic sites. In the case of MOF-5, all the oxygen atoms forming the zinc oxide tetrahedra are equivalent in terms of "spatial arrangement" (Fig. 5.9). Consequently, any change of structure between the GM-Znn composites must be related to the oxygen groups of GO. GO contains oxygen groups on the basal planes (i.e. epoxy, hydroxyl, ketone) and on the edges of the layers (carboxyl and sulfonic groups) [12, 26, 27]. Depending on the type of groups interacting with
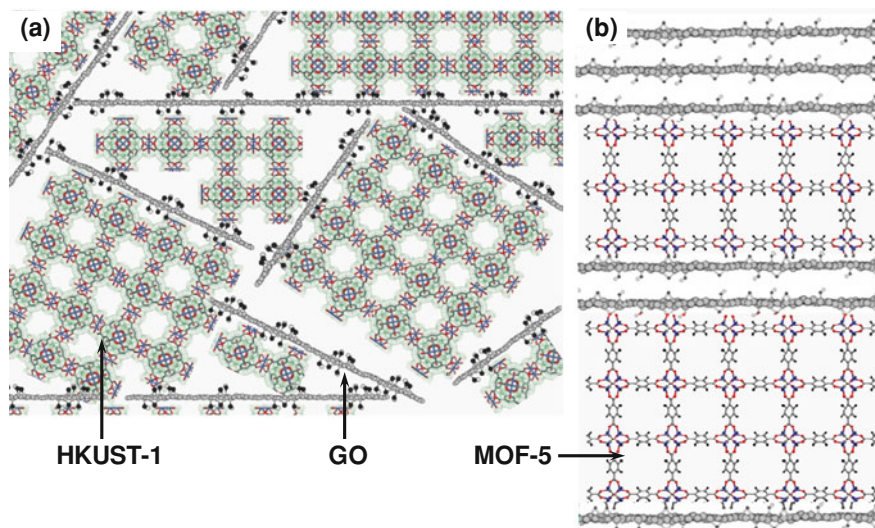
Fig. 5.11 Proposed composite structures: HKUST-1-based composites (**a**) and MOF-5-based composites (**b**). With kind permission from Springer Science + Business Media. Ref. [20], Copyright 2010

MOF-5 metallic sites, the structure of the composites can change. This mechanism is also applicable to the GM-Cu*n* materials. However, in this case, an additional "degree of modification" must be taken into account since the coordination sites to copper are not all equivalent (see Fig. 5.9). Because of this, one might expect a more disordered structure in the case of GM-Cu*n* composites compared to the GM-Zn*n* materials. Examples of possible coordinations between GO functional groups and the MOF metallic centers in HKUST-1 are presented in Fig. 5.10 for some oxygen groups.

Considering all the above, envisioned structures for the GM-Zn*n* and GM-Cu*n* composites are proposed in Fig. 5.11. The more regular arrangement of the MOF-5-based compounds and their layered structure is visualized. On the contrary, the copper-based composites exhibit a more disordered structure. Moreover, in both series of samples, a new pore space is created between the MOF blocks and the graphene layers. However, the new pores are smaller in GM-Zn*n* composites than in the GM-Cu*n* materials as suggested by the results of nitrogen adsorption analyses. In the case of GM-Cu*n* composites, the nitrogen adsorption analysis presented above indicated a trend in the porosity of the materials with first an increase in porosity as the GO content increased up to about 20 wt% and then a decrease for higher GO contents. This evolution of structure is represented in Fig. 5.12. As the content of GO increases (Fig. 5.12b), the larger pores between the graphene flakes are formed as a result of the interactions of more carboxylic groups (and sulfonic groups) on the edges of flakes with the copper sites. This is supported by N_2 sorption analyses, which

Fig. 5.12 Schematic representations of the composites with low (**a**), medium (**b**) and high (**c**) content of GO. Reprinted from Ref. [19], Copyright 2011, with permission from Elsevier
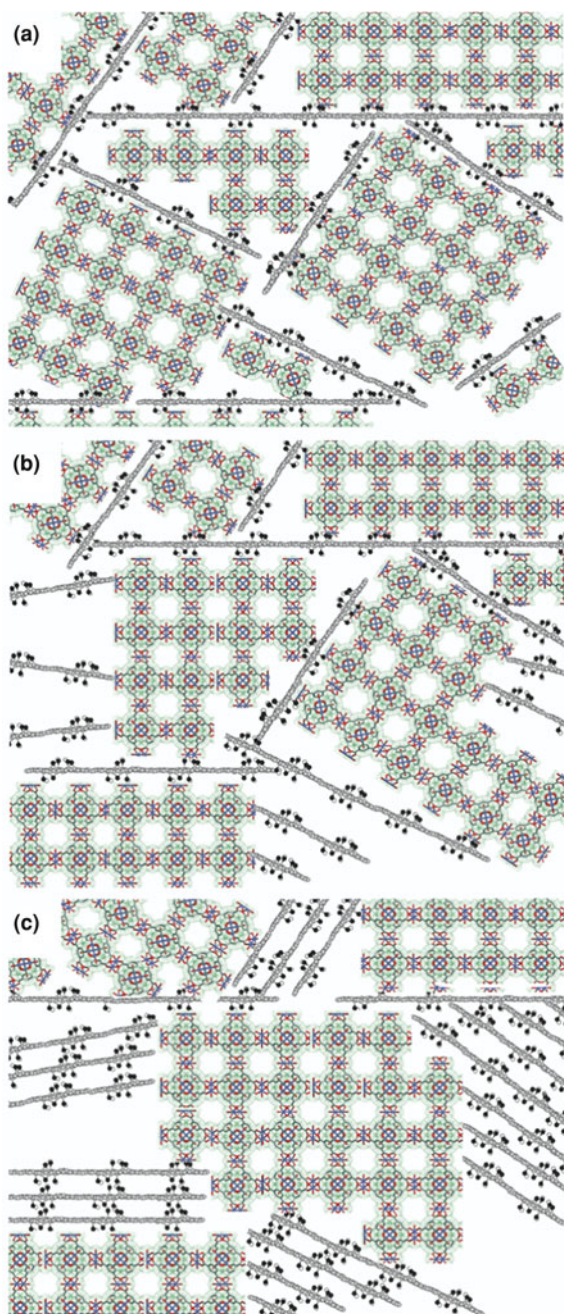
showed that the volumes of mesopores increased with the GO content (see Table 5.1). When even higher amounts of GO are present, the number of groups from GO can exceed the number of accessible MOF sites they can react with and the graphene layers remain as agglomerates (Fig. 5.12). This causes that smaller volumes of new small pores are formed.

References

1. J. M. D. MacElroy, *et al.*, "Sorption rate processes in carbon molecular sieves," in *Equilibria and dynamics of gas adsorption on heterogeneous solid surfaces*, W. Rudziński, et al., Eds., ed: Elsevier, 1997, pp. 837–873.
2. T. J. Bandosz, *Activated carbon surfaces in environmental remediation*. Oxford, UK: Elsevier, 2006.
3. M. Seredych, *et al.*, "Role of graphite precursor in the performance of graphite oxides as ammonia adsorbents," *Carbon,* vol. 47, pp. 445–456, 2009.
4. C. Moreno-Castilla, *et al.*, "Changes in surface chemistry of activated carbons by wet oxidation," *Carbon,* vol. 38, pp. 1995–2001, 2000.
5. G. Johansson, "On the crystal structure of some basic aluminium salts," *Acta Chem. Scand.,* vol. 14, pp. 771–773, 1960.
6. J. C. Thompson, "Compressibility of Metal-Ammonia Solutions," *Physical Review A,* vol. 4, p. 802, 1971.
7. K. S. W. Sing, "The use of physisorption for the characterization of microporous carbons," *Carbon,* vol. 27, pp. 5–11, 1989.
8. T. J. Bandosz and C. Petit, "On the reactive adsorption of ammonia on activated carbons modified by impregnation with inorganic compounds," *Journal of Colloid and Interface Science,* vol. 338, pp. 329–345, 2009.
9. C. L. McCallum, *et al.*, "A Molecular Model for Adsorption of Water on Activated Carbon: Comparison of Simulation and Experiment," *Langmuir,* vol. 15, pp. 533–544, 1998.
10. F. Rodríguez-reinoso, "The role of carbon materials in heterogeneous catalysis," *Carbon,* vol. 36, pp. 159–175, 1998.
11. K. Aligizaki, "Gas sorption," in *Pore structure of cement-based materials: testing, interpretation and requirements*, ed: Taylor & Francis, 2006, pp. 108–167.
12. C. Petit, *et al.*, "Revisiting the chemistry of graphite oxides and its effect on ammonia adsorption," *Journal of Materials Chemistry,* vol. 19, pp. 9176–9185, 2009.
13. S. L. James, "Metal-organic frameworks," *Chemical Society Reviews,* vol. 32, pp. 276–288, 2003.
14. C. Petit, *et al.*, "Reactive Adsorption of Ammonia on Cu-Based MOF/Graphene Composites," *Langmuir,* vol. 26, pp. 15302–15309, 2010.
15. C. Petit and T. J. Bandosz, "Enhanced Adsorption of Ammonia on Metal-Organic Framework/Graphite Oxide Composites: Analysis of Surface Interactions," *Advanced Functional Materials,* vol. 20, pp. 111–118, 2010.
16. E. Biemmi, *et al.*, "High-throughput screening of synthesis parameters in the formation of the metal-organic frameworks MOF-5 and HKUST-1," *Microporous and Mesoporous Materials,* vol. 117, pp. 111–117, 2009.
17. S. S. Kaye, *et al.*, "Impact of Preparation and Handling on the Hydrogen Storage Properties of $Zn_4O(1,4$-benzenedicarboxylate$)_3$ (MOF-5)," *Journal of the American Chemical Society,* vol. 129, pp. 14176–14177, 2007.
18. C. Petit and T. J. Bandosz, "MOF–Graphite Oxide Composites: Combining the Uniqueness of Graphene Layers and Metal–Organic Frameworks," *Advanced Materials,* vol. 21, pp. 4753–4757, 2009.

19. C. Petit and T. J. Bandosz, "The synthesis and characterization of copper-based metal organic framework/graphite oxide composites," *Carbon,* vol. 49, pp. 563–572, 2011.
20. C. Petit and T. J. Bandosz, "MOF/graphite oxide hybrid materials: exploring the new concept of adsorbents and catalysts," *Adsorption,* vol. 17, pp. 5–16, 2011.
21. A. Lerf, *et al.*, "Structure of Graphite Oxide Revisited," *The Journal of Physical Chemistry B,* vol. 102, pp. 4477–4482, 1998.
22. L. Huang, *et al.*, "Synthesis, morphology control, and properties of porous metal-organic coordination polymers," *Microporous and Mesoporous Materials,* vol. 58, pp. 105–114, 2003.
23. Y.-K. Seo, *et al.*, "Microwave synthesis of hybrid inorganic-organic materials including porous $Cu_3(BTC)_2$ from Cu(II)-trimesate mixture," *Microporous and Mesoporous Materials,* vol. 119, pp. 331–337, 2009.
24. R. J. T. Houk, *et al.*, "Silver Cluster Formation, Dynamics, and Chemistry in Metal−Organic Frameworks," *Nano Letters,* vol. 9, pp. 3413–3418, 2009.
25. S. J. Yang, *et al.*, "Preparation and Enhanced Hydrostability and Hydrogen Storage Capacity of CNT@MOF-5 Hybrid Composite," *Chemistry of Materials,* vol. 21, pp. 1893–1897, 2009.
26. C. Hontoria-Lucas, *et al.*, "Study of oxygen-containing groups in a series of graphite oxides: Physical and chemical characterization," *Carbon,* vol. 33, pp. 1585–1592, 1995.
27. T. Szabó, *et al.*, "DRIFT study of deuterium-exchanged graphite oxide," *Carbon,* vol. 43, pp. 3186–3189, 2005.

Chapter 6
Role of Surface Chemistry

The secondary role of porosity in ammonia removal was evidenced above for samples providing weak dispersive forces. An indication that surface chemistry is a controlling factor in this process was also underlined above and is investigated in more detail in this chapter. Surface chemistry can originate from the functional groups of the adsorbent tested and/or from new chemical species introduced to modify the initial adsorbent. In other words, it includes several parameters such as the type and amount of the functional groups and inorganic matter, or the acidity (pH, type/amount of acidic groups) of a material tested. Various techniques are available to evaluate these properties.

This chapter offers a thorough description of the materials surface chemistry as well as its impact on ammonia adsorption. It focuses more specifically on the effects of the materials' acidity, of the presence of oxygen- or sulfur-containing groups and that of inorganic matter.

6.1 Role of Acidity

As mentioned above, a convenient way to retain ammonia is by developing acid–base interactions between the ammonia molecule and the adsorbent surface. That is why a study of the adsorbent acidic properties and their impact on the reactive adsorption of ammonia is considered important. These acidic features include the type, strength and amount of acidic groups present on the adsorbent surface.

One way to assess the acidity of the various samples is the measurement of their surface pH. The surface pH values of the different samples tested are listed in Table 6.1. The composites based on GO and MOF are not presented here since their dispersion in water, required for pH measurement (Chap. 3, Sect. 3.2), causes their collapse [1, 2]. Therefore these kinds of data are not representative of the surface pH experienced by ammonia during adsorption. For the other materials,

Table 6.1 Surface pH and number of groups for the samples studied

Sample	pH	Amount of groups with $pK_a < 7$ (mmol. g^{-1})	Amount of groups with $pK_a > 7$ (mmol. g^{-1})	Total amount of groups (mmol. g^{-1})
CC	7.47	0.14	0.14	0.28
CC-Zn	6.15	–	–	–
CC-Cu1	4.69	–	–	–
CC-Cu2	4.19	–	–	–
CW	6.01	0.27	0.57	0.84
CW-Al	4.15	0.60	0.51	1.11
CW-Zr	3.86	0.34	0.73	1.07
CW-Zr-c	5.13	0.58	1.13	1.71
CW-V	3.15	0.86	1.30	2.16
CW-Mo1	3.74	1.03	0.32	1.65
CW-Mo2	3.82	2.11	0.66	2.77
CS	8.66	0.09	0.22	0.31
CS-Mo1	5.28	1.03	0.29	1.32
CS-Mo2	4.47	1.37	0.40	1.77
CP-1	4.78	0.27	0.24	0.51
CP-1A	3.24	1.27	0.70	2.24
CP-1B	3.55	0.23	0.58	0.81
CP-2	2.79	0.27	0.22	0.49
CP-2A	3.26	0.45	0.65	1.10
CP-2B	3.45	0.19	0.57	0.76
GO	1.93	0.58	1.98	2.56
GP-W	2.20	0.52	3.97	4.49
GP-Mo	2.30	4.80	1.37	6.17

a significant decrease in pH is observed for each series of samples after impregnation or oxidation (except for GO and CP-2). The most dramatic change is found for the CS impregnated carbon with a 4-pH unit decrease for the CS-Mo2 sample. For the other samples, a decrease of about 1–3-pH unit is found. These measurements indicate that the introduction of the inorganic matter and oxidation treatments have a pronounced effect on the acidity of the resulting materials.

As seen in Table 6.1, an overall decrease in pH is associated with an increase in the breakthrough capacity for each series of samples (except for GO and CP-2). Dependence of the breakthrough capacity on pH values for CW, CS and GO before and after impregnation with metal oxides (for CW and CS) or POMs (for GO) is plotted in Fig. 6.1. All these materials were selected on the basis of the similarity in chemical species used for modifications and because they represent a rather large panel of samples which offers more reliable trends. As found in a previous study [3], ammonia breakthrough capacity increases continuously with an increase in the acidity of the adsorbents. The trend is well represented by an exponential fit (correlation factor above 0.9). It is interesting that a steep increase is noticed at pH about 5. This might be related to the dissociation constants of carboxyl acids present on the surface and their reactions with NH_3 (benzoic acid's $pK_a = 4.2$ [4]).

Fig. 6.1 Dependence of ammonia breakthrough capacity on the surface pH for the CW and CS carbons (untreated and impregnated with metal oxides) and for GO, GP-W and GP-Mo materials. Reprinted from Ref. [10], Copyright 2009, with permission from Elsevier
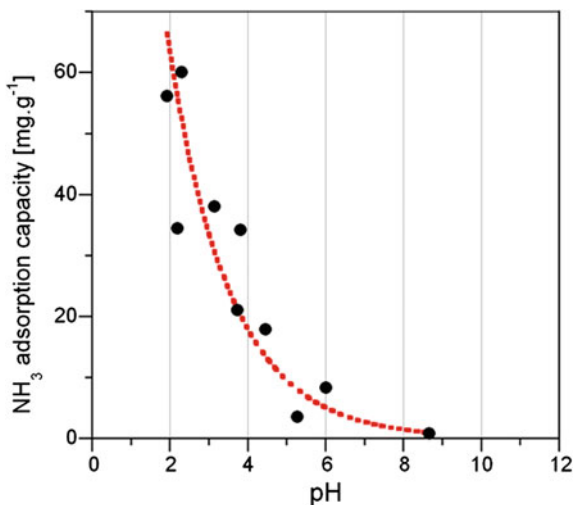
This particular trend is not observed for the other samples containing metal chlorides and oxycations or for the polymer-based carbons. For instance, although CC-Cu1 and CC-Zn are more acidic than the corresponding untreated carbon and show better adsorption capacities, CC-Cu1 has a smaller pH than CC-Zn but adsorbs less ammonia. This lack of direct correlation might not be surprising if one takes into account that surface pH represents the average of the strength and number of acidic groups, and does not distinguish between the two. Moreover, factors other than acid–base interactions can be predominant in the adsorption process on these materials. Complexation is an example [5–9].

To differentiate between the effect of the amount of functional groups and that of their strength, potentiometric titration can be useful. Indeed, using this method, the various groups present on the adsorbent surface are identified by their pK_a (strength) and the amount of each type of group is calculated [11, 12]. The pK_a distributions for the various samples are plotted in Fig. 6.2. For each sample, several peaks can be seen indicating the chemical heterogeneity of the materials' surface. In the case of the non-impregnated samples, these peaks usually correspond to oxygen-containing groups commonly classified as carboxyl groups ($pK_a < 8$) and phenolic groups ($pK_a > 8$) [13]. One can notice that GO-B and GO-H exhibit similar pK_a distribution except in the low pK_a range, where more strongly acidic groups are detected on the surface of GO-H. After impregnation (for the activated carbons) or formation of composites (for GO), new pK_a distributions are observed. A precise assignment of each peak remains impossible since the nature of interactions between the inorganic matter and the carbonaceous "support" is unknown. However, it seems reasonable to think that these new distributions result from the combined effect of the functional groups of the carbon matrix and those of the impregnates. For instance, in the case of CS-Mo and CW-Mo, a new peak at pK_a about 5 can be attributed to $Mo_7O_{24}^{6-}$ or MoO_4^{2-} [14, 15]. The latter species is also observed on the surface of GP-Mo
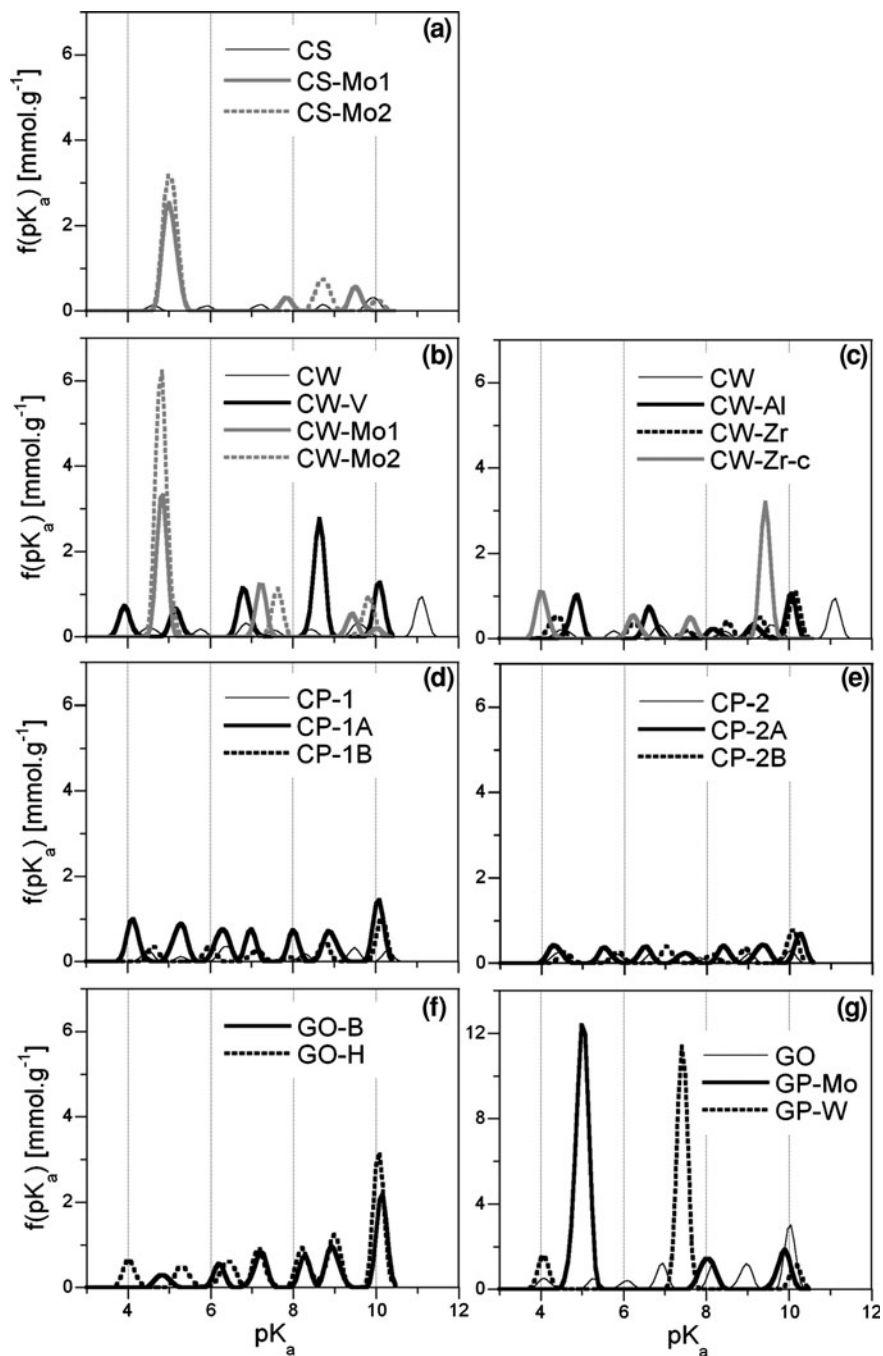
Fig. 6.2 pK$_a$ distributions for various samples before exposure to ammonia

(pK$_a$ about 5) and corresponds to the product of depolymerization of $PMo_{12}O_{40}^{3-}$ [15]. Similarly, the peak at pK$_a$ about 7 on GP-W distribution curve likely results from the presence of WO_4^{2-} (as a result of $PW_{12}O_{40}^{3-}$ depolymerization). It has to be noted that for the GP-Mo and GP-W samples, the Y-axis scale is different from the other samples for the sake of clarity. In the case of CW impregnated with polycations, the new peaks at pK$_a$ about 4.9, 6.5, 9.5 and 10 can be related to (OH)-Al^{IV}, (OH)-Al^{VI} and (OH)-Zr ("IV" refers to tetrahedral and "VI" to octahedral) [16, 17]. The amount of each group (calculated by integration of the area under a peak) is reported for the untreated and modified samples in Table 6.1. It has to be noted that no data are listed for the carbon impregnated with metal chlorides since chlorides, as water soluble species, can be washed out from the surface and can chemically react with the titrant (HCl or NaOH) and thus skew the results. The MOF/GO composites are not presented either for the same reason and/or the reason explained for the pH measurement. Untreated carbons CC and CS have very small amounts of groups, whereas CP-1, CP-2 and CW carbons contain about two to three times more groups. Finally, the highest degree of functionalization among the untreated materials is found for GO. As expected, impregnation and oxidation lead to an increase in the amount of functional groups of strongly acidic (pK$_a$ < 7) and weakly acidic character (pK$_a$ > 7). To analyze the role of the amount and type of functional groups on ammonia retention, we studied the dependence of ammonia breakthrough capacity on the total amount of acidic groups and on the amount of strongly acidic groups. Although no overall correlation was found for all samples studied, a general trend can be observed within each series of samples (except for CW loaded with oxycations): breakthrough capacity increases with an increase in the amount of functional groups. This general trend, which is not linear, is better observed when the total amount of functional groups is considered and not the amount of strongly acidic groups (pK$_a$ < 7). These observations suggest that ammonia retention is not directly influenced by only the strength and amount of functional groups but also by the type of functional groups and their interactions with the ammonia molecule.

The complexity of ammonia interactions with surface species is particularly well-illustrated by comparing the behaviors of CW-Zr and CW-Zr-c samples [10, 18]. For the former sample, adsorption likely occurs via Brønsted acid–base interactions, due to the hydroxyl groups provided by the polycations [19, 20]. For CW-Zr-c, on the contrary, ammonia retention must be governed by Lewis acid–base interactions since the polycations were dehydrated and partially dehydroxylated, leaving only metal oxides for interactions. In dry air (ED), breakthrough capacity of CW-Zr is higher than that of CW-Zr-c due to ammonia preference for Brønsted interactions [21]. In moist air (EM) however, the difference between the breakthrough capacity obtained for CW-Zr and that obtained for CW-Zr-c is reduced. Indeed, water forms Brønsted sites on CW-Zr-c sample in addition to the Lewis sites. This explains that no correlation between the breakthrough capacity and the pH or the amount of groups could be found for this series of samples. More generally, it indicates the importance of considering the types of groups in the ammonia removal process.

6.2 Role of Oxygen-Containing Groups

As evidenced above, the nature of the groups present on the adsorbent's surface can influence ammonia adsorption. It is thus of interest to investigate in more detail the effect(s) of these specific functionalities on the ammonia removal. Several types of groups can be encountered in adsorbent materials, however the predominant ones are with no doubt oxygen-containing groups [22]. This "family" of functionalities includes different types of oxygen-groups of which, only the following are discussed in this section: carboxyl, epoxy and hydroxyl groups. All of them are most of the time incorporated into the surface of carbonaceous adsorbents via an oxidation treatment [23, 24].

6.2.1 Role of Carboxyl Groups

Carboxyl groups are well known for their acidity and it seems natural to believe that they can react with ammonia via acid–base reactions. A first sign of such mechanism was presented in the previous section (Fig. 6.1) where a significant increase in the ammonia retention was observed for the materials with pH below 4.2, which is close to the pK_a of benzoic acid [4].

The ability of these groups to react with ammonia via acid–base reactions is also well-illustrated by the comparison of the FT-IR spectra of samples before and after exposure to ammonia (Fig. 6.3). For instance, the spectra of the initial carbon-based samples (Fig. 6.3a) exhibit various bands at 1715, 1590 and 1190 cm^{-1}. The first band is commonly assigned to C=O vibration in carboxyl groups [25]. The band at 1590 cm^{-1} is related to carbonyl or carboxylate and that at 1190 cm^{-1} to C–O vibration in phenolic groups [25]. After exposure to ammonia, changes in the vibrations bands are observed indicating modifications in the surface chemistry of the sample caused by ammonia adsorption. In particular, the band at 1715 cm^{-1} disappears after the exposure to ammonia in the moist conditions, which is likely due to the reactions of the carboxyl groups with ammonia to form ammonium ions. Similar changes are observed in the carboxyl groups vibration band for the GO samples (Fig. 6.3b). On the GO-H spectrum, C–O vibration appears at 1060 cm^{-1} [26]. Vibration of O–H bond in water and/or oxygen surface groups is observed at 1630 cm^{-1} and C=O vibration from carboxyl and/or carbonyl groups is detected at 1730 cm^{-1} [26, 27]. In addition to these vibrations, two bands are observed: one at 990 cm^{-1} and another at 1230 cm^{-1} with a small shoulder. The first band can be assigned to epoxy/peroxide groups [27]. The second can be related to S=O asymmetric stretching vibration in sulfonic groups [4, 28] and/or vibration of C–O in epoxides [27]. It has to be noted that the symmetric vibration of S=O from sulfonic groups appears at 1060 cm^{-1} as for the vibration of C–O [4, 28]. In the range of higher wavenumbers (3000–3700 cm^{-1}), broad overlapping bands are observed. They must represent the vibrations of O–H in phenol or water [26].
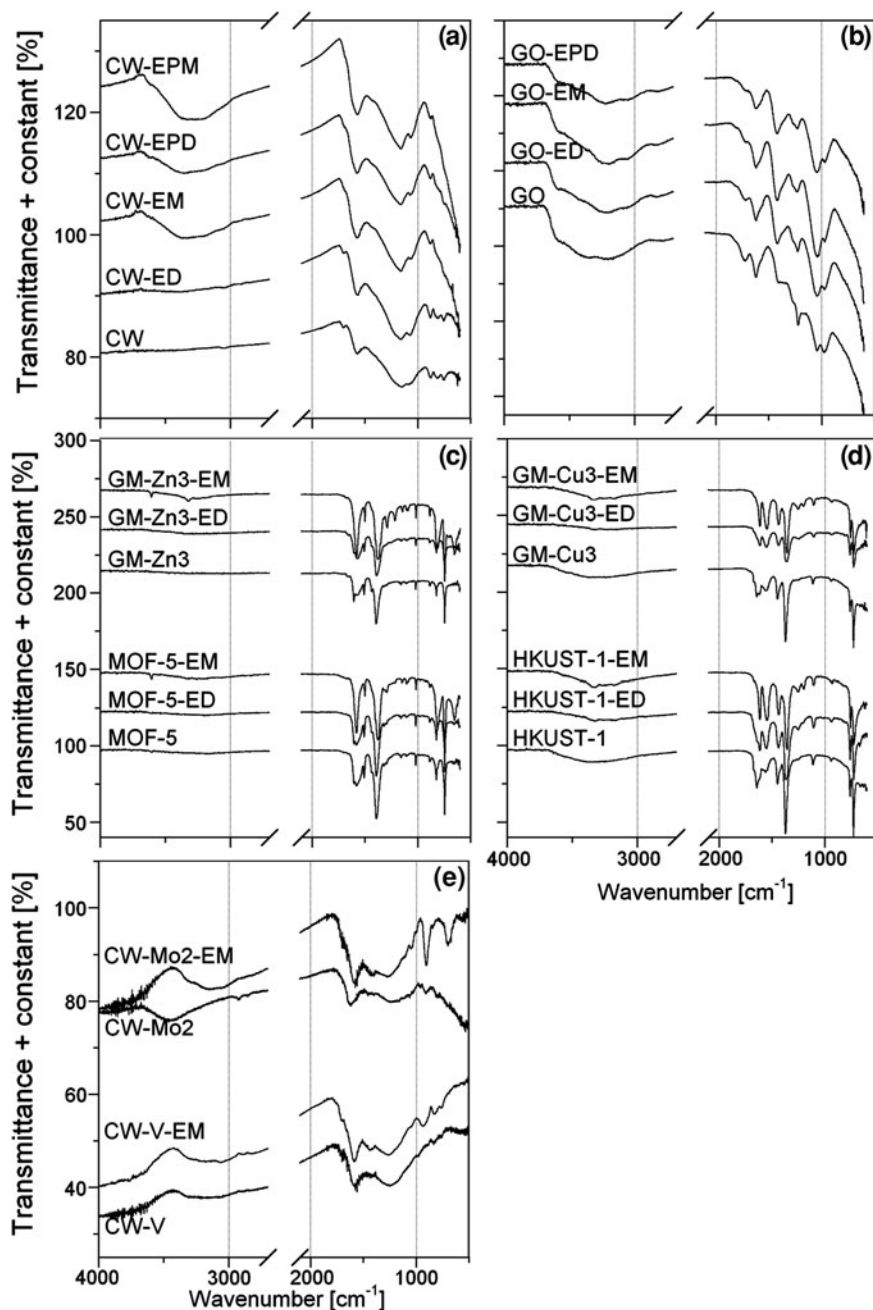
Fig. 6.3 FT-IR spectra of CW carbon (**a**), GO-H (**b**), MOF-based materials (**c**, **d**) and modified CW carbon (**e**) before and after exposure to ammonia

As one can see in Fig. 6.3b, as in the case of activated carbons, ammonia adsorption leads to a decrease in the band at 1730 cm^{-1} suggesting the acid–base reaction between ammonia and carboxyl groups. The formation of ammonium ions as a result of this reaction is supported by the spectra of the exhausted GO sample via the appearance of a new band at about 1410 cm^{-1} for the GO materials, related to N–H vibration in NH_4^+ [29].

Further details and support on the occurrence of acid–base reaction between ammonia and carboxyl groups are provided by the FT-IR spectra of the GM-Zn*n* and GM-Cu*n* samples (Fig. 6.3c, d). The spectra of the initial samples (composites and MOFs) can be divided into two regions. The first one, below 1300 cm^{-1}, shows various bands assigned to the out-of-plane vibrations of the organic ligands (BDC or BTC). The region between 1300 and 1700 cm^{-1} is related to the carboxylate groups of the ligands and is thus indicative of the coordination of these groups to the metallic sites of the MOFs [30]. More precisely, the bands at 1645 and 1590 cm^{-1} and at 1450 and 1370 cm^{-1} correspond to the asymmetric and symmetric stretching vibrations of the carboxylate groups in BDC and BTC, respectively [31–33]. New bands are observed for all exhausted MOFs and composite materials after exposure to ammonia. In the case of MOF-5 and the corresponding composites, new bands appear at 1295, 1220 and 655 cm^{-1}. This is accompanied by more intense bands at 1500 and 1385 cm^{-1} while the initial broad band around 1600 cm^{-1} "is replaced" by a thinner one at 1585 cm^{-1}. New bands appear as well in the high wavenumber range at 3350 and 3190 cm^{-1} and are assigned to ammonia and water vibrations [29]. All of these features are more pronounced for the samples run in the moist conditions. The changes in the region 1350–1600 cm^{-1} can be attributed to modifications in the coordination of the carboxylate groups from BDC to the zinc centers [30]. These modifications are related to the decomposition of the MOF-5 structure with the "release" of the BDC ligands (not coordinated to zinc). Since no band at about 1720 cm^{-1} is observed on the spectrum of the exhausted sample, the presence of the acidic form of BDC is excluded [34]. This suggests that ammonia might be interacting with the carboxylate groups of BDC. A similar analysis can be made for HKUST-1 and its composites. New bands are observed at 1620, 1255 and 1215 cm^{-1} and a broadening of the bands at 1450, 1370 and 730 cm^{-1} is seen with an increase in the intensity of the band at 1560 cm^{-1}. The latter feature is assigned to a change in the coordination of the carboxylate ligands from BTC [30]. Moreover, the appearance of the thin band at about 1620 cm^{-1} and the ones at about 1255 and 1215 cm^{-1}, as well as the broadening of the bands at 1370 and 1450 cm^{-1}, suggest the presence of BTC "alone" (not coordinated to copper) [35]. Once again, the absence of the band at about 1720 cm^{-1} excludes the presence of the acidic form of BTC [36, 37]. The progressive changes in the spectra of the materials upon the exposure to ammonia are illustrated in Fig. 6.4, which collects the spectra of HKUST-1 exposed to ammonia and taken at different time intervals. As seen, the more ammonia is supplied to the system, the more the alterations become visible in the vibrations and they are directly related to the changes in the structure of the material. More precisely, after about 5 minutes of exposure,
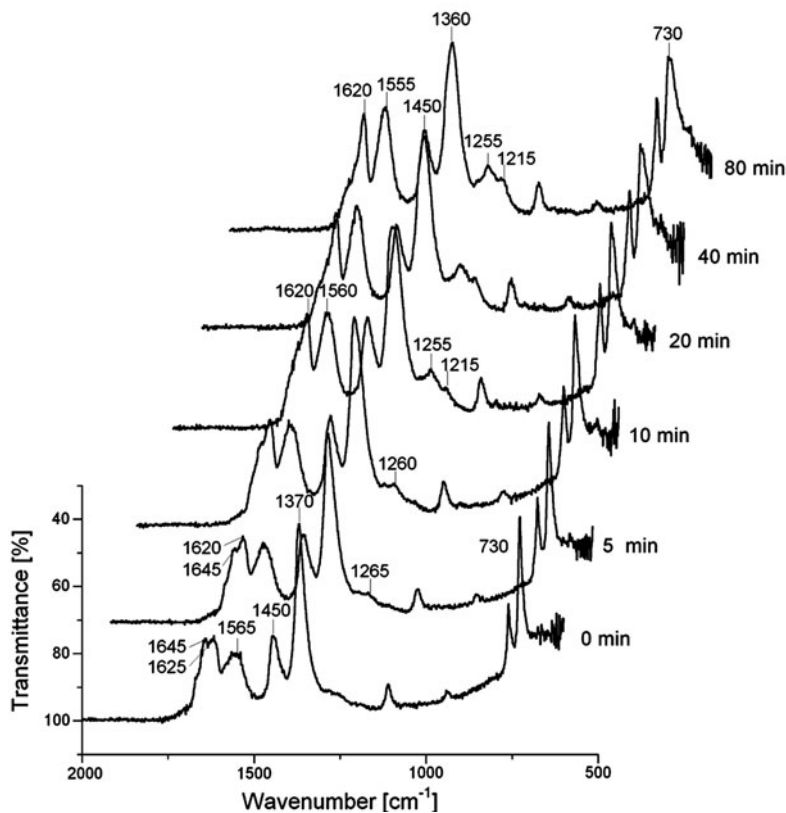
**Fig. 6.4** FT-IR spectra of HKUST-1 exposed to ammonia and taken at different time intervals

the spectrum of HKUST-1 is only slightly modified suggesting that at that time, the MOF network is not visibly affected by the presence of ammonia. This is in accordance with the fact that ammonia molecules first coordinate to the copper centers of the MOF as do water molecules. This is evidenced by a first change of color of the bed as explained later in this chapter [38, 39]. After 10 minutes, the changes are better visible and the asymmetric vibrations of the carboxylate group (1550–1650 cm^{-1}) become more intense, where the symmetric vibrations for the same functionality (1350–1450 cm^{-1}) broaden and their intensity slightly decreases. This indicates that the symmetry of the carboxylate groups (related to the bridging configuration of the COO in the MOF) is progressively lost and a less symmetric configuration linked to monodentate carboxylates is adopted [40]. Another interesting feature is the appearance of a new band at about 1260 cm^{-1} related to C–OH vibration in carboxylate-based species [41]. This suggests that ammonia is now interacting (via the hydrogen atom) with the carboxylate groups, causing the transition from the bridging to the monodentate configuration. All these features indicate the collapse of the MOF network and explain the
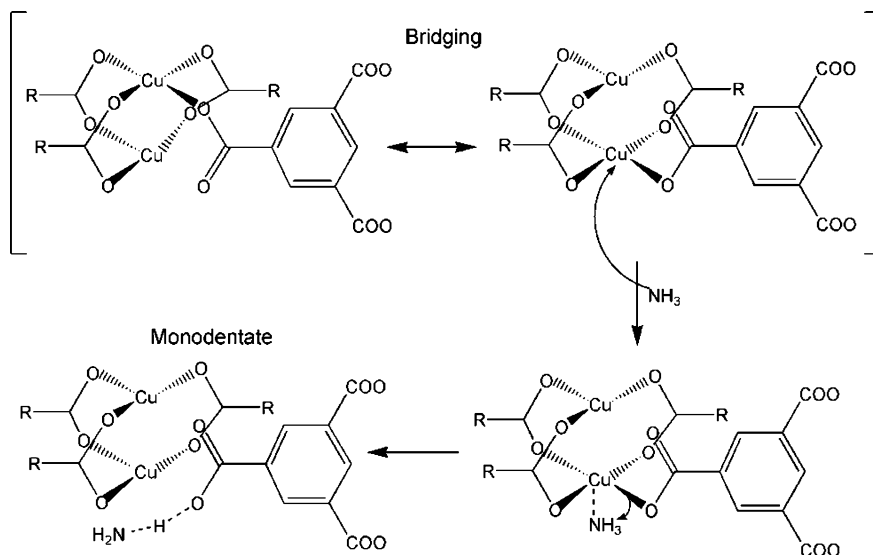
Fig. 6.5 Proposed mechanism of ammonia interactions with HKUST-1

appearance of the second color change of the adsorbent (explained in this chapter). A reaction mechanism proposed to illustrate the above-discussed results is presented in Fig. 6.5. In this proposed mechanism, the delocalized structure of the MOF, indicating that the oxygen atoms of the carboxylate groups (from BTC) are equivalent, is justified by the fact that no band from the corresponding acid is present (usually seen at about 1700 cm^{-1} [36, 37]). The intensification of the asymmetric bands, the broadening of the symmetric bands and the appearance of the C–OH vibration band become more pronounced as more ammonia is supplied to the system. This is related to the fact that more of the material is decomposed. After about 40 minutes, which is close to the breakthrough point, no further changes are observed since almost all the adsorbent has reacted with ammonia. These observations are also visible in the different color of the material at the end of the breakthrough tests compared to the color of the fresh adsorbent. Indeed, during the adsorption tests, the materials color changes from dark blue to a Cyan blue and then to Maya blue as seen in Fig. 6.6. The first color change is assigned to the coordination of ammonia to the copper site and is discussed in more detail in Sect. 6.4 [38, 39]. The second color change indicates modifications in the Cu–Cu vibration [39]. This perturbation is likely related to the formation of a new copper-based complex resulting from the decomposition of the MOF caused by the interactions between ammonia and the organic ligand [39].

All of these indicate the enhancement in ammonia adsorption via its acid–base reaction with carboxyl groups. Figure 6.7a shows the details of ammonia reaction with carboxyl groups. Other mechanisms are also presented in this figure and they will be discussed later.
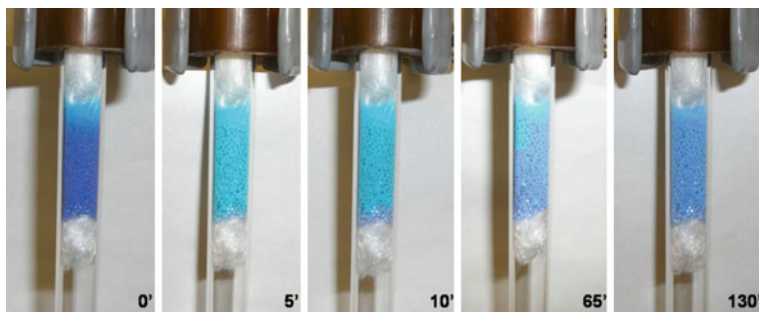
Fig. 6.6 Color changes in HKUST-1 during ammonia adsorption with the progress of adsorption. Reprinted with permission from Ref. [39]. Copyright 2010, American Chemical Society

Not only do carboxyl groups react with ammonia via acid–base reaction but they are also involved in the formation of amides incorporated into the adsorbent's surface. This latter mechanism is of special interest since it enables the "immobilization" of ammonia on the adsorbent and thus prevents its gradual desorption from the surface. This specific process was evidenced in the case of ammonia adsorption on GO material prepared by the Brodie method as explained below [42].

GO-B was analyzed by XPS before and after exposure to ammonia. The XPS deconvoluted spectra of C1s, O1s and S2p for the fresh material are presented in Fig. 6.8, while the spectrum of N1s obtained after exposure to ammonia is presented in Fig. 6.9. Tables 6.2, 6.3 provide the elemental composition of the sample and the chemical states of various atoms (along with their relative percentage and binding energy), respectively. Data for other samples are also included but will be discussed in more detail later. The analyses indicate two types of oxygen with binding energies at 533.0 and 535.0 eV (O-II and O-III) on the surface of the GO-B sample. They are linked to oxygen in C–O configuration (epoxy, phenol or carboxyl groups) and oxygen in water or chemisorbed oxygen species, respectively [43, 44]. The C1 s spectrum consists of peaks at 285.8, 287.4 and 289.3 eV assigned to C–C, C–O and O–C=O groups, respectively [43, 45–47]. As seen in Tables 6.2, 6.3, after ammonia adsorption, nitrogen is detected on the surface of GO-B and its amount consists of 1.1 wt%. The latter amount represents about 60% of the total ammonia adsorbed, which is significant but likely even lower than the actual value. Indeed, one has to consider the limited inaccuracy of the XPS method (only the material's surface is studied) and the fact that only a small amount of ammonia is desorbed during outgassing (Chap. 8). Deconvolution of the N1s spectra (Fig. 6.9) for the exhausted samples shows two peaks with their binding energies equal to 399.8 and 401.9 eV (Table 6.3). The first peak represents nitrogen involved in C–N (from amines and/or amides), whereas the second peak can be assigned to C–N$^+$ (from quaternary nitrogen) or NH$_4^+$ [48–50]. All of these indicate that ammonia is converted into new compounds strongly retained on the surface of GO-B or is incorporated to it via reactive adsorption/chemisorption.
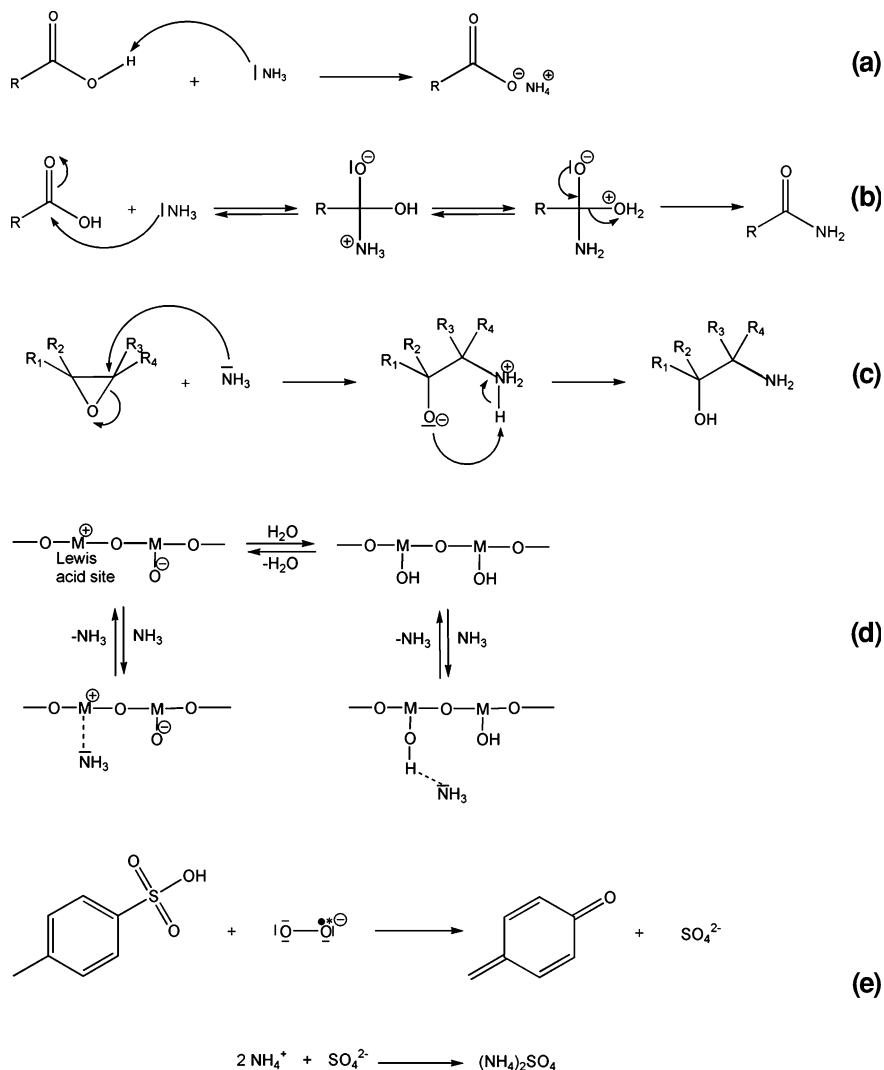
Fig. 6.7 Reactions between ammonia and the functional groups present on the adsorbents' surface (M = metal)

Moreover, as evidenced from the data collected in Table 6.3, the relative contributions of other functional groups change for the exhausted samples. The most significant change is the decrease in the percentage of carboxyl groups (O–C=O) noticed after exposure to ammonia. An explanation for this can be the reaction of ammonia with carboxyl groups leading to the formation of amides. This is supported by the formation of C–N bonds detected by XPS analyses, as described
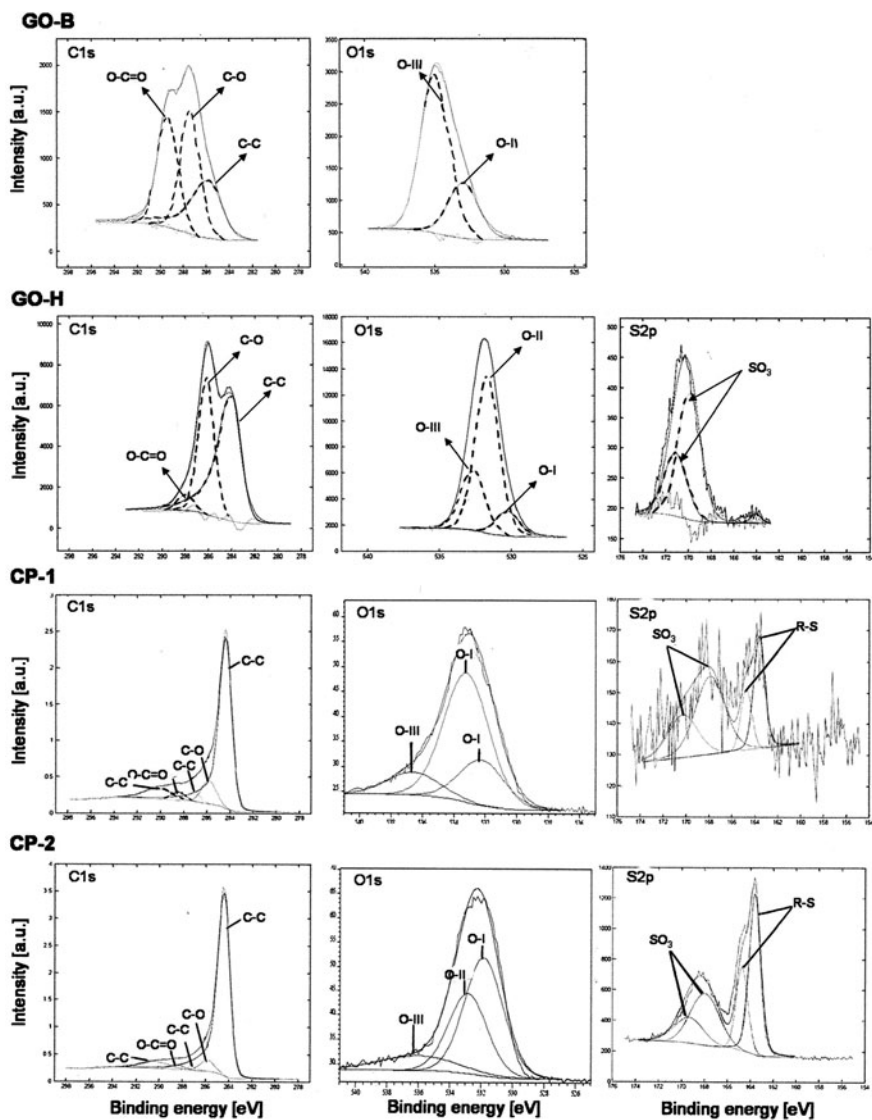
Fig. 6.8 XPS spectra of C1s, O1s and S2p for the graphite oxide and activated carbon samples before exposure to ammonia

above. The deconvolution curves for O1s confirm the decrease in the amount of carboxyl groups as seen by the disappearance of the peak at 535.0 eV (O-III). The mechanism leading to the amide formation is shown in Fig. 6.7b.
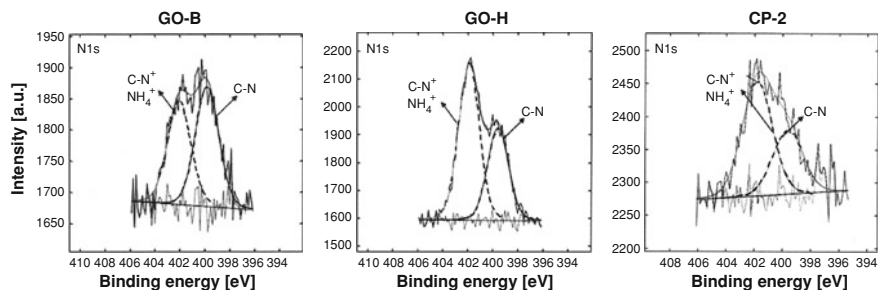
Fig. 6.9 XPS spectra of N1s for the graphite oxide and activated carbon samples after exposure to ammonia

Table 6.2 Elemental composition of graphite oxide and activated carbon samples before and after exposure to ammonia determined by various methods (in wt%)

Sample	Elemental analysis				EDX analysis			XPS analysis			
	C	O	N	H	C	O	S	C	O	N	S
GO-B	59.2	38.3	<0.5	2.5	66.6	33.4	0	63.0	37.0	0	0
GO-B-ED	–	–	–	–	–	–	–	65.7	33.2	1.1	0
GO-H	46.9	50.6	<0.1	2.5	61.5	35.1	3.4	58.7	39.4	0	1.9
GO-H-ED	–	–	–	–	–	–	–	57.9	38.0	2.2	1.9
CP-1	–	–	–	–	86.7	13.3	0	87.4	12.1	0	0.5
CP-1A	–	–	–	–	80.3	19.7	0	–	–	–	–
CP-1B	–	–	–	–	84.4	15.6	0	–	–	–	–
CP-2	–	–	–	–	82.4	6.5	11.1	83.6	9.3	<0.1	6.7
CP-2-EM	–	–	–	–	–	–	–	80.8	11.8	1.0	6.4
CP-2A	–	–	–	–	81.1	10.8	8.1	–	–	–	–
CP-2B	–	–	–	–	84.9	10.5	4.7	–	–	–	–

6.2.2 Role of Epoxy Groups

Epoxy groups also play a role in ammonia retention as observed in the case of ammonia removal using the GO material [42]. The FT-IR spectrum of the GO-H sample before exposure to ammonia was presented and described above (Fig. 6.3). After exposure to ammonia, changes in the vibration bands, other than those described previously for the carboxyl groups, are observed. A decrease in intensity is noticed for the band at about 1230 cm^{-1} (related to C–O and/or C–S vibrations). This decrease can be related to the reaction of ammonia with epoxy groups leading to the formation of amine [27]. Moreover, the broadening of the band at 1630 cm^{-1} indicates the formation of OH groups [4, 29]. The latter remark supports the formation of amines via the reaction of NH_3 with epoxy groups since this reaction implies the formation of OH groups [42]. The reaction mechanism is presented in Fig. 6.7c. In the range of higher wavenumbers (2800–4000 cm^{-1}),

Table 6.3 Chemical states of C, O, N and S atoms in graphite oxide and activated carbon samples before and after exposure to ammonia, with their relative concentration (in %) and binding energy (in parenthesis, in eV)

Sample	C–C	C–O	C=O	O–C=O	O-I	O-II	O-III	R-S	SO$_3$	SO$_4$	C–N	C–N$^+$, NH$_4^+$
GO-B	30.0 (285.8)	36.8 (287.4)	–	33.2 (289.3)	–	26.5 (533.0)	73.5 (535.0)	–	–	–	–	–
GO-B-ED	20.8 (285.6)	76.6 (287.4)	–	2.6 (289.8)	18.9 (531.4)	81.1 (532.8)	– (–)	–	–	–	53.6 (399.8)	46.4 (402.0)
GO-H	57.1 (284.4)	38.5 (286.6)	–	4.4 (288.5)	10.3 (530.8)	65.2 (532.2)	24.5 (533.2)	–	100 (168.1)	–	–	–
GO-H-ED	44.6 (284.8)	48.0 (286.9)	–	7.4 (288.8)	16.6 (530.8)	71.8 (532.2)	11.6 (533.1)	–	– (–)	100 (168.4)	37.5 (399.6)	62.5 (401.9)
CP-1	86.0 (284.4)	10.2 (286.0)	–	3.8 (288.5)	22.7 (532.2)	64.3 (533.2)	12.8 (536.6)	50 (163.6)	50 (167.9)	–	–	–
CP-2	92.4 (284.4)	5.5 (285.8)	–	2.1 (288.4)	51.9 (531.8)	35.1 (532.8)	13.0 (536.0)	57.1 (163.6)	42.9 (168.0)	–	–	–
CP-2-EM	97.4 (285.5)	1.3 (286.7)	–	1.3 (288.7)	22.8 (531.3)	70.9 (532.9)	6.3 (535.9)	53.8 (163.8)	15.4 (166.7)	30.8 (168.6)	33 (399.6)	67 (401.8)

broad overlapping bands are visible. They represent the vibrations of O–H (phenol) and N–H (NH_4^+, NH_3, NH_2) [4, 26, 29, 51]. The large increase in the intensity of the overlapping bands between 3100 and 3700 cm^{-1} after exposure to ammonia, even though the experiment was run in the dry conditions, supports the reaction of ammonia with epoxy groups leading to the formation of hydroxyl groups whose vibrations are in this range.

The formation of amine as a result of ammonia reaction with the epoxy groups of GO-H is supported by XPS analyses. Indeed, as can be seen in Fig. 6.9 and Table 6.3, a peak with a binding energy of 399.6 eV related to C–N bonds is observed on the surface of the exhausted sample. This binding energy can be related to C–N in amines or amides groups [48–50]. Since no nitrogen was present in the initial material (Table 6.2), it suggests that ammonia reacted with the functionalities of GO-H.

X-ray diffraction analysis brings additional evidence for the formation of amines via reaction with epoxy groups. Figure 6.10 presents the X-ray diffraction patterns of GO-H before and after the exposure to ammonia. As one can see, the d_{002} distance (related to the distance between the graphene layers) decreases after ammonia adsorption. This phenomenon is unexpected since an intercalation of ammonia between the graphene layers (and thus the increase in the d_{002} distance) is usually observed on GO materials prepared by the Brodie method [52]. A possible explanation for that behavior would be the ring opening caused by the reaction of epoxy groups with ammonia. Indeed, epoxy groups are thought to cause the wrinkled texture of GO by inducing a bending in the graphene layers [53, 54]. Thus, when epoxy groups react with ammonia, the ring strain is released. This may lead to a more "flat" surface and a more efficient stacking of the layers. Figure 6.7c shows the reaction between GO epoxy groups and ammonia with the subsequent formation of amine and hydroxyl groups.

6.2.3 Role of Hydroxyl Groups

First, it has to be noted that hydroxyl groups can be present on the surface of the adsorbent itself but can also originate from the metal oxides used to modify the samples. The influence of these groups on the ammonia removal can be more subtle to detect than for the previous two types of groups. This is because ammonia usually interacts with OH functionalities via weak forces [21]. Indeed, with hydroxyl groups, the main mechanism one can envision is hydrogen bonding. The lone pair of electrons on ammonia can interact with the hydrogen atom of OH and in the same way the lone pair of electrons on OH can interact with the hydrogen atoms of NH_3. A "proof" of this ability to form hydrogen bonds is the high solubility of ammonia in water. Since hydrogen bonds are rather weak for these two mechanisms (between 10 and 30 kJ mol^{-1} [21]), ammonia is only weakly retained on OH groups and most of it is likely removed from the adsorbent's surface during air purging.
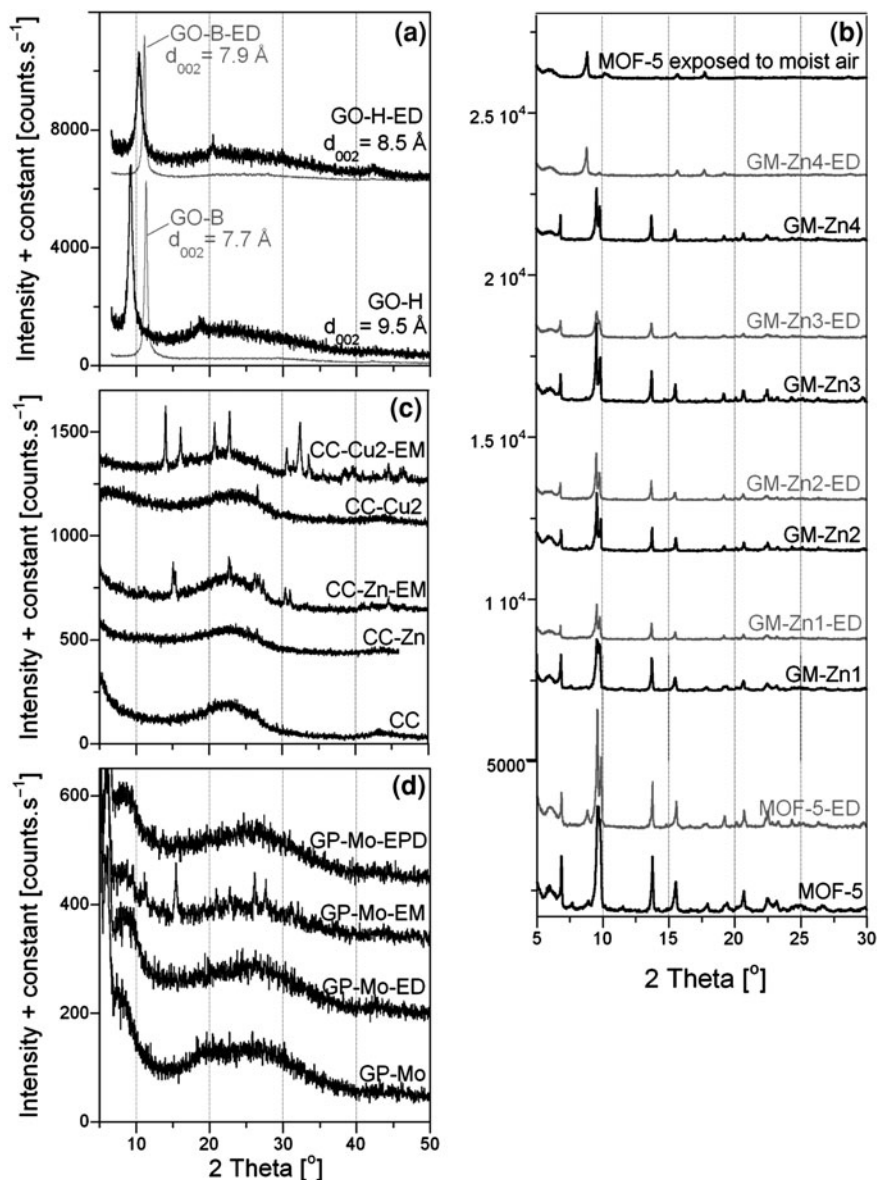
Fig. 6.10 X-ray diffraction patterns for graphite oxide (**a**), graphite oxide/MOF composites (**b**), modified activated carbons (**c**), and graphite oxide/POMs composites before and after exposure to ammonia

Despite all of these, two of the samples studied provide an indirect indication of the role of hydroxyl groups in the ammonia retention [18]. These samples are the modified activated carbons CW-Zr and CW-Zr-c [18]. As mentioned previously

Table 6.4 Exchange capacities and breakthrough capacities of sulfonated resins tested for ammonia removal in moist conditions	Sample	Exchange capacity (mmol g^{-1})	NH$_3$ breakthrough capacity (mmol g^{-1})
	R1	7.1	6.2
	R2	8.0	8.6

(Sect. 6.1), the former material contains several hydroxyl groups (i.e. those from the polycations used for the modification) whereas for the latter material, many of those groups have been removed as a result of the calcination process. As underlined before (Sect. 6.1), the breakthrough capacity of CW-Zr is higher than that of CW-Zr-c in the dry conditions. This is explained by the enhancement of adsorption via hydrogen bonding for CW-Zr. In the moist conditions however, the performance of the two samples is similar. This is related to the fact that, in the presence of water, the oxides on CW-Zr-c become protonated, which favors the hydrogen bonding of ammonia. These various mechanisms are presented in Fig. 6.7d.

6.3 Role of Sulfur-Containing Groups

Sulfur-containing functionalities, although less frequent than their oxygen counterparts, are sometimes encountered on the surface of carbonaceous materials [22]. These groups usually come from the precursor used to derive the carbon materials [22]. Sulfur-containing groups can take various forms such as sulfonic, thiophenic, sulfide, disulfide, thioquinone and thioloactone [22]. The influence of the former two types of groups on ammonia removal is discussed in the following two sections.

6.3.1 Role of Sulfonic Groups

As carboxyl groups, sulfonic groups can react with ammonia via acid–base reaction leading to the formation of ammonium ions. This predictable outcome can be however difficult to detect on the adsorbents tested. This is related to the fact that many materials containing sulfonic groups also bear carboxyl functionalities. Owing to the similar acid–base properties of these two groups, their effects on ammonia adsorption become hardly distinguishable. Nevertheless, the study of ammonia adsorption on sulfonated gel resins can somehow support the above. The exchange capacities and ammonia adsorption capacities of the two sulfonate resins, R1 and R2, are listed in Table 6.4. As seen in this table, the amount of ammonia adsorbed is very close to that of exchangeable protons, suggesting that

ammonia (in the form of NH_4^+ since experiments were conducted in moist conditions) interact with the functional groups present.

Besides their acidic properties, sulfonic groups also participate in the enhancement of ammonia reactive adsorption on the carbonaceous adsorbents via the formation of ammonium sulfate. This mechanism is observed on materials with relatively high oxygen contents such as the GO-H and CP-2 series of samples [42, 55]. As seen in Table 6.2, the oxygen content in the polymer-based carbons CP-2 ranges from 6 to 11 wt% depending on the oxidation treatment (twice less than for the CP-1 series) while it is about 50 wt% for GO-H sample. In both cases, several types of oxygen groups are detected on the surface of the materials. They include oxygen in C=O configuration (O-I, carbonyl, carboxyl), in C–O configuration (O-II, phenol, epoxy, carboxyl) and in water or chemisorbed oxygen species (O-III) [43, 44]. Sulfur is also detected on the GO-H sample and CP-2 series of materials. Its amount reaches to about 2 wt% for GO-H and between 5 and 11 wt% for the CP-2 samples depending on the preparation method (Table 6.2). On the contrary, the CP-1 samples contain only trace amounts of sulfur. The results of XPS analyses indicate that sulfur is in the form of sulfonic groups (SO_3) for GO-H sample, whereas both sulfonic (SO_3) and thiophenic (R-S) functionalities are present on the surface of CP-1 and CP-2 samples [56–58]. The C1s, O1s and S2p XPS spectra for the fresh GO-H, CP-1 and CP-2 samples are displayed in Fig. 6.8. After exposure to ammonia, XPS analyses of the exhausted GO-H and CP-2 samples were performed and the results obtained are collected in Tables 6.2, 6.3. For both exhausted samples, changes in the relative amounts of each oxygen groups are noticed especially for the CP-2 sample. This suggests that the reactive adsorption of ammonia on the surface of these adsorbents takes place. Another interesting feature is the conversion of a part of (for CP-2) or all of (for GO-H) the sulfonic groups into sulfates (SO_4). This is indicated by a shift in the S2p peak towards higher binding energies [59]. In the case of GO-H, the formation of sulfates is further supported by analyzing the filtrate of a GO-H-ED/deionized water suspension with $BaCl_2$. Briefly, a suspension of GO-H-ED and deionized water was stirred overnight, and then filtrated. $BaCl_2$ was then added to the filtrate and formation of a white precipitate of $BaSO_4$ was observed. The presence of sulfate can be explained if one takes into account the presence of superoxide anions O_2^{-*} on the surface of GO-H and CP-2 samples. Indeed, previous findings demonstrate that in the presence of C–O-C (epoxy) or C = O (carbonyl) groups on carbon, O_2 is converted into O_2^{-*} [60–62]. Besides, this phenomenon is favored in the presence of nitrogen atoms on the surface of carbon, which is the case for the exhausted GO-H and CP-2 samples since XPS analyses show the incorporation of ammonia into their structure (see Tables 6.2, 6.3 and Fig. 6.9) [60–62]. The superoxide anion O_2^{-*} is then able to react with the sulfonic groups present on the surface of the materials and cleave the C–S bond to form SO_4^{2-}. The sulfates are then free to react with ammonia, which is continuously supplied to the system. The presence of ammonium ions on the surface of the exhausted samples is also found by XPS analyses (Table 6.3 and Fig. 6.9). Once again, XPS analyses indicate the strong retention of ammonia on the samples tested. Figure 6.7e illustrates the mechanisms leading to the formation of ammonium sulfate. It has to be noted that in the latter reaction, the benzene ring and the carbon atom connected to it (in para

position of the sulfonic acid functionality) are considered as part of the carbon structure of the adsorbent.

The oxidation of sulfonic groups and the subsequent formation of ammonium sulfates can explain the enhanced ammonia adsorption on GO-H and CP-2 compared to their counterpart materials (GO-B and CP-1) deprived (or with only trace amounts) of sulfonic groups. For instance, the adsorption capacities of the CP-1 and CP-2 samples significantly differ in the dry conditions whereas they are similar in the moist conditions. Taking into account that these samples have the same amounts of acidic groups and especially the same amounts of strongly acidic groups (Sect. 6.1), and that the porosity (and microporosity) of CP-1 is higher than that of CP-2 (Chap. 5, Sect. 5.1), the trend found for the data obtained in the dry conditions suggests that another parameter must affect the ammonia adsorption. This parameter can be the presence of sulfonic groups in the CP-2 sample. Moreover, when no (or a small amount of) sulfonic groups are present on the surface, the adsorption capacities seem to be governed by the oxygen groups [63, 64]. This is seen when the CP-1B and CP-2B samples are compared. These two samples, which have similar distributions of functional groups and no sulfonic groups (removed by heat treatment [55]), show the same trends towards the ammonia retention in both dry and moist conditions. A rigorous comparison between the CP-1A and CP-2A samples is not possible due to the much higher amount of functional groups on the surface of CP-1A (Sect. 6.1). Nevertheless, it is worth noticing that the adsorption capacities of CP-1A are not much higher those ones of CP-2A despite the high amount of functional groups on the surface of the former material. This is another support for the enhancing effect of sulfonic groups in ammonia retention.

6.3.2 Role of Thiophenic Groups

Unlike sulfonic groups, thiophenic functionalities do not seem to have any impact on ammonia adsorption. This is suggested by studying the polymer-based carbons [55]. For the CP-2 series, in dry conditions, the best performance is found for CP-2A followed by CP-2 and then CP-2B. Despite its larger amount of oxygen groups (and similar amount of acidic groups) and higher porosity (and volume of micropores), CP-2B adsorbs less ammonia than CP-2. This behavior is different from that of the CP-1 series where CP-1 and CP-1B show the similar breakthrough capacities. As neither the oxygen-containing groups nor the porosity seem to be a key element to explain this trend, the sulfur-containing group should be analyzed. On the CP-2 sample both sulfonic and thiophenic functionalities are detected (Table 6.3). On the contrary, for the CP-2B sample, only thiophenic groups are present since the heat treatment applied during oxidation causes the removal of the sulfonic groups [55]. All of these suggest that sulfur-containing groups in the form of sulfonic groups (CP-2) enhance ammonia retention, whereas the R-S groups (CP-2B) lead to a decreased performance.

Given the similarity between hydroxyl groups and thiol functionalities, one could expect the presence of hydrogen bonding between –SH groups and N. However, such interactions involve a very weak binding energy, even weaker than in the case of –OH groups [65]. Consequently, if the presence of hydrogen bonding between –SH and ammonia cannot be ruled out, it likely does not account for the strong retention of NH$_3$ on the adsorbent surface.

6.4 Role of Inorganic Matter

The inorganic matter which, in the case of the materials studied, is limited to metal oxides, metal chlorides, polyoxometalates and metallic species in MOFs, can influence the removal of ammonia from air [5–7, 9, 18, 39, 66]. Nevertheless, the extent of such an effect as well as the nature of interactions between ammonia and inorganic matter greatly depends on the nature of the inorganic compound considered. Considering the materials tested, three types of interactions can be identified (Lewis, hydrogen bonding, complexation) and are described in this section.

6.4.1 Lewis Interactions

Ammonia molecule can be considered as a Lewis base owing to its lone pair of electrons. Metals, on the other hand, can act as Lewis acids [67]. For these reasons, it is easy to envision Lewis acid–base interactions between ammonia molecules and metals deposited on the surface of adsorbents. Nevertheless, as in the case of hydrogen bonding, the energy of such interactions is often very weak [21]. Upon air purging, most of the ammonia involved in Lewis acid–base interactions is likely released from the surface and the detection of ammonia on the surface of the exhausted samples can thus be impaired.

FT-IR spectroscopy is often employed to identify ammonia adsorbed on Lewis acidic sites [29]. Although this technique was used to characterize many of our exhausted samples, the specific detection of ammonia involved in Lewis interactions remains difficult. The reasons for this are that: (i) only small amount of ammonia involved in Lewis interactions must be present making its detection difficult, and (ii) the vibration band of ammonia adsorbed on Lewis sites appears in the same region as physisorbed ammonia and carboxyl groups (which are commonly found in our materials) [4, 29].

Whereas evidence of ammonia interacting with Lewis acids is hardly obtained via "regular" analytical methods in the case of modified activated carbons, the visualization of this process becomes straightforward for some MOF materials with unsaturated metallic sites (and the derived composites as well) [39]. Example of such MOF is HKUST-1 which contains the unsaturated copper sites that can act as Lewis acids [68]. Under ambient conditions, these centers are coordinated to water and the

Fig. 6.11 Pictures of
HKUST-1 before (*left*) and
after a 5-min exposure to
ammonia (*right*), and
visualization of the Lewis
interactions between
ammonia and the copper sites
of HKUST-1 (*grey* carbon,
red oxygen, *blue* copper).
Reprinted with permission
from Ref. [39]. Copyright
2010, American Chemical
Society
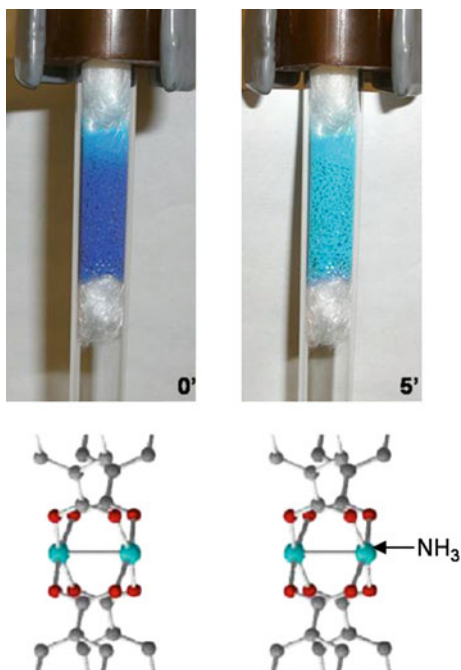
resulting material has a light blue color. Upon drying, water molecules are removed
and the MOF adopts a much darker blue color linked to the change in a vibration of
the copper–copper bond [69]. Upon the exposure to ammonia, the material turns back
to its original light blue color owing to the coordination of ammonia to the copper
centers [38]. This was clearly seen when both HKUST-1 and the derived composites
were tested for ammonia adsorption [39]. The pictures of the bed with color changes
are presented in Fig. 6.11 together with a schematic representation of the interactions
taking place.

6.4.2 Hydrogen Bonding

The evidence that metallic species can enhance ammonia adsorption via hydrogen
bonding was discussed in Sect. 6.2. In the case of the samples modified by the
addition of the metallic species (CW-Mo1, CW-Mo2, CW-V, CS-Mo1,
or CSMo2), hydrogen bonding originates from the hydroxyl groups present in
metal oxides deposited on the surface of activated carbons.

Such interactions are also encountered in the case of ammonia adsorption on
MOF-5 and its composites with GO [66]. Indeed, the metallic component of the MOF
is made of zinc oxide tetrahedra able to interact with ammonia. Figure 6.10 shows

the X-ray diffraction patterns of MOF-5 and the composites before and after the exposure to ammonia. The pattern of MOF-5 after a prolonged contact with moisture is also presented. After the exposure to ammonia, the splitting of the peak at 2 Theta 9.78° becomes more pronounced. For GM-Zn3-ED, this peak is even slightly shifted toward lower angles, but the overall pattern is preserved. In contrast, for GM-Zn4-ED, the spectrum is completely modified and shows features similar to those of the spectrum of MOF-5 exposed to humid air. These observations indicate that ammonia retained on the composites leads to a distortion of the structure of the MOF-5 component. This distortion is the greatest for GM-Zn3-ED, and it leads to a complete collapse of the structure for GM-Zn4-ED, which is also observed in the spectrum when MOF-5 is exposed to water [70]. The collapse of the MOF structure upon an exposure to humidity has been described by Greathouse and Allendorf [1]. They found that the destruction of the MOF network was caused by: (i) the "replacement" of the oxygen atoms in the zinc oxide tetrahedra by the oxygen atoms from water and (ii) hydrogen bonding between the hydrogen atoms in water and the oxygen atoms in the zinc oxide tetrahedra. Given its similarity with water, ammonia can induce the formation of hydrogen bonds and leads to the progressive collapse of the MOF structure. The decomposition of the MOF-5 component is also detected by nitrogen adsorption analyses which indicate that most of the porosity of the material is lost after the exposure to ammonia [66]. Although in the case of MOF-5 and GM-Znn composites, hydrogen bonding ensures an enhanced adsorption of ammonia, it also prevents any regeneration of the exhausted adsorbents since the decomposition of the MOF structure is an irreversible phenomenon.

6.4.3 Complexation

Many transition metal complexes involve ammonia as a ligand. Consequently, it seems natural to envision the formation of complexes involving ammonia when metallic species are present on the surface of adsorbents. Such a phenomenon is for instance observed in the case of activated carbon or graphite oxide impregnated with metallic species (metal oxides, metal chlorides or polyoxometalates) [5–7, 9].

Figure 6.3 shows the FT-IR spectra of several samples before and after exposure to ammonia. As seen in Fig. 6.3e, new bands are detected at 1430, 940 and 840 cm^{-1}, on the surface of the CW-V sample after the exposure to ammonia. The peaks correspond to the vibrations of NH$_4^+$, V=O and V–O–V in ammonium vanadate (NH$_4$VO$_3$) [29, 51, 71, 72], and confirm the formation of a new product. Similarly, the FT-IR spectra for CW-Mo2 show new bands after ammonia adsorption at 1420, 910 and 710 cm^{-1}. These bands, related to the vibration of NH$_4^+$, Mo=O and Mo–O–Mo, indicate the presence of ammonium molybdate ((NH$_4$)$_6$Mo$_7$O$_{24}$) [29, 51, 73]. All of these suggest that the reactive adsorption of ammonia occurs via complexation. Other signs of complexation are found for the CC carbon. X-ray diffraction patterns, plotted in Fig. 6.10, provide an evidence for the reactive adsorption on its surface. Whereas for the initial samples, only a broad hump related to the presence of amorphous carbon is

Fig. 6.12 DTG curves before and after exposure to ammonia for the CC carbon impregnated with copper chloride (**a**) and zinc chloride (**b**). Reprinted from Ref. [10], Copyright 2009, with permission from Elsevier
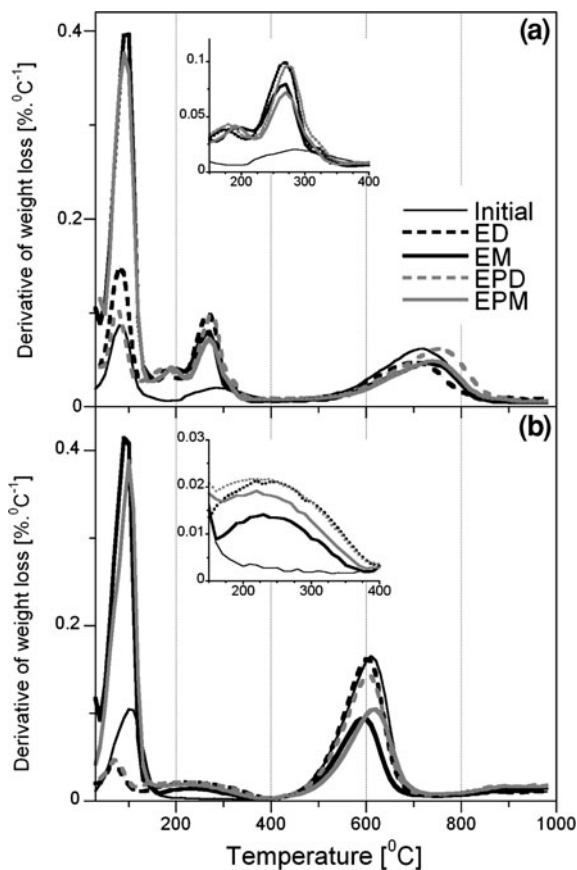
observed, additional peaks are detected after the exposure to ammonia, especially for CC-Cu2 on which a large amount of ammonia has been retained. Peaks at 2 Theta 16.1, 32.5 and 33.9° for CC-Cu2 indicate the formation of ammonium copper chloride ($CuCl_2 \cdot 2NH_4Cl \cdot 2H_2O$) [74]. For the CC-Zn sample, peaks at 2 Theta 15.1, 27.5° and 15.5, 1.2° correspond to the presence of zinc chloride ($ZnCl_2$) and ammonium tetrachlorozincate ($ZnCl_2 \cdot 2NH_4Cl$), respectively [74]. Additional support for these hypotheses is obtained by means of thermal analysis. Figure 6.12 presents the DTG curves for CC-Zn and CC-Cu2 before and after ammonia adsorption. On the curves for the initial materials, a peak at about 100 °C is noticed for both samples and it is assigned to the release of physically adsorbed water [4]. A second peak at about 710 °C for CC-Cu2 and about 600 °C for CC-Zn is revealed and linked to $CuCl_2$ and $ZnCl_2$, respectively [4]. After the exposure to ammonia, additional peaks are found in the temperature range 150–400 °C: one additional peak for CC-Zn and two new ones for CC-Cu2. These peak positions are in agreement with the decomposition of ammonium tetrachlorozincate for CC-Zn, and ammonium copper chloride and copper diamine chloride for CC-Cu2 [4]. Besides metal oxides and metal chlorides, polyoxometalates

$$V_2O_5 + 2NH_3 + H_2O \rightleftharpoons 2NH_4VO_3 \tag{a}$$

$$7MoO_3 + 2NH_3 + 3H_2O \rightleftharpoons (NH_4)_6Mo_7O_{24} \tag{b}$$

$$H_3OMo_{12}O_{40} + 3NH_3 \rightleftharpoons (NH_4)_3PMo_{12}O_{40} \tag{c}$$

$$CuCl_2 + 2NH_3 \rightleftharpoons Cu(NH_3)_2Cl_2 \tag{d}$$
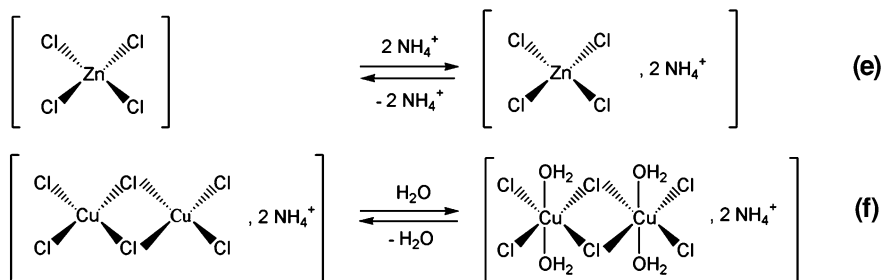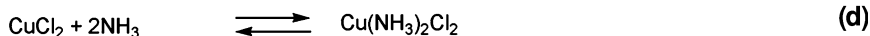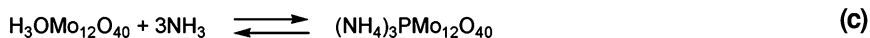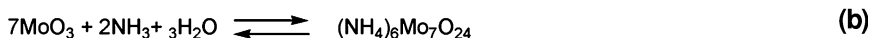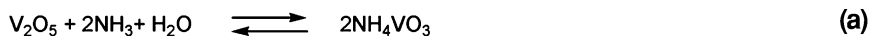
Fig. 6.13 Reactions between ammonia and the inorganic compounds present on the adsorbents' surface

are also able to form complexes with ammonia. As seen in Fig. 6.10, the apparition of new peaks at 2 Theta about 11.3, 15.4, 26.1 and 27.7° is observed for the GP-Mo composites after the exposure to ammonia in the moist conditions. A plausible explanation for these peaks is the formation of a compound involving ammonia and phosphomolybdic acid. Taking into account the formula of the POM and the stoichiometry of the reactions, the formation of $(NH_4)_3PMo_{12}O_{40}$ is proposed. The peaks found on the diffractogram are consistent with the ones characteristic for this compound [75]. These peaks are not found in the dry conditions, likely because of the smaller amount of ammonia adsorbed and also because formation of NH_4^+ is not favored without the presence of water. Reactions leading to the formation of all the complexes addressed above are proposed in Fig. 6.13.

6.4.4 Influence of the Amount of Metal

Besides the nature of interactions between ammonia and the inorganic matter, it is also interesting to analyze the effect of the amount of these metallic species on the breakthrough capacity. Given the possible reactions between ammonia and the inorganic compounds described above, it can be expected that an increase in the amount of metallic species leads to an increase in the breakthrough capacity. Nevertheless, one must consider that by increasing the amount of an inorganic matter used for impregnation, the risk that these species form large clusters rather than well-dispersed inorganic species increases as well [76]. This possible

Fig. 6.14 Dependence of the ammonia breakthrough capacity on the metal content for various modified activated carbons
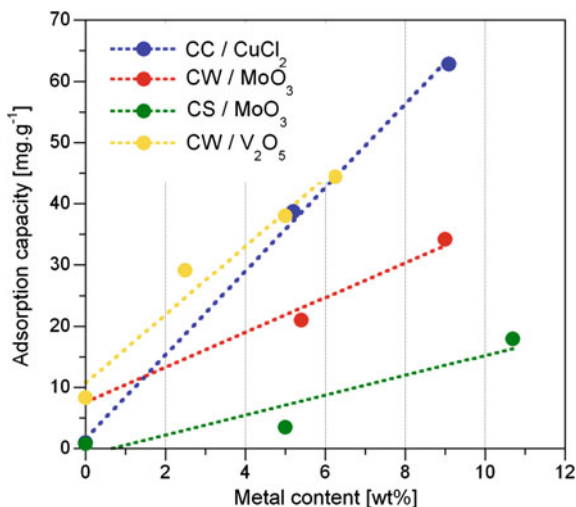
outcome would render a part of the inorganic matter inactive for reaction with ammonia.

Figure 6.14 shows the trends between the amount of metal present on the adsorbent and the corresponding breakthrough capacity. Very good linear correlations are found (R^2 higher than 0.9 for each series). It is important to notice that the Y-intercept of the curves does not necessarily equal 0 indicating that the carbon matrix itself is also responsible for the adsorption process. The latter was addressed in detail by Le Leuch and Bandosz and Helminen and coworkers [23, 77]. From these trends, one can see that the situation where a part of the inorganic matter becomes ineffective (because of the formation of large clusters) is not reached. This is likely due to the small amount of the inorganic matter (always below 10 wt%) that was used for modification of the activated carbons (Chap. 3, Sect. 3.1).

References

1. J. A. Greathouse and M. D. Allendorf, "The Interaction of Water with MOF-5 Simulated by Molecular Dynamics," *Journal of the American Chemical Society,* vol. 128, pp. 10678–10679, 2006.
2. P. Küsgens, et al., "Characterization of metal-organic frameworks by water adsorption," *Microporous and Mesoporous Materials,* vol. 120, pp. 325–330, 2009.
3. H. Fortier, et al., "Ammonia, cyclohexane, nitrogen and water adsorption capacities of an activated carbon impregnated with increasing amounts of $ZnCl_2$, and designed to chemisorb gaseous NH_3 from an air stream," *Journal of Colloid and Interface Science,* vol. 320, pp. 423–435, 2008.
4. R. C. Weast and M. J. Astle, *Handbook of Chemistry and Physics*, 62 ed. Boca Raton, FL: CRC Press, 1981.
5. C. Petit, et al., "Interactions of Ammonia with the Surface of Microporous Carbon Impregnated with Transition Metal Chlorides," *The Journal of Physical Chemistry C,* vol. 111, pp. 12705–12714, 2007.

6. C. Petit and T. J. Bandosz, "Complexity of ammonia interactions on activated carbons modified with V_2O_5," *Journal of Colloid and Interface Science,* vol. 325, pp. 301–308, 2008.

7. C. Petit and T. J. Bandosz, "Role of surface heterogeneity in the removal of ammonia from air on micro/mesoporous activated carbons modified with molybdenum and tungtsen oxides," *Microporous and Mesoporous Materials,* vol. 118, pp. 61–67, 2009.

8. V. E. Sharonov and Y. I. Aristov, "Ammonia adsorption by $MgCl_2$, $CaCl_2$ and $BaCl_2$ confined to porous alumina: the fixed bed adsorber," *Reaction Kinetics and Catalysis Letters,* vol. 85, pp. 183–188, 2005.

9. C. Petit and T. J. Bandosz, "Graphite Oxide/Polyoxometalate Nanocomposites as Adsorbents of Ammonia," *The Journal of Physical Chemistry C,* vol. 113, pp. 3800–3809, 2009.

10. T. J. Bandosz and C. Petit, "On the reactive adsorption of ammonia on activated carbons modified by impregnation with inorganic compounds," *Journal of Colloid and Interface Science,* vol. 338, pp. 329–345, 2009.

11. J. Jagiello, "Stable Numerical Solution of the Adsorption Integral Equation Using Splines," *Langmuir,* vol. 10, pp. 2778–2785, 1994.

12. J. Jagiello, et al., "Carbon surface characterization in terms of its acidity constant distribution," *Carbon,* vol. 32, pp. 1026–1028, 1994.

13. G. Kortum, et al., *Dissociation constants of organic acids in aqueous solution.* London: Butterworth, 1961.

14. H. Hu, et al., "Surface Structures of Supported Molybdenum Oxide Catalysts: Characterization by Raman and Mo L3-Edge XANES," *The Journal of Physical Chemistry,* vol. 99, pp. 10897–10910, 1995.

15. P. Vázquez, et al., "Catalysts based on supported 12-molybdophosphoric acid," *Catalysis Letters,* vol. 60, pp. 205–215, 1999.

16. C. Contescu, et al., "Heterogeneity of proton binding sites at the oxide/solution interface," *Langmuir,* vol. 9, pp. 1754–1765, 1993.

17. T. J. Bandosz, et al., "Characterization of acidity of pillared clays by proton affinity distribution and DRIFT spectroscopy," *Journal of the Chemical Society, Faraday Transactions,* vol. 90, pp. 3573–3578, 1994.

18. C. Petit and T. J. Bandosz, "Activated carbons modified with aluminium-zirconium polycations as adsorbents for ammonia," *Microporous and Mesoporous Materials,* vol. 114, pp. 137–147, 2008.

19. H. J. Chae, et al., "Physicochemical characteristics of pillared interlayered clays," *Catalysis Today,* vol. 68, pp. 31–40, 2001.

20. C. Flego, et al., "The influence of the composition on the thermal and acid characteristics of multi-component oxide pillared montmorillonite," *Applied Catalysis A: General,* vol. 168, pp. 323–331, 1998.

21. X. Yin, et al., "NH_3 Adsorption on the Brönsted and Lewis Acid Sites of V_2O_5(010): A Periodic Density Functional Study," *The Journal of Physical Chemistry B,* vol. 103, pp. 4701–4706, 1999.

22. T. J. Bandosz, *Activated carbon surfaces in environmental remediation.* Oxford, UK: Elsevier, 2006.

23. L. M. Le Leuch and T. J. Bandosz, "The role of water and surface acidity on the reactive adsorption of ammonia on modified activated carbons," *Carbon,* vol. 45, pp. 568–578, 2007.

24. H. Tamon and M. Okazaki, "Influence of acidic surface oxides of activated carbon on gas adsorption characteristics," *Carbon,* vol. 34, pp. 741–746, 1996.

25. R. Bansal and M. Goyal, *Activated carbon adsorption*: Taylor & Francis, 2005.

26. T. Szabó, et al., "DRIFT study of deuterium-exchanged graphite oxide," *Carbon,* vol. 43, pp. 3186–3189, 2005.

27. C. Hontoria-Lucas, et al., "Study of oxygen-containing groups in a series of graphite oxides: Physical and chemical characterization," *Carbon,* vol. 33, pp. 1585–1592, 1995.

28. U. Boehner and G. Zundel, "Sulfonic acid-oxygen base systems as a function of the $\Delta.pK_a$," *The Journal of Physical Chemistry,* vol. 89, pp. 1408–1413, 1985.

29. J. Zawadzki and M. Wisniewski, "In situ characterization of interaction of ammonia with carbon surface in oxygen atmosphere," *Carbon,* vol. 41, pp. 2257–2267, 2003.

30. K. Nakamoto, "Complexes of alkoxides, alcohols, ethers, ketones, aldehydes, esters and carboxylic groups," in *Infrared and Raman Spectra of Inorganic and Coordination Compounds, Applications in Coordination, Organometallic, and Bioinorganic Chemistry*, ed: Wiley, 2009, pp. 62–67.

31. E. Biemmi, et al., "Synthesis and characterization of a new metal organic framework structure with a 2D porous system: (H$_2$NEt$_2$)$_2$[Zn$_3$(BDC)$_4$].3DEF," *Solid State Sciences,* vol. 8, pp. 363–370.

32. S. Hermes, et al., "Loading of porous metal-organic open frameworks with organometallic CVD precursors: inclusion compounds of the type [LM]@MOF-5," *Journal of Materials Chemistry,* vol. 16, pp. 2464–2472, 2006.

33. S. Vairam and S. Govindarajan, "New hydrazinium salts of benzene tricarboxylic and tetracarboxylic acids–preparation and their thermal studies," *Thermochimica Acta,* vol. 414, pp. 263–270, 2004.

34. Y. Wang, et al., "Two-dimensional metal-organic frameworks (MOFs) constructed from heterotrinuclear coordination units and 4,4'-biphenyldicarboxylate ligands," *Dalton Transactions,* pp. 689–696, 2007.

35. N. Shi, et al., "Self-Assembly of Two Different Hierarchical Nanostructures on Either Side of an Organic Supramolecular Film in One Step," *Chemistry – A European Journal,* vol. 14, pp. 6255–6259, 2008.

36. Y.-K. Seo, et al., "Microwave synthesis of hybrid inorganic-organic materials including porous Cu$_3$(BTC)$_2$ from Cu(II)-trimesate mixture," *Microporous and Mesoporous Materials,* vol. 119, pp. 331–337, 2009.

37. Y. Wang, et al., "Two-dimensional metal-organic frameworks (MOFs) constructed from heterotrinuclear coordination units and 4,4'-biphenyldicarboxylate ligands," *Dalton Transactions,* pp. 689–696, 2007.

38. D. Britt, et al., "Metal-organic frameworks with high capacity and selectivity for harmful gases," *Proceedings of the National Academy of Sciences,* vol. 105, pp. 11623–11627, August 19, 2008 2008.

39. C. Petit, et al., "Reactive Adsorption of Ammonia on Cu-Based MOF/Graphene Composites," *Langmuir,* vol. 26, pp. 15302–15309, 2010.

40. H. Emeleus, et al., *Advances in inorganic chemistry and radiochemistry*: Academic Press, 1977.

41. A. Baes and P. Bloom, "Diffuse reflectance and transmission Fourier Transform infrared (DRIFT) spectroscopy of humic and fluvic acids," *Soil Science Society of America Journal,* vol. 53, pp. 695–700, 1989.

42. C. Petit, et al., "Revisiting the chemistry of graphite oxides and its effect on ammonia adsorption," *Journal of Materials Chemistry,* vol. 19, pp. 9176–9185, 2009.

43. E. Desimoni, et al., "XPS/XAES study of carbon fibres during thermal annealing under UHV conditions," *Carbon,* vol. 30, pp. 521–526, 1992.

44. S. Biniak, et al., "The characterization of activated carbons with oxygen and nitrogen surface groups," *Carbon,* vol. 35, pp. 1799–1810, 1997.

45. H.-K. Jeong, et al., "Evidence of Graphitic AB Stacking Order of Graphite Oxides," *Journal of the American Chemical Society,* vol. 130, pp. 1362–1366, 2008.

46. T. Szabó, et al., "Evolution of Surface Functional Groups in a Series of Progressively Oxidized Graphite Oxides," *Chemistry of Materials,* vol. 18, pp. 2740–2749, 2006.

47. S. Stankovich, et al., "Synthesis of graphene-based nanosheets via chemical reduction of exfoliated graphite oxide," *Carbon,* vol. 45, pp. 1558–1565, 2007.

48. J. R. Pels, et al., "Evolution of nitrogen functionalities in carbonaceous materials during pyrolysis," *Carbon,* vol. 33, pp. 1641–1653, 1995.

49. H. Schmiers, et al., "Change of chemical bonding of nitrogen of polymeric N-heterocyclic compounds during pyrolysis," *Carbon,* vol. 37, pp. 1965–1978, 1999.

50. R. J. J. Jansen and H. van Bekkum, "XPS of nitrogen-containing functional groups on activated carbon," *Carbon,* vol. 33, pp. 1021–1027, 1995.

51. B. Onida, et al., "Spectroscopic Characterization of Hydroxyl Groups in SAPO-40. 1. Study of the Template-Free Samples and Their Interaction with Ammonia," *The Journal of Physical Chemistry,* vol. 100, pp. 11072–11079, 1996.
52. A. Hamwi and V. Marchand, "Some chemical and electrochemical properties of graphite oxide," *Journal of Physics and Chemistry of Solids,* vol. 57, pp. 867–872.
53. H. C. Schniepp, et al., "Functionalized Single Graphene Sheets Derived from Splitting Graphite Oxide," *The Journal of Physical Chemistry B,* vol. 110, pp. 8535–8539, 2006.
54. A. Incze, et al., "Mechanical properties of graphite oxides: Ab initio simulations and continuum theory," *Physical Review B,* vol. 70, p. 212103, 2004.
55. C. Petit, et al., "The role of sulfur-containing groups in ammonia retention on activated carbons," *Carbon,* vol. 48, pp. 654–667, 2010.
56. J. G. C. Shen, et al., "Synthesis and Characterization of [NaO$_3$SOCH$_2$CH$_2$OSO$_3$Na] and Its Anchored Form: Surface-Grafted Acid Groups on Zirconium Hydroxide," *Chemistry of Materials,* vol. 13, pp. 4479–4485, 2001.
57. J. G. C. Shen, et al., "Sulfonic Acid-Functionalized Mesoporous Silica: Synthesis, Characterization, and Catalytic Reaction of Alcohol Coupling to Ethers," *The Journal of Physical Chemistry B,* vol. 106, pp. 9975–9978, 2002.
58. M. M. Nasef and H. Saidi, "Surface studies of radiation grafted sulfonic acid membranes: XPS and SEM analysis," *Applied Surface Science,* vol. 252, pp. 3073–3084, 2006.
59. M. Descostes, et al., "Use of XPS in the determination of chemical environment and oxidation state of iron and sulfur samples: constitution of a data basis in binding energies for Fe and S reference compounds and applications to the evidence of surface species of an oxidized pyrite in a carbonate medium," *Applied Surface Science,* vol. 165, pp. 288–302, 2000.
60. V. V. Strelko, et al., "Mechanism of reductive oxygen adsorption on active carbons with various surface chemistry," *Surface Science,* vol. 548, pp. 281–290, 2004.
61. B. Stöhr, et al., "Enhancement of the catalytic activity of activated carbons in oxidation reactions by thermal treatment with ammonia or hydrogen cyanide and observation of a superoxide species as a possible intermediate," *Carbon,* vol. 29, pp. 707–720, 1991.
62. C. L. Mangun, et al., "Adsorption of sulfur dioxide on ammonia-treated activated carbon fibers," *Carbon,* vol. 39, pp. 1689–1696, 2001.
63. W. H. Lee and P. J. Reucroft, "Vapor adsorption on coal- and wood-based chemically activated carbons: (III) NH$_3$ and H$_2$S adsorption in the low relative pressure range," *Carbon,* vol. 37, pp. 21–26, 1999.
64. F. Stoeckli, et al., "Specific and non-specific interactions between ammonia and activated carbons," *Carbon,* vol. 42, pp. 1619–1624, 2004.
65. M. Solimannejad and S. Scheiner, "Unconventional H-bonds: SH⋯N interaction," *International Journal of Quantum Chemistry,* vol. 111, pp. 3196–3200, 2011.
66. C. Petit and T. J. Bandosz, "Enhanced Adsorption of Ammonia on Metal-Organic Framework/Graphite Oxide Composites: Analysis of Surface Interactions," *Advanced Functional Materials,* vol. 20, pp. 111–118, 2010.
67. J. Moore, et al., *Principles of Chemistry: The Molecular Science*: Cengage Learning, 2009.
68. L. Alaerts, et al., "Probing the Lewis Acidity and Catalytic Activity of the Metal–Organic Framework [Cu$_3$(btc)$_2$] (BTC = Benzene-1,3,5-tricarboxylate)," *Chemistry – A European Journal,* vol. 12, pp. 7353–7363, 2006.
69. C. Prestipino, et al., "Local Structure of Framework Cu(II) in HKUST-1 Metallorganic Framework: Spectroscopic Characterization upon Activation and Interaction with Adsorbates," *Chemistry of Materials,* vol. 18, pp. 1337–1346, 2006.
70. S. S. Kaye, et al., "Impact of Preparation and Handling on the Hydrogen Storage Properties of Zn$_4$O(1,4-benzenedicarboxylate)$_3$ (MOF-5)," *Journal of the American Chemical Society,* vol. 129, pp. 14176–14177, 2007.
71. L. D. Frederickson and D. M. Hausen, "Infrared Spectra-Structure Correlation Study of Vanadium-Oxygen Compounds," *Analytical Chemistry,* vol. 35, pp. 818–827, 1963.
72. L. Kotai, et al., "A Convenient Method to Prepare Alkali- and Chloride-free Ammonium Metavanadate (NH$_4$VO$_3$)," *Chemistry Letters,* vol. 35, pp. 384–385, 2006.

73. R. Díaz and R. S. Mann, "ESR and FTIR spectroscopy study of Sb-Mo oxide catalysts," *Materials Letters,* vol. 33, pp. 19–22, 1997.

74. Joint Committee on Powder Diffraction Standards, *Inorganic index to the powder diffraction file*. Swarthmore, PA: Joint committee on powder diffraction standards, 1971.

75. C. Srilaxmi, et al., "In situ synthesis and ammoxidation activity of ammonium salt of molybdophosphoric acid on VOPO4 catalysts," *Catalysis Communications,* vol. 5, pp. 199–203, 2004.

76. F. Rodríguez-reinoso, "The role of carbon materials in heterogeneous catalysis," *Carbon,* vol. 36, pp. 159–175, 1998.

77. J. Helminen, et al., "Adsorption Equilibria of Ammonia Gas on Inorganic and Organic Sorbents at 298.15 K," *Journal of Chemical & Engineering Data,* vol. 46, pp. 391–399, 2001.

Chapter 7
Role of Water

In addition to the role of the adsorbent's features (porosity and surface chemistry), the experimental conditions of the breakthrough tests can affect the removal process as well. In particular, the role of water, either in the air stream or on the adsorbent's surface must be considered.

7.1 Influence of the Moisture During Adsorption

7.1.1 Water as an Enhancing Factor

As seen from Figs. 4.1 and 4.2, in most cases, the breakthrough capacity follows these trends: ED < EM, EPD < EPM and ED < EPD, EM < EPM. The first two trends are related to the influence of water in the air stream and the two others refer to the role of water on the adsorbent surface. These results indicate that both "types of water" have a positive effect on the ammonia breakthrough capacity.

An improvement in the performance of an adsorbent with water can originate from various phenomena. First, due to the high affinity of small pores to retain water at high humidity levels [1], it is likely that in moist conditions, a water film fills the micropores [1]. In this film, ammonia can easily be retained by dissolution because of its high solubility in water [2]. This is very well-illustrated in the case of HKUST-1 and the GM-Cun composites [3]. These materials are characterized by high microporosity (Chap. 5, Sect. 5.1) and they can adsorb the significant amounts of water. From Fig. 4.2, one can see that the breakthrough capacity is between about 1.2 to 2.0 times higher in the moist conditions than in the dry conditions.

Moreover, the water film favors the deprotonation of carboxylic groups present on the carbons surface [4], which are then able to react with NH_4^+ ions. Indeed, ammonium ions are present in the system due to the Brønsted acidity of water. In addition to its action on the functional groups present in the carbon matrix, water

forms Brønsted centers in the inorganic matter present on the carbons and thus enables the reactions of those centers with an ammonia molecule. For metal oxide impregnates, water leads to the formation of hydroxyl groups [5, 6], which are able to interact with ammonia via acid–base reactions or hydrogen bonding. This was also discussed previously in Chap. 6 (Sect. 6.2).

7.1.2 Water as a Neutral Component or Obstacle in Adsorption Processes

Although based on the above discussion, water has a positive effect in most cases, its action is sometimes not noticeable and can even lead to a decrease in the ammonia retention. Such behaviors do not invalidate the previous statements but rather indicates that for some materials, additional features are involved in the process of adsorption and they sometimes predominate.

For instance, in the case of CW-Al sample, the presence of water does not improve ammonia retention and similar adsorption capacities are found regardless the experimental conditions [7]. A plausible explanation for this is that enough Brønsted sites are already available for the ammonia retention in the dry conditions due to the many hydroxyl groups on the polycations (Fig. 4.1) [7–9]. The CW-V sample also exhibits similar performances whether water is present or not (Fig. 4.1) [10]. This is very different from the behavior of CW-Mo1 and CW-Mo2 samples, even though the types of the impregnate are similar (Fig. 4.1) [11]. This phenomenon can be attributed to a competition between water and ammonia adsorption on vanadium oxide that would counterbalance that of ammonia dissolution in water. This is supported by the fact that the favorite site for ammonia adsorption on vanadium oxide is the same one as for water, as determined by computational methods [12, 13].

In the case of GP-W and GP-Mo composites, water, as well, seems to have a critical influence on the ammonia uptake [14]. As seen in Fig. 4.2, water present on the adsorbent surface (EPD) enhances the ammonia uptake, whereas water present in the challenging gas (EM) has a negative effect on the adsorption. This is in agreement with the results showing the influence of water on the acidity, catalytic activity and ammonia uptake of both bulk and supported POMs [15]. Indeed, Bardin and co-workers showed that increasing the pretreatment temperature of bulk $H_3PW_{12}O_{40}$ and $H_3PMo_{12}O_{40}$ (and thus decreasing their hydration level) leads to a decrease in the material acidity and more precisely in the ammonia uptake [15]. This was explained by the stronger acidity of hydrated POMs than their anhydrous counterparts. This would explain why GP-W-EPD and GP-Mo-EPD have a better breakthrough capacity than GP-W-ED and GP-Mo-ED, respectively. On the contrary, in the moist conditions (EM), water adsorption seems to be in competition with ammonia adsorption. Based on the study of Kozhevnikov, water combines with the protons in the POM to form $H_2O_5^+$ acidic clusters [16]. These molecules of water are hydrogen bonded to the terminal oxygens of the Keggin unit. Since Bardin and co-workers demonstrated that

ammonia adsorbs on both the bridging and terminal oxygens of $H_3PW_{12}O_{40}$ and $H_3PMo_{12}O_{40}$ [17], when both water and ammonia are present in the challenging gas, a competition between the adsorption of the two molecules might occur, leading to a decrease in the NH_3 uptake. In the dry conditions (ED), owing to the fact that there is no competition between water and ammonia present in the challenging gas, and there is no water present on the surface either, all existing acidic centers are available for interactions with ammonia. Nevertheless, the breakthrough capacity values in these cases are between the ones obtained in EM and EPD conditions owing to the weaker acidity.

7.2 Influence of the Moisture on the Strength of Adsorption

Not only does water influence the breakthrough capacity, but it can also play a role in the desorption process. This is true for water present in the air stream as well as water preadsorbed on the adsorbent surface.

Figure 7.1 presents adsorption and desorption curves for selected samples. In the case of HKUST-1 and the derived composites (Fig. 7.1a, b) we can see that desorption curves are much steeper in the dry conditions than in the moist conditions. This indicates the stronger retention of ammonia in the former case. This phenomenon is related to the part of ammonia adsorbed via dissolution in water. In the moist conditions, a water film is created inside the micropores of the materials [1] in which ammonia dissolves. This mechanism of adsorption involves only weak retention forces and results in the release of the "dissolved" ammonia when the adsorbent bed is purged with air. It has to be mentioned that if water impairs the strong retention of ammonia, it also enhances the breakthrough capacity since in addition to other adsorption mechanisms, the dissolution of ammonia in water occurs as well. Consequently, depending on the preferred point of view (breakthrough capacity or retention), a trade-off has to be made.

The detrimental role of water is also observed when moisture is present on the adsorbent itself (as a result of prehumidification). From Fig. 7.1c, one can also notice that when prehumidification is performed, the ammonia concentration always exceeds 100 ppm (sensor's limit) resulting in the absence of data (gap) due to the inability of its collection. More generally, for the samples studied (see Appendix, Figs. A1, A2, A3, A4, A5, A6), prehumidification usually results in a larger gap between the breakthrough curve and the desorption curve than in the absence of prehumidification [7, 11, 12, 18, 19]. All of these suggest that more ammonia is desorbed when water is preadsorbed before running the adsorption test. This behavior can be explained by considering the process of pores filling and ammonia dissolution in water. Water is first adsorbed in the small pores, and then it starts to fill larger pores [1]. Consequently, at the end of the adsorption step, more water is present in the large pores when prehumidification is performed than without prehumidification (since more water was injected to the system). A similar conclusion can be made for ammonia since it dissolves in water. When adsorbent beds are purged, water
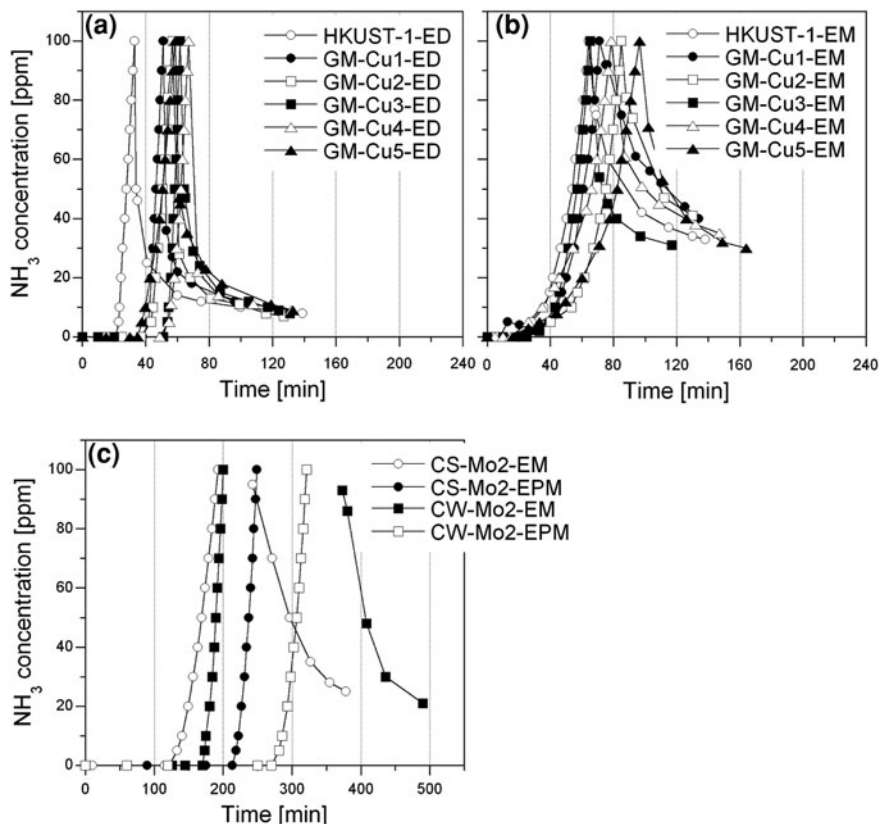
Fig. 7.1 Breakthrough and desorption curves for HKUST-1 and the derived composites in dry (**a**) and moist conditions (**b**) and for modified activated carbons in various conditions (**c**)

(with dissolved ammonia) contained in large pores, where adsorptive forces are the weakest, is removed first. As more water is contained in large pores for the samples run after prehumidification, there is more water removed during the desorption and thus more ammonia released. This might explain the higher amount of ammonia desorbed when prehumidification is performed than without it.

References

1. C. L. McCallum, *et al.*, "A Molecular Model for Adsorption of Water on Activated Carbon: Comparison of Simulation and Experiment," *Langmuir,* vol. 15, pp. 533–544, 1998.
2. R. C. Weast and M. J. Astle, *Handbook of Chemistry and Physics*, 62 ed. Boca Raton, FL: CRC Press, 1981.
3. C. Petit,   *et al*., "Reactive Adsorption of Ammonia on Cu-Based MOF/Graphene Composites," *Langmuir,* vol. 26, pp. 15302–15309, 2010.
4. L. M. Le Leuch and T. J. Bandosz, "The role of water and surface acidity on the reactive adsorption of ammonia on modified activated carbons," *Carbon*, vol. 45, pp. 568–578, 2007.

5. I. E. Wachs, "Raman and IR studies of surface metal oxide species on oxide supports: Supported metal oxide catalysts," *Catalysis Today,* vol. 27, pp. 437–455, 1996.

6. G. Deo and I. E. Wachs, "Predicting molecular structures of surface metal oxide species on oxide supports under ambient conditions," *The Journal of Physical Chemistry,* vol. 95, pp. 5889–5895, 1991.

7. C. Petit and T. J. Bandosz, "Role of Aluminum Oxycations in Retention of Ammonia on Modified Activated Carbons," *The Journal of Physical Chemistry C,* vol. 111, pp. 16445–16452, 2007.

8. H. J. Chae, *et al.*, "Physicochemical characteristics of pillared interlayered clays," *Catalysis Today,* vol. 68, pp. 31–40, 2001.

9. C. Flego, *et al.*, "The influence of the composition on the thermal and acid characteristics of multi-component oxide pillared montmorillonite," *Applied Catalysis A: General,* vol. 168, pp. 323–331, 1998.

10. C. Petit and T. J. Bandosz, "Complexity of ammonia interactions on activated carbons modified with V_2O_5," *Journal of Colloid and Interface Science,* vol. 325, pp. 301–308, 2008.

11. C. Petit and T. J. Bandosz, "Role of surface heterogeneity in the removal of ammonia from air on micro/mesoporous activated carbons modified with molybdenum and tungtsen oxides," *Microporous and Mesoporous Materials,* vol. 118, pp. 61–67, 2009.

12. X. Yin, *et al.*, "NH_3 Adsorption on the Brönsted and Lewis Acid Sites of $V_2O_5(010)$: A Periodic Density Functional Study," *The Journal of Physical Chemistry B,* vol. 103, pp. 4701–4706, 1999.

13. X. Yin, *et al.*, "Adsorption of H_2O on the $V_2O_5(010)$ Surface Studied by Periodic Density Functional Calculations," *The Journal of Physical Chemistry B,* vol. 103, pp. 3218–3224, 1999.

14. C. Petit and T. J. Bandosz, "Graphite Oxide/Polyoxometalate Nanocomposites as Adsorbents of Ammonia," *The Journal of Physical Chemistry C,* vol. 113, pp. 3800–3809, 2009.

15. B. B. Bardin, *et al.*, "Acidity of Keggin-Type Heteropolycompounds Evaluated by Catalytic Probe Reactions, Sorption Microcalorimetry, and Density Functional Quantum Chemical Calculations," *The Journal of Physical Chemistry B,* vol. 102, pp. 10817–10825, 1998.

16. I. V. Kozhevnikov, *Russ. Chem. Rev.,* vol. 56, p. 1417, 1987.

17. B. B. Bardin, *et al.*, "Ammonia Adsorption on Keggin-Type Heteropolyacid Catalysts Explored by Density Functional Quantum Chemistry Calculations," *The Journal of Physical Chemistry B,* vol. 104, pp. 3556–3562, 2000.

18. C. Petit and T. J. Bandosz, "Removal of Ammonia from Air on Molybdenum and Tungsten Oxide Modified Activated Carbons," *Environmental Science & Technology,* vol. 42, pp. 3033–3039, 2008.

19. C. Petit and T. J. Bandosz, "Activated carbons modified with aluminium-zirconium polycations as adsorbents for ammonia," *Microporous and Mesoporous Materials,* vol. 114, pp. 137–147, 2008.

Chapter 8
Mechanisms of Adsorption and Strength of Retention

As addressed in the preceding chapters, ammonia can be adsorbed on the surface of adsorbents in various ways. These processes can be classified according to several criteria such as the strength of retention (weak/strong), the specificity of ammonia interactions with the adsorbent (specific/non-specific), the reversible or irreversible character of the adsorption interactions (usually related to the strength of adsorption) or the types of interactions (e.g. acid–base reactions). In this chapter, we intend to summarize/classify the different mechanisms of adsorption addressed above. These various paths of adsorption are discussed according to the type of interactions involved. For each type of mechanism, we try to indicate its specificity and strength, along with the materials for which the mechanism is observed. A more in-depth and quantitative analysis of the strength of retention is also proposed at the end of this chapter.

8.1 Physisorption

In porous materials, physical adsorption of ammonia can be expected and it takes place in the case of our samples [1]. In such mechanisms, van der Waals forces between ammonia and the adsorbent's surface are involved [2, 3] and a simple pore filling governs the process [4]. Since physisorption does not depend on the nature of ammonia (and that of the adsorbent), it is considered as a non-specific mechanism. Because of this nonspecificity, physical adsorption, in most cases, results in weak retention. This is the case for the virgin and modified activated carbons discussed above [5–11]. For the latter materials, the desorption curves are most of the time absent (lack of data due to the sensor's limit), or a gap between the breakthrough and desorption curve was observed. All of these indicate a weak retention. For some adsorbents, however, stronger physical forces are observed. Examples of such materials are the two series of GO/MOF composites (GM-Znn

and GM-Cun). Indeed, in these cases, the dispersive forces (a type of van der Waals forces) are enhanced compared to the parent materials [12, 13].

8.2 Dissolution in Water

Dissolution of ammonia in water during the breakthrough tests represents another mechanism of retention. This process occurs when moisture is present either in the challenging gas or on the adsorbent's surface (as a result of prehumidification). It can be considered as a specific mechanism since it is related to the hydrophilic character of ammonia [14]. Ammonia dissolved in water is most of the time only weakly retained on the surface and progressively desorbs together with water upon air purging, as evidenced in Chap. 7 (Sect. 7.2). This mechanism is enhanced by the presence of surface functional groups, which increases the hydrophilicity of the surface and thus increases the formation of hydrogen bonding between the surface and polar adsorbates. The presence of small pores also enhances the adsorption of water [15] and thus the dissolution of ammonia. Considering our adsorbents, the dissolution of ammonia in water is favored in the case of activated carbons modified with metal oxides or polycations (oxygen groups from the inorganic matter and the carbon matrix), polymer-based activated carbons (high oxygen content), GO or HKUST-1 and the GM-Cun composites [6–9, 12, 13, 16–18].

8.3 Hydrogen Bonding

Owing to its lone pair of electrons, ammonia can also be adsorbed via hydrogen bonding. This mechanism represents a specific process as it depends on the particular electronic structure of ammonia. Despite this specificity, hydrogen bonding usually involves weak retention forces which makes its detection difficult as explained in Chap. 6 (Sect. 6.2). Generally speaking, hydrogen bonding is favored on materials with oxygen-containing groups and in particular hydroxyl functionalities. This is the case of the activated carbons either nonmodified or after the modifications with metal oxides and polycations [6–9]. The polymer-based carbons and GO-based materials, owing to their high oxygen content, can be included to this category of materials as well [16]. For the GO-based materials, indirect evidences of hydrogen bonding are found using X-ray diffraction [17]. In Fig. 6.10, one can see that the interlayer distance of GO-B increases after the exposure to ammonia in the dry conditions. This finding indicates that a part of the ammonia adsorbed was retained via intercalation between the graphene layers [17, 19]. Intercalation is possible owing to the hydrophilic character of the interlayer space of GO (due to the oxygen groups decorating the basal planes [20]) which attracts ammonia molecules and drives them between the graphene layers. This phenomenon has already been reported by Hamwi and Marchand [19]. Considering

this, it might seem unexpected that the interlayer distance of GO-H does not increase after the exposure to ammonia despite the fact that more ammonia was adsorbed on this material than on GO-B and that oxygen groups are also present its surface. Nevertheless, as explained in Chap. 6 (Sect. 6.2), in the case of GO-H, other reactions of ammonia with the oxygen groups causes a more "efficient" stacking of the graphene layers (and thus a decrease in the interlayer distance). This process does not contradict that of adsorption via the intercalation but rather suggests that the effect of the intercalation does not counterbalance the effect of the ammonia reaction with GO groups. MOF-5 and the GM-Zn composites also adsorb ammonia via hydrogen bonding due to the presence of zinc oxide as their metallic component as explained in Chap. 6 (Sect. 6.2).

8.4 Lewis Acid–Base Reactions

Besides hydrogen bonding, the lone pair of electrons on ammonia molecules also enables adsorption via Lewis acid–base interactions. As in the case of hydrogen bonding, the mechanism is specific since it relies on the electronic structure of ammonia. Lewis acid–base interactions can be expected on adsorbents with metallic species. This is the case of all our adsorbents except the polymer-based carbons and GO materials [5–9, 12, 13, 18, 21]. Such mechanism involves mainly weak retention forces. This is supported by the study of ammonia adsorption on HKUST-1 and GM-Cun composites. In this case, as explained in Chap. 6 (Sect. 6.4), ammonia interactions with the metallic sites are detected via a change of color of the adsorbent from dark blue to a lighter blue. If the breakthrough test is stopped before ammonia reacts with the MOF, which is related to a second change of color (Chap. 6, Sect. 6.2), then the process is reversible. Indeed, upon purging the bed with dry air or heating the material at 100 °C, the bed recovers its original dark blue color. All of these indicate the weakness of Lewis acid–base interactions.

8.5 Brønsted Acid–Base Reactions

Not only does ammonia behave as a Lewis base, but it can also be considered as a Brønsted base. Brønsted interactions are thus also involved in the ammonia retention. This specific mechanism results in the strong retention of ammonia on the adsorbent's surface and can be detected via the presence of ammonium ions. This is, for instance, the case in Fig. 6.3, where a band at about 1410 cm^{-1} related to N–H vibration in NH_4^+ is observed on the spectrum of GO-H after exposure to ammonia followed by air purging [22]. This type of adsorption is enhanced on materials with acidic properties. Among the adsorbents studied here, adsorbents with acidic functional groups (i.e. carboxyl and sulfonic groups) and/or impregnated with acidic polycations can be considered. Such materials are the CW and CP activated carbons

as well as GO samples [6, 7, 9, 16, 21]. The MOF compounds and their derived composites, owing the carboxyl groups of the organic ligands, can also adsorb ammonia via Brønsted interactions, as described in Chap. 6 (Sect. 6.2).

8.6 Complexation

Ammonia is often encountered as a component of complexes. Formation of complexes involving ammonia is observed as a result of reactive adsorption on our materials such as: the activated carbons modified with metal chlorides or metal oxides and the GO/POMs composites [5–9, 18, 21]. This specific mechanism allows the strong retention of ammonia. Indeed, even after air purging, evidences of the presence of these complexes are found, for instance, in the results of X-ray diffraction (Fig. 6.10). Besides, as observed from the DTG analysis in the case of CW impregnated with metal chlorides (Fig. 6.12), these complexes are stable up to 200 or 250 °C depending on their nature (ammonium tetrachlorozincate, ammonium copper chloride or copper diamine chloride, respectively).

8.7 Nucleophilic Addition

A last mechanism detected on the adsorbents studied is the reaction of ammonia with oxygen groups on the surface of the adsorbents via nucleophilic addition. It is found that ammonia can react with epoxy or carboxyl groups to form amine or amide functionalities incorporated into the matrix of the materials (Chap. 6, Sect. 6.2). Such specific mechanisms are evidenced in the XPS results obtained for GO and the polymer-based activated carbons, two materials with the high oxygen content [16, 17]. It has to be mentioned here that XPS analyses were not performed on the other materials and although their oxygen content is likely smaller, such reactions cannot be completely ruled out. Since nucleophilic addition leads to the incorporation of ammonia in the adsorbent's matrix, the retention is considered as strong. The fact that amine/amide groups are usually desorbed from a carbonaceous surface at temperature slightly below 500 °C confirms the strong retention of ammonia via this route [23–25].

8.8 Complexity of Ammonia Retention

Considering the above, one can understand that ammonia adsorption on a given adsorbent can occur via multiple ways depending on the material's features. Indeed, most adsorbents combine high porosity and the presence of functional groups and/or inorganic matter. Consequently, ammonia adsorption becomes a rather complex process since the relative extent of each mechanism of adsorption

Table 8.1 Proposed mechanisms of reactive adsorption evidenced on the adsorbents studied along with their properties

Mechanism	Specificity	Strength of retention	Adsorbents involved
Physisorption	No	Weak (except if strong dispersive forces are present)	CC, CP, CS, CW (fresh or modified) MOF-5, HKUST-1 GM-Znn, GM-Cun
Dissolution in water	Yes	Weak	All materials when water is present in the system
Hydrogen bonding	Yes	Weak	CP, CS, CW (fresh or modified) GO, GP-Mo, GP-W MOF-5, HKUST-1 GM-Znn, GM-Cun
Lewis acid–base interactions	Yes	Weak	CC-Zn, CC-Cu, CS-Mo, CW-Al, CW-Zr, CW-Zr-c, CW-V, CW-Mo GP-Mo, GP-W HKUST- 1, GM-Cun
Brønsted acid– base interactions	Yes	Strong	CP, CW (fresh or modified) GO, GP-Mo, GP-W MOF-5, HKUST-1 GM-Znn, GM-Cun
Complexation	Yes	Strong	CC-Zn, CC-Cu, CP, CW-V, CW-Mo GP-Mo, GP-W
Nucleophilic addition	Yes	Strong	CP GO

remains unknown. However, considering the structural and chemical features of our adsorbents, we can envision the possible ways of retention on these materials. Table 8.1 proposes the various paths of adsorption along with evaluation of their level of specificity and strength of ammonia retention for the materials studied. Unlike the other materials presented here, the GM-Znn and GM-Cun composites (and the MOFs) exhibit a rather well-defined structure, which makes it possible to localize precisely the different types of adsorption sites. For these materials, ammonia is adsorbed via: (i) intercalation between the graphene layers and reaction with the functional groups of these layers, (ii) adsorption at the interface between the carbon layers and the MOF units and (iii) interactions with the metallic sites of the MOF. These mechanisms are visualized in Fig. 8.1.

8.9   Strength of Adsorption

If the amount of ammonia adsorbed is a criterion to assess the performance of an adsorbent, the amount of ammonia retained on the surface after the test is another one to be considered. Indeed, when the strength of interactions between the
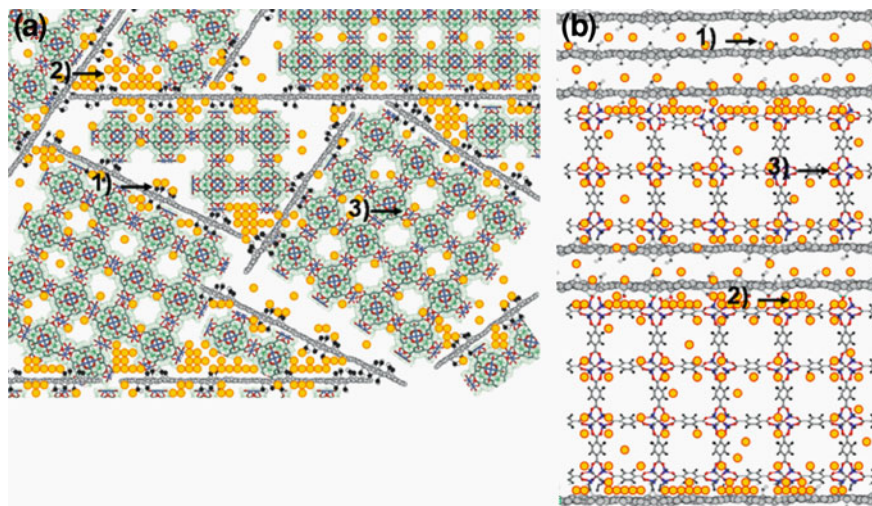
Fig. 8.1 Schematic representation of the mechanisms of ammonia adsorption in GM-Cun (**a**) and GM-Znn (**b**) composites including: 1 Intercalation/reaction in/with GO, 2 physisorption at the interface between the graphene layers and the MOF units and 3 interactions with the MOF metallic centers (simple coordination or hydrogen bonding). Reprinted with permission from Ref. [12, 13]. Copyright 2010, American Chemical Society and Wiley

adsorbent surface and NH_3 molecule is weak, ammonia easily desorbs from the surface. On the contrary, when these interactions are strong, most of the adsorbed ammonia will be retained on the surface. The latter case is of course the desired outcome. Although a qualitative discussion on the strength of retention was addressed in Sect. 8.9, a quantitative analysis can be useful to fully evaluate the performance of an adsorbent for potential applications.

As described above, qualitative analysis of the strength of adsorption can be obtained either via the study of the shape of the desorption curve or via the detection of ammonia or products of ammonia reactive adsorption on the surface of the exhausted adsorbent using techniques such as FT-IR spectroscopy, thermal analysis, X-ray diffraction, XPS analysis or potentiometric titration.

Among the latter methods, thermal analysis, XPS analysis and potentiometric titration allow for the quantitative determination of the amount of ammonia left on the adsorbent surface after the adsorption and desorption runs. For CC carbon loaded with $ZnCl_2$ and $CuCl_2$, the thermal stability of ammonia-/ammonium-containing complexes (Fig. 6.12) is a sign of the strong retention. Thus, based on the difference in the weight loss between the exhausted and initial samples in the temperature range corresponding to the decomposition of those complexes, the amount of ammonia strongly adsorbed can be calculated. Similarly, for the modified samples based on the CW carbon, the polymer-based samples, the graphite oxide and GO/POMs composites, ammonium ions are detected by potentiometric titration on the surface of the exhausted samples as a new peak at pK_a about 9.4 [14]. The pK_a distributions for selected samples are plotted in Fig. 8.2. For the sake
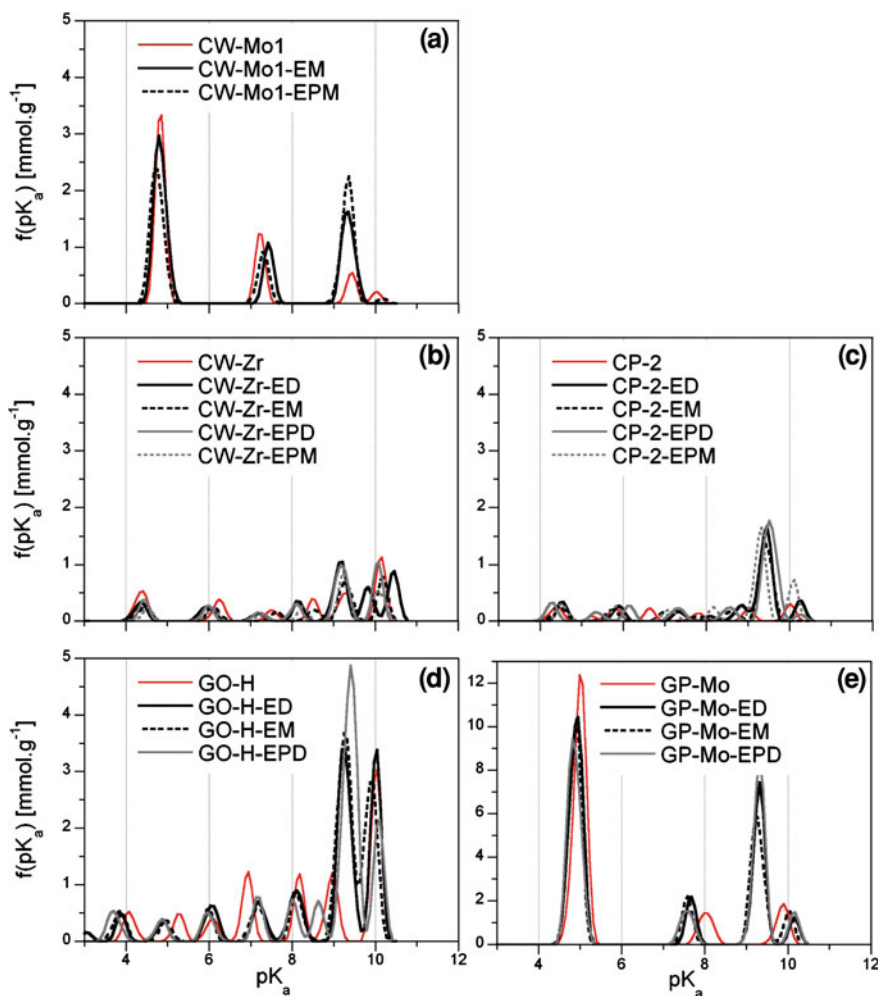
Fig. 8.2 pK_a distributions for selected samples before and after exposure to ammonia in various conditions

of clarity, only selected samples are presented (for each series of materials). The curves for all the materials tested can be found in the Appendix (Figs. A.10, A.11, A.12). Based on the area under the new peak, the amount of ammonia retained in its ionic form can be determined. For the polymer-based carbons, as well as for the GO-B and GO-H materials, ammonia retained in C–N (amine/amide), $C–N^+$ and/or NH_4^+ configuration can be quantified by XPS analysis (Tables 6.2, 6.3). Results of these three approaches are summarized in the plot shown in Fig. 8.3. In this graph, the Y-axis represents the percentage of ammonia strongly retained compared to the initial amount of gas adsorbed (breakthrough capacity). The values are for the samples exposed to ammonia in the dry conditions.
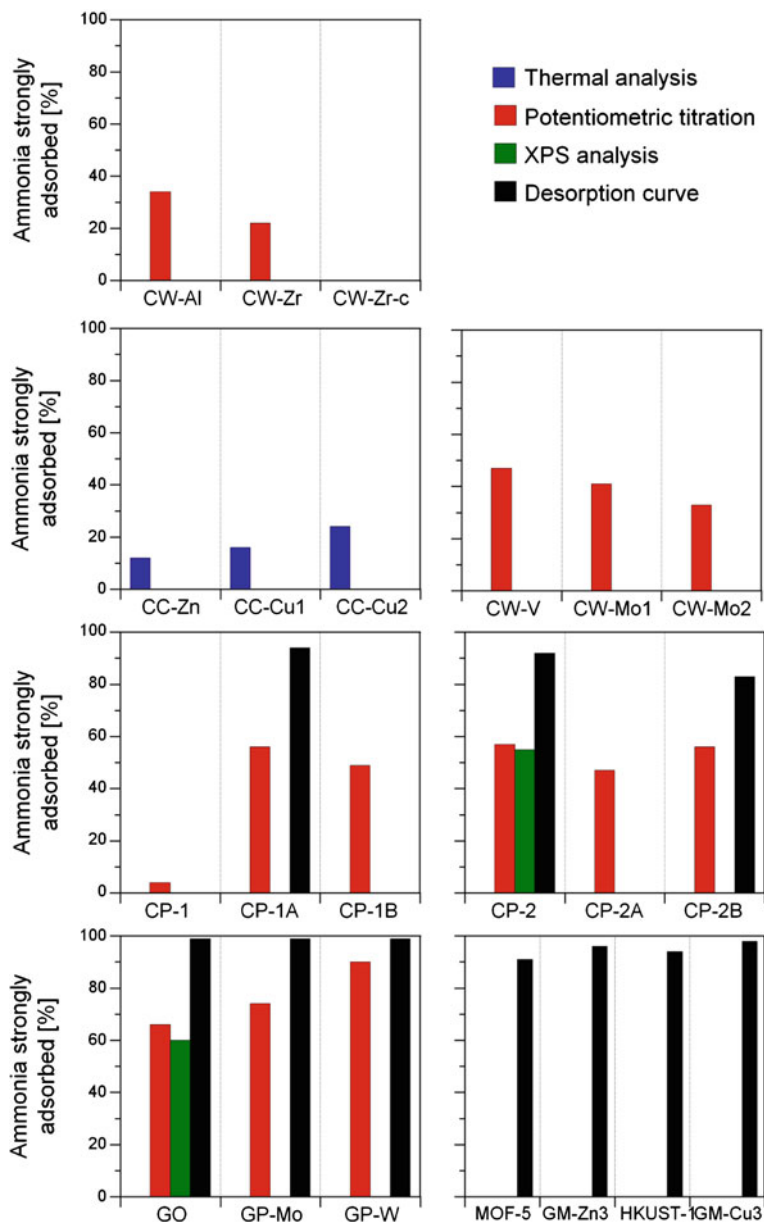
Fig. 8.3 Percentage of ammonia strongly retained on the adsorbents tested in dry conditions evaluated by various experimental methods

As observed in the plot, 7–25% of the adsorbed ammonia is strongly retained on the CC carbon modified with metal chlorides. This percentage reaches up to 34% for the CW carbon impregnated with oxycations and 33–47% for the same carbon impregnated with metal oxides. For the polymer-based carbons, between 4 and 57% of the ammonia adsorbed is detected by potentiometric titration on the surface of the exhausted samples. Finally, the highest amount of strongly retained ammonia is found for GO and GO/POMs composites (66–91%). One obvious remark here is that these values indicate a minimum in terms of ammonia strongly retained. Indeed, it is likely that not all the ammonia strongly adsorbed is considered in these measurements. In fact, for some samples, it is possible to evaluate the amount of ammonia desorbed upon purging using the data of the desorption curve. As for the breakthrough capacity, the amount of ammonia desorbed during air purging can be calculated via a mass balance between the inlet concentration of ammonia (0 ppm) and the outlet concentration of ammonia (given by sensor). Details of the calculations are given in Eqs. (8.5–8.7). This can be performed only when no gap between the adsorption curve and the breakthrough curve is observed. From these results, one can evaluate the actual amount of ammonia left on the surface at the end of the breakthrough test. The results are displayed in Fig. 8.3. The percentages of ammonia strongly adsorbed for the samples considered range from 83 to 99%. GO and the derived composites (with POMs or MOFs) appear as the best materials in terms of strength of adsorption. Overall, the percentages are rather high and suggest that some samples fulfill the strong retention requirement of real-life applications. Besides, the values obtained confirm the fact that a part of the ammonia strongly retained is not detected by the techniques used.

$$D_{t+dt} = D_t + dt \times \left(\frac{C_t + C_{t+dt}}{2} \right) \times \frac{Q_{\text{air}}}{m_{\text{ads}}} \times \frac{M_{\text{gas}} \times 273}{10^6 \times 22.4 \times (273 + T)} \qquad (8.5)$$

$$D_{t_{\text{final}}} = \sum_{t=0}^{t_{\text{final}}} D_t \qquad (8.6)$$

$$\%NH_3 \text{ strongly adsorbed} = \frac{D_{t_{\text{final}}}}{A_b} \times 100 \qquad (8.7)$$

D_t amount of ammonia desorbed at t (mg g^{-1} of adsorbent)

$D_{t_{\text{final}}}$ amount of ammonia desorbed at the end of the desorption test (mg g^{-1} of adsorbent)

A_b breakthrough capacity (mg g^{-1} of adsorbent)

t time (min)

t_{final} time at the end of the desorption test (min)
dt time interval between two points of the desorption curve (min)
C_0 inlet concentration of targeted gas (ppm)
C_t outlet concentration of targeted gas at t (ppm)
m_{ads} weight of adsorbent's bed (g)
Q_{air} air flow rate (mL min^{-1})
M_{gas} gas molecular weight (g mol^{-1})
T temperature (in °C)

References

1. F. Rodríguez-reinoso, "The role of carbon materials in heterogeneous catalysis," *Carbon,* vol. 36, pp. 159–175, 1998.
2. T. J. Bandosz, *Activated carbon surfaces in environmental remediation.* Oxford, UK: Elsevier, 2006.
3. J. Keller and R. Staudt, *Gas adsorption equilibria.* New York: Springer, 2005.
4. H. Tamon and M. Okazaki, "Influence of acidic surface oxides of activated carbon on gas adsorption characteristics," *Carbon,* vol. 34, pp. 741–746, 1996.
5. C. Petit , *et al.*, "Interactions of Ammonia with the Surface of Microporous Carbon Impregnated with Transition Metal Chlorides," *The Journal of Physical Chemistry C,* vol. 111, pp. 12705–12714, 2007.
6. C. Petit and T. J. Bandosz, "Complexity of ammonia interactions on activated carbons modified with V$_2$O$_5$," *Journal of Colloid and Interface Science,* vol. 325, pp. 301–308, 2008.
7. C. Petit and T. J. Bandosz, "Role of surface heterogeneity in the removal of ammonia from air on micro/mesoporous activated carbons modified with molybdenum and tungtsen oxides," *Microporous and Mesoporous Materials,* vol. 118, pp. 61–67, 2009.
8. C. Petit and T. J. Bandosz, "Removal of Ammonia from Air on Molybdenum and Tungsten Oxide Modified Activated Carbons," *Environmental Science & Technology,* vol. 42, pp. 3033–3039, 2008.
9. C. Petit and T. J. Bandosz, "Role of Aluminum Oxycations in Retention of Ammonia on Modified Activated Carbons," *The Journal of Physical Chemistry C,* vol. 111, pp. 16445–16452, 2007.
10. C. Petit and T. J. Bandosz, "Activated carbons modified with aluminium-zirconium polycations as adsorbents for ammonia," *Microporous and Mesoporous Materials,* vol. 114, pp. 137–147, 2008.
11. T. J. Bandosz, "On the Adsorption/Oxidation of Hydrogen Sulfide on Activated Carbons at Ambient Temperatures," *Journal of Colloid and Interface Science,* vol. 246, pp. 1–20, 2002.
12. C. Petit, *et al.*, "Reactive Adsorption of Ammonia on Cu-Based MOF/Graphene Composites," *Langmuir,* vol. 26, pp. 15302–15309, 2010.
13. C. Petit and T. J. Bandosz, "Enhanced Adsorption of Ammonia on Metal-Organic Framework/Graphite Oxide Composites: Analysis of Surface Interactions," *Advanced Functional Materials,* vol. 20, pp. 111–118, 2010.
14. R. C. Weast and M. J. Astle, *Handbook of Chemistry and Physics*, 62 ed. Boca Raton, FL: CRC Press, 1981.
15. C. L. McCallum, *et al.* "A Molecular Model for Adsorption of Water on Activated Carbon: Comparison of Simulation and Experiment," *Langmuir,* vol. 15, pp. 533–544, 1998.

16. C. Petit, *et al.*, "The role of sulfur-containing groups in ammonia retention on activated carbons," *Carbon,* vol. 48, pp. 654–667, 2010.
17. C. Petit, *et al.*, "Revisiting the chemistry of graphite oxides and its effect on ammonia adsorption," *Journal of Materials Chemistry,* vol. 19, pp. 9176–9185, 2009.
18. C. Petit and T. J. Bandosz, "Graphite Oxide/Polyoxometalate Nanocomposites as Adsorbents of Ammonia," *The Journal of Physical Chemistry C,* vol. 113, pp. 3800–3809, 2009.
19. A. Hamwi and V. Marchand, "Some chemical and electrochemical properties of graphite oxide," *Journal of Physics and Chemistry of Solids,* vol. 57, pp. 867–872.
20. T. Szabó, *et al.*, "DRIFT study of deuterium-exchanged graphite oxide," *Carbon,* vol. 43, pp. 3186–3189, 2005.
21. T. J. Bandosz and C. Petit, "On the reactive adsorption of ammonia on activated carbons modified by impregnation with inorganic compounds," *Journal of Colloid and Interface Science,* vol. 338, pp. 329–345, 2009.
22. J. Zawadzki and M. Wisniewski, "In situ characterization of interaction of ammonia with carbon surface in oxygen atmosphere," *Carbon,* vol. 41, pp. 2257–2267, 2003.
23. J. R. Pels, *et al.*, "Evolution of nitrogen functionalities in carbonaceous materials during pyrolysis," *Carbon,* vol. 33, pp. 1641–1653, 1995.
24. H. Schmiers, *et al.*, "Change of chemical bonding of nitrogen of polymeric N-heterocyclic compounds during pyrolysis," *Carbon,* vol. 37, pp. 1965–1978, 1999.
25. Q. Zhu, *et al.*, "Determination of the Fate of Nitrogen Functionality in Carbonaceous Materials during Pyrolysis and Combustion Using X-ray Absorption Near Edge Structure Spectroscopy," *Langmuir,* vol. 13, pp. 2149–2157, 1997.

Chapter 9
Conclusions

This dissertation provides a summary of our research regarding ammonia adsorption on various carbonaceous materials.

The results obtained indicate that porosity does not play a primary role in ammonia adsorption since most of the adsorbents tested exhibit large pores compared to ammonia's size which reduces the strength of physical forces (van der Waals). Nevertheless, if the dispersive forces (a type of van der Waals interactions) increase when adsorbents with small micropores (<10 Å) and a high density of atoms are used, then the retention process is enhanced. Porous adsorbents also enable the deposition of inorganic matter used to enhance ammonia reactive adsorption.

Reactive adsorption, unlike physisorption, represents the main mechanism of ammonia retention. This process is governed by the surface chemistry of the adsorbents, which arises from both the presence on the surface of the materials functional groups and inorganic compounds (either initially present or added via impregnation or oxidation). Among the chemical features responsible for the enhanced adsorption of ammonia is the acidity of the adsorbent. However, even though a general trend between acidity (low pH) and the breakthrough capacity was found, more parameters must be considered to provide a full understanding of the adsorption mechanism. Indeed, it was demonstrated that the role of acidity is more complex than just the presence of a low surface pH, and a proper combination of factors such as surface pH, strength (see pK_a), type (e.g. Brønsted versus Lewis acidic centers) and the amount of functional groups is required. In addition to acidity, the presence of specific oxygen-containing groups able to interact with ammonia was indicated as a positive factor for ammonia removal. These groups are sometimes already present on the adsorbent or result from a surface treatment (e.g. oxidation or impregnation with metal oxides). These oxygen functionalities include carboxyl groups, hydroxyl groups and epoxy groups. The former functionalities lead to Brønsted acid–base reactions with ammonia and/or the formation of amides. Hydroxyl groups are responsible for ammonia adsorption via hydrogen-

bonding. Finally, epoxy groups can react with ammonia to form amines. Besides oxygen-containing groups, sulfur functionalities also play a role in the ammonia retention. While thiophenic groups are not effective in ammonia adsorption, sulfonic groups can enhance ammonia adsorption via Brønsted acid–base reactions or formation of ammonium sulfate. The presence of inorganic matter, and in particular that of metals (in the form of ions, oxides or chlorides), represents another important surface chemistry feature. These metals can be a part of the adsorbent material itself or can originate from an impregnation process. The inorganic compounds can act as active centers as they allow ammonia reactive adsorption via Lewis interactions, hydrogen-bonding (for metal oxides) or a complexation reaction.

Moisture, present in the challenging gas or on the adsorbent's surface, influences the ammonia removal as well. The effect of water is dual. On the one hand, humidity enhances the breakthrough capacity since it enables the formation of a water film on the pore walls of the adsorbent where ammonia can easily dissolve due to its high water solubility. On the other hand, the competition between ammonia and water adsorption for the same active sites is observed for some adsorbents. Moreover, the strength of the ammonia retention via dissolution in water is rather weak which causes the gradual release of ammonia upon air purging. The amount of adsorbed water is increased on materials with hydrophilic functionalities (i.e. oxygen-containing groups) and small pores.

Owing to these various influencing parameters, the mechanisms of ammonia adsorption are diverse and include: physisorption, dissolution in water, hydrogen-bonding, Lewis and Brønsted acid–base interactions, complexation and nucleophilic addition with formation of amines and/or amides. Consequently, ammonia can be retained on the adsorbent's surface in the form of NH_3, NH_4^+ or nitrogen-containing groups incorporated into the adsorbent's matrix (NH_2). The three last mechanisms allow for the strong retention of ammonia. Generally speaking, for the materials tested, the amount of ammonia retrieved on the adsorbent's surface after air purging ranges from 10 to 99% depending on the materials tested.

Among the adsorbents tested in this study for ammonia adsorption, GO and the derived composites (GO/POMs and GO/copper-based MOFs) appear as the best candidates for the ammonia removal media in terms of the breakthrough capacity, performance in the presence of water and strength of adsorption. Overall, all the materials synthesized exhibit similar or much higher breakthrough capacities than those reported for activated carbons, which currently represent the "standard" adsorbents in the industrial field.

To conclude, all the above indicates that one can act upon several parameters to enhance ammonia adsorption. Consequently, the challenge is more to define the requirements (i.e. cost of preparation, conditions of applications such as the temperature and humidity level, minimum breakthrough capacity, etc.…) of a specific application for an ammonia adsorbent and then find an adsorbent allowing the best trade-off.

Chapter 10
Paths Toward Future Research

The research on ammonia removal from air is far from exhausted and still represents the object of study of many research groups. In this chapter, some thoughts on directions of research related to the ammonia removal are proposed.

- The influence of other functionalities than the ones described above on ammonia adsorption could be studied. Examples of such groups include the phosphorus-containing groups. They can be incorporated to the surface of activated carbons in different forms such as phosphonic or pyrophosphate groups [1]. Given the acidity of the former functionalities, interactions with ammonia are expected to take place.
- In the presented work, adsorption of ammonia "alone" was studied. The only potential "competitor" considered was water. It could thus be interesting to extend that study to the adsorption of mixture of gases containing ammonia and other pollutants. This could provide some information on the selectivity of the materials described.
- Although materials can exhibit a good performance on the laboratory-scale, studies are needed to evaluate their capability for larger applications. In particular, gas masks require the immobilization of a filter on a given cloth. Considering both the various research projects currently focusing on the preparation of films for diverse applications and the chemistry of ammonia adsorbents ways to prepare flexible filters could be proposed.
- The sustainability of an adsorbent is in part dictated by the possibility of its regeneration or recycling. The first option relies on the fact that products of ammonia adsorption can be removed without (or with minor) alteration of the adsorbent. Due to the strong adsorption requirement in ammonia removal, this might not be possible. Indeed, it was underlined that most of the time ammonia reacts with the adsorbent's surface to form new products incorporated in the materials matrix or deposited in the pores network. Consequently, heat treatment or chemical extraction processes would affect both the chemistry and texture of

the adsorbents and thus do not represent "real" regeneration processes. For this reason, the second option (recycling) appears as the most viable. Heat treatment can be used to prepare materials with nitrogen-containing functionalities which can find applications as, for instance, a support for metallic nanoparticles [2–4] or adsorbents for other toxic gases [5]. Some of the adsorbents discussed in this study allow the reactive adsorption of ammonia with subsequent deposition of water-soluble species (i.e. ammonium sulfate). Based on this, one could envision a process to extract the products of reactive adsorption. Although the surface chemistry of the final material would be different than that of the fresh adsorbent, the texture should be fairly recovered. As porous structures are needed in many fields such as catalysis or gas purification/separation, one could imagine a way to reuse the porous materials for these applications.

References

1. T. J. Bandosz, *Activated carbon surfaces in environmental remediation*. Oxford, UK: Elsevier, 2006.
2. Z. Lei,*et al.*, "Highly dispersed platinum supported on nitrogen-containing ordered mesoporous carbon for methanol electrochemical oxidation," *Microporous and Mesoporous Materials,* vol. 119, pp. 30–38, 2009.
3. K. Jiang*, et al.*, "Selective Attachment of Gold Nanoparticles to Nitrogen-Doped Carbon Nanotubes," *Nano Letters,* vol. 3, pp. 275–277, 2003.
4. F. Li*, et al.*, "Nitrogen-doped porous carbon microspherules as supports for preparing monodisperse nickel nanoparticles," *Carbon,* vol. 44, pp. 128–132, 2006.
5. J. Keller and R. Staudt, *Gas adsorption equilibria*. New York: Springer, 2005.

Appendix

Table A.1 The parameters of porous structure derived from nitrogen isotherms for the polymer-based carbons before and after exposure to ammonia

Sample	S_{BET} (m^2 g^{-1})	V_{tot} (cm^3 g^{-1})	V_{meso} (cm^3 g^{-1})	V_{mic} (cm^3 g^{-1})	V_{mic}/V_{tot}
CP-1	1331	0.991	0.370	0.621	0.63
CP-1-ED	1297	0.969	0.369	0.600	0.62
CP-1-EM	1326	0.963	0.333	0.630	0.65
CP-1-EPD	1434	1.026	0.358	0.668	0.65
CP-1-EPM	1323	0.933	0.314	0.619	0.66
CP-1A	1049	0.871	0.375	0.496	0.57
CP-1A-ED	1081	0.868	0.358	0.510	0.59
CP-1A-EM	1031	0.841	0.356	0.485	0.58
CP-1A-EPD	1017	0.789	0.299	0.490	0.62
CP-1A-EPM	952	0.744	0.296	0.448	0.60
CP-1B	1449	1.076	0.385	0.691	0.64
CP-1B-ED	1419	1.034	0.360	0.674	0.65
CP-1B-EM	1369	1.025	0.365	0.660	0.64
CP-1B-EPD	1454	1.038	0.313	0.725	0.70
CP-1-EPM	1473	1.083	0.397	0.686	0.63
CP-2-ED	295	0.263	0.120	0.143	0.54
CP-2-EM	308	0.279	0.131	0.148	0.53
CP-2-EPD	311	0.294	0.147	0.147	0.50
CP-2-EPM	257	0.243	0.118	0.125	0.51
CP-2A	531	0.399	0.140	0.259	0.65
CP-2A-ED	508	0.391	0.147	0.244	0.62
CP-2A-EM	501	0.380	0.136	0.244	0.64
CP-2A-EPD	493	0.374	0.131	0.243	0.65
CP-2A-EPM	494	0.378	0.136	0.242	0.64
CP-2B	742	0.533	0.164	0.369	0.69
CP-2B-ED	734	0.528	0.167	0.361	0.68
CP-2B-EM	738	0.518	0.149	0.369	0.71
CP-2B-EPD	730	0.513	0.151	0.362	0.71
CP-2B-EPM	743	0.527	0.162	0.365	0.69

Table A.2 The parameters of porous structure derived from nitrogen isotherms for activated carbon-based samples before and after exposure to ammonia

Sample	S_{BET} (m^2 g^{-1})	V_{tot} (cm^3 g^{-1})	V_{meso} (cm^3 g^{-1})	V_{mic} (cm^3 g^{-1})	V_{mic}/V_{tot}
CC	1033	0.614	0.139	0.475	0.774
CC-ED	1033	0.614	0.135	0.479	0.780
CC-Zn	726	0.437	0.095	0.342	0.78
CC-Zn-ED	562	0.353	0.096	0.257	0.73
CC-Zn-EM	593	0.370	0.102	0.268	0.72
CC-Zn-EPD	603	0.373	0.102	0.271	0.73
CC-Zn-EPM	555	0.349	0.104	0.245	0.70
CC-Cu1	914	0.539	0.124	0.415	0.770
CC-Cu1-ED	801	0.471	0.109	0.362	0.769
CC-Cu1-EM	778	0.458	0.092	0.366	0.799
CC-Cu1-EPD	839	0.494	0.096	0.398	0.805
CC-Cu1-EPM	846	0.498	0.098	0.400	0.803
CC-Cu2	565	0.345	0.095	0.250	0.73
CC-Cu2-ED	552	0.339	0.089	0.250	0.74
CC-Cu2-EM	648	0.387	0.090	0.297	0.77
CC-Cu2-EPD	580	0.353	0.092	0.261	0.74
CC-Cu2-EPM	558	0.339	0.085	0.254	0.75

Table A.3 The parameters of porous structure derived from nitrogen isotherms for MOF-5 and the GM-Zn*n* composites before and after exposure to ammonia

Sample	S_{BET} (m^2 g^{-1})	V_{tot} (cm^3 g^{-1})	V_{meso} (cm^3 g^{-1})	V_{mic} (cm^3 g^{-1})	V_{mic}/V_{tot}
MOF-5	793	0.408	0.023	0.385	0.94
MOF-5-ED	739	0.399	0.010	0.389	0.97
MOF-5-EM	10	0.057	0.052	0.005	0.09
GM-Zn1	706	0.365	0.024	0.341	0.93
GM-Zn1-ED	710	0.365	0.024	0.341	0.93
GM-Zn1-EM	8	0.025	0.021	0.004	0.16
GM-Zn2	806	0.416	0.028	0.388	0.93
GM-Zn2-ED	807	0.415	0.027	0.388	0.93
GM-Zn2-EM	4	0.021	0.019	0.002	0.01
GM-Zn3	603	0.325	0.037	0.288	0.89
GM-Zn3-ED	475	0.254	0.025	0.229	0.90
GM-Zn3-EM	7	0.026	0.022	0.004	0.15
GM-Zn4	742	0.399	0.002	0.397	0.99
GM-Zn4-ED	93	0.211	0.168	0.043	0.20
GM-Zn4-EM	0	0	0	0	–
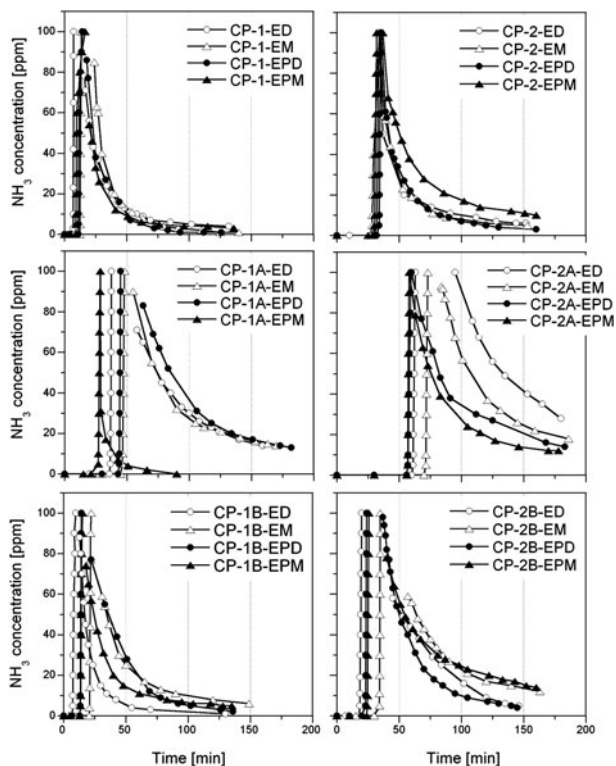
Fig. A.1 Ammonia breakthrough and desorption curves for the polymer-based carbons in the various conditions tested. Reprinted from Ref. [1], Copyright 2010, with permission from Elsevier
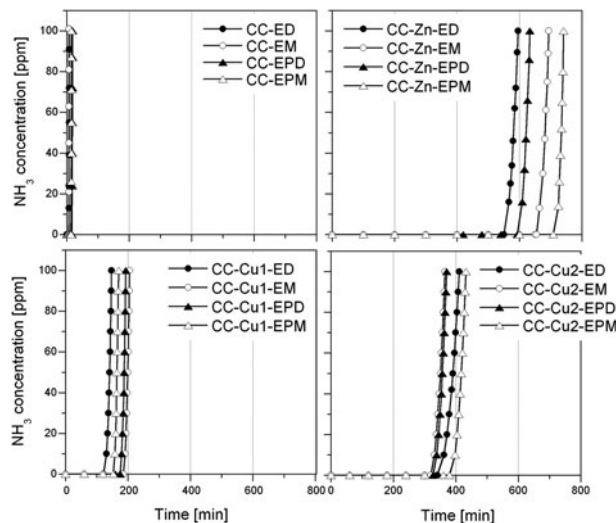
Fig. A.2 Ammonia breakthrough curves for the activated carbon-based samples (virgin and modified with metal chlorides) in the various conditions tested
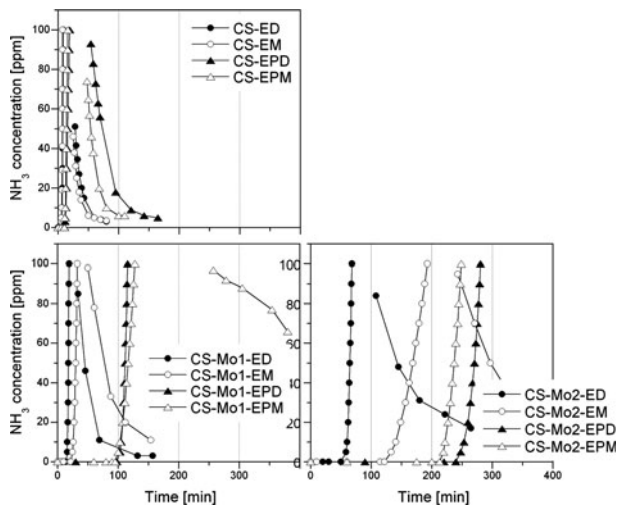
Fig. A.3 Ammonia breakthrough and desorption curves for the coconut shell-based carbon (virgin and modified with metal oxides) in the various conditions tested
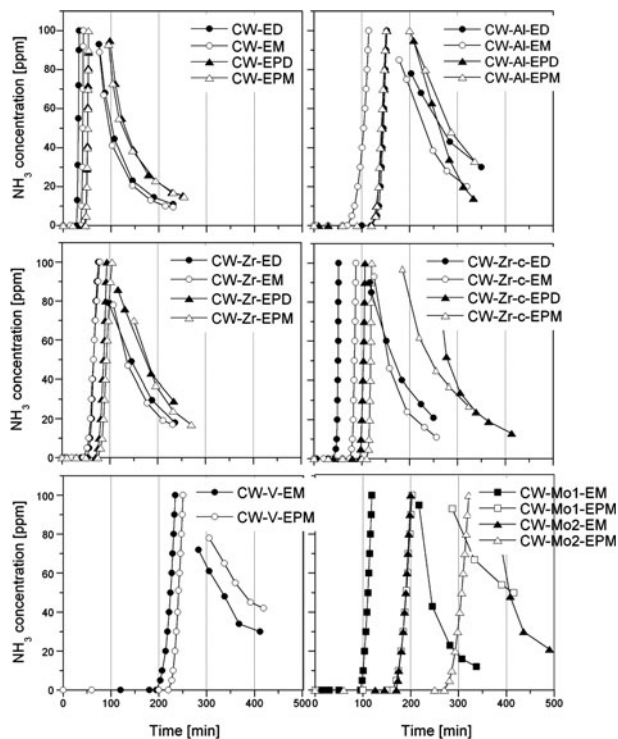
Fig. A.4 Ammonia breakthrough and desorption curves for the wood-based carbon (virgin and modified with metal oxides or polycations) in the various conditions tested
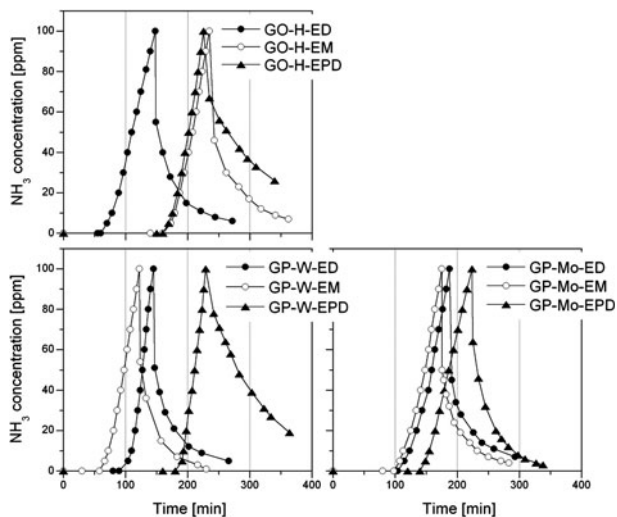
Fig. A.5 Ammonia breakthrough and desorption curves for the graphite oxide and graphite oxide/polyoxometalate composites in the various conditions tested
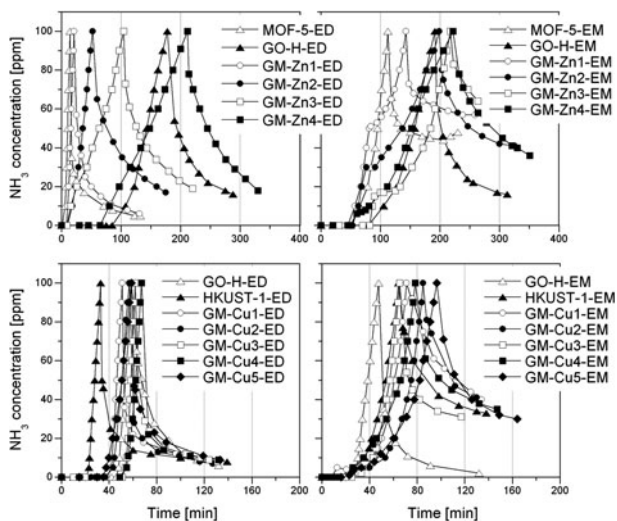
Fig. A.6 Ammonia breakthrough and desorption curves for the zinc and copper-based metal-organic frameworks and the derived metal-organic frameworks/graphite oxide composites in the various conditions tested
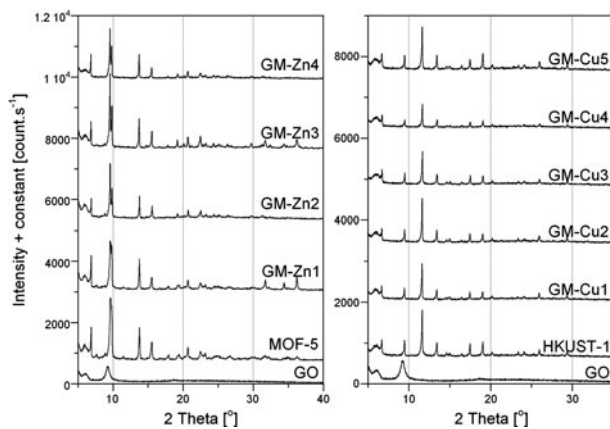
Fig. A.7 X-ray diffraction patterns for GO, MOF-5, HKUST-1 and the zinc- and copper-based composites

Fig. A.8 DTG curves for GO, MOF-5, HKUST-1 and the zinc- and copper-based composites
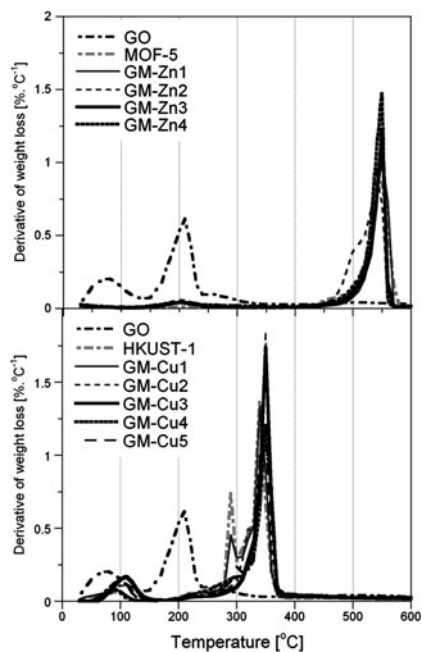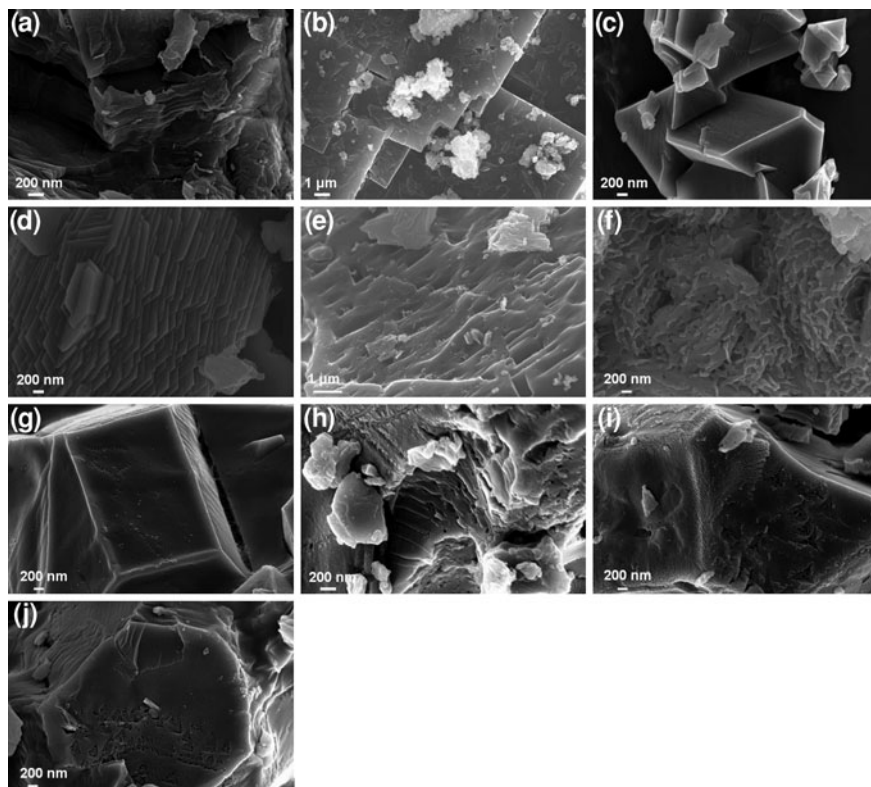
Fig. A.9 SEM micrographs for GO (**a**), MOF-5 (**b**), HKUST-1 (**c**) and the zinc- and copper-based composites: GM-Zn1 (**d**), GM-Zn2 (**e**), GM-Zn3 (**f**), GM-Cu1 (**g**), GM-Cu2 (**h**), GM-Cu3 (**i**), GM-Cu4 (**j**). Reprinted with permission from Refs. [2, 3]. Copyright 2009 and 2010, Wiley and American Chemical Society
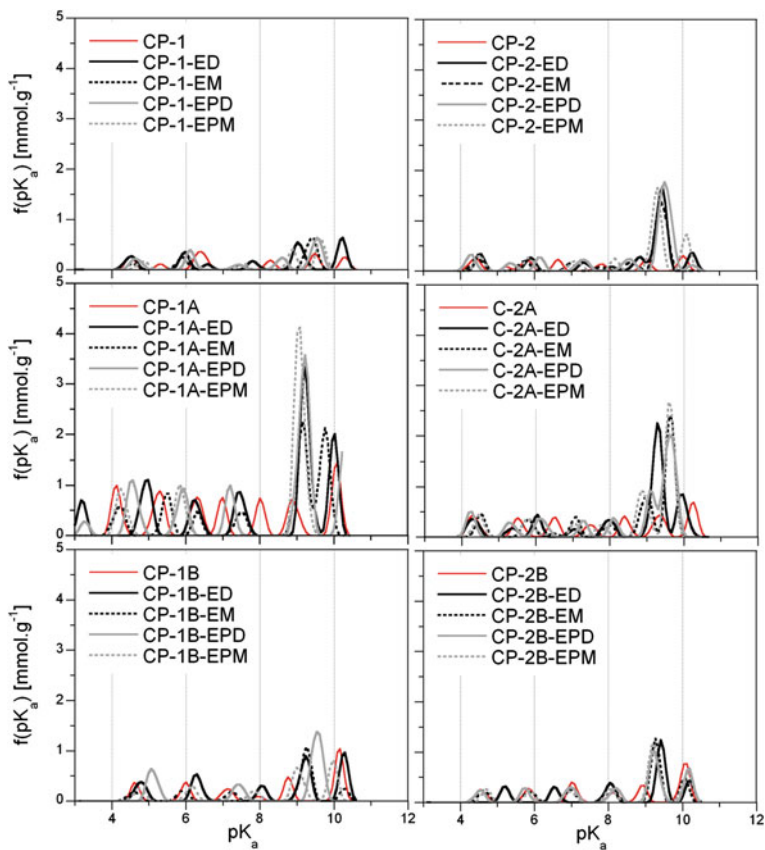
Fig. A.10 pK$_a$ distributions for the polymer-based carbons before and after exposure to ammonia. Reprinted from Ref. [1], Copyright 2010, with permission from Elsevier

Fig. A.11 pK$_a$ distributions for the wood-based carbon (virgin and impregnated with metal oxides or polycations) before and after exposure to ammonia
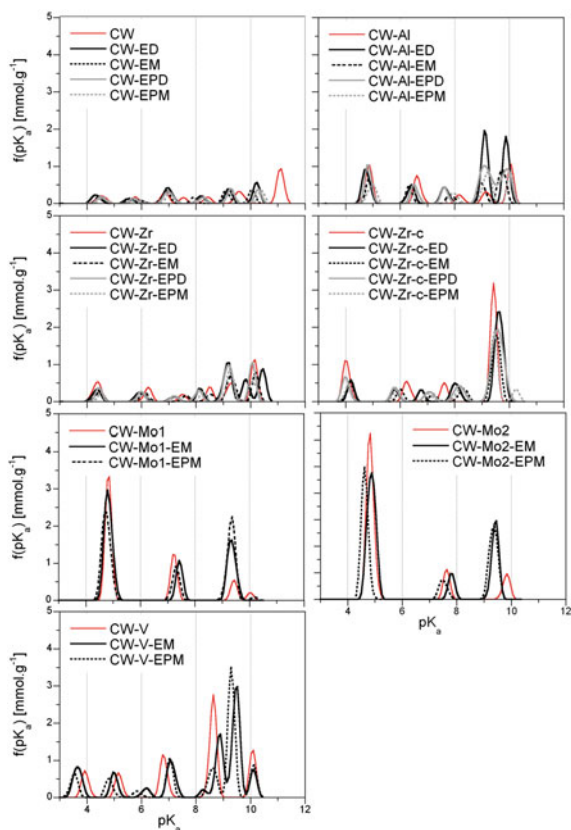
Fig. A.12 pK$_a$ distributions for the graphite oxide materials and the graphite oxide/polyoxometalate composites before and after exposure to ammonia
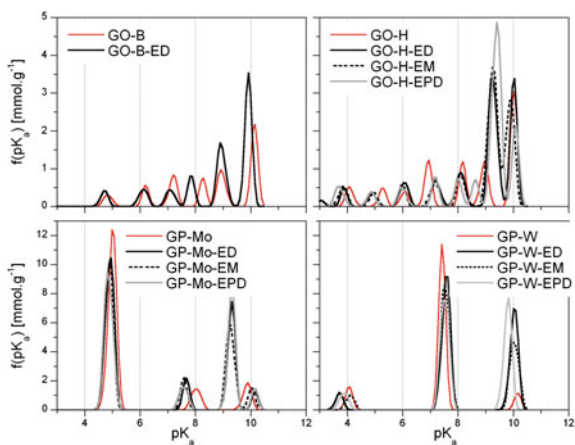
References

1. C. Petit, *et al.*, "The role of sulfur-containing groups in ammonia retention on activated carbons," *Carbon,* vol. 48, pp. 654–667, 2010.
2. C. Petit and T. J. Bandosz, "MOF–Graphite Oxide Composites: Combining the Uniqueness of Graphene Layers and Metal–Organic Frameworks," *Advanced Materials,* vol. 21, pp. 4753–4757, 2009.
3. C. Petit, *et al.*, "Reactive Adsorption of Ammonia on Cu-Based MOF/Graphene Composites," *Langmuir,* vol. 26, pp. 15302–15309, 2010.

Index